UNIVERSITÀ
DEGLI STUDI
DI PADOVA

Sede Amministrativa: Università degli Studi di Padova

Dipartimento di Scienze Chimiche

SCUOLA DI DOTTORATO DI RICERCA IN: Scienze Molecolari

INDIRIZZO: Scienze Chimiche

CICLO: XXVII

Study, analysis and identification of degradation by-products in ancient and artificially aged papers

Direttore della Scuola: Prof. Antonino Polimeno

Coordinatore d'indirizzo: Prof. Antonino Polimeno

Supervisore: Dr. Alfonso Zoleo

Dottorando: Maddalena Bronzato

Table of contents

ABSTRACT

The aims of this research is the identification of the degradation by-products in ancient papers by means of chemical, spectroscopic and chromatographic analyses and the development of innovative methods of artificial ageing that should be able to simulate the natural degradation in these materials.

For many centuries paper has been representing the main writing support for storing human knowledge. Paper is a material prone to degradation, and its conservation is a main concern, due to its obvious wide diffusion. A considerable effort has been dedicated to the paper preservation issue and it is widely recognized that a proper knowledge of the degradation reactions is essential in designing an efficient conservation treatment.[1]

To this purpose, a relevant amount of data has been collected about artificially aged paper, but just a few articles deal with naturally aged materials, since generally paper from ancient books has an artistic or historical value, and either non-destructive or micro-destructive spectroscopic techniques can be applied.

In the first part of this work, ("Analysis of degradation by-products in ancient papers", Chapter 4) a new comprehensive protocol is proposed for assessing the degradation of ancient books. The protocol is based on a multi-technique spectroscopic, chemical and analytical study of material obtained by washing leaves of ancient books. Indeed, the conservation treatments on ancient books involve frequently washing the paper leaves with water to remove the acidic by-products, which is considered a safe treatment.[2] If the waters used for washing are collected rather than wasted, the cross-referencing of the analysis results of these "wasted waters" can provide a broad and deep insight into paper degradation by-products, thus furnishing much valuable information on both the conservation state of the books/documents in question and the degradation reactions occurring within their leaves. The proposed protocol is applied here, as a case-of-study, to the "wasted waters" obtained from washing leaves of a 16th-century-printed book, the *De Divina Providentia*. The widest range of analytical techniques was applied to the degradation by-products extracted from leaves in different conservation state, ranging from not degraded to very degraded.

The here-proposed method is meant to become a *pilot protocol* for the study of ancient/historical paper degradation processes: it represents the starting point of a wider

study on ancient and historical papers. Its potential application on a broad range of books and papers of different ages, origins and in different conservation state could allow for the creation of the first database on the natural by-products generated by aging in ancient books.

Furthermore, a fruitful comparison with the data collected directly on ancient sheets can represent the basis for the development and the optimization of an innovative method for paper ageing (accelerated or artificial ageing methods, AAMs), able to closely simulate the natural degradation of cellulosic materials, depending on their chemical composition.

In the second part of this research ("Artificial ageing by ozonation", Chapter 5) a method for the artificial ageing of paper is proposed, aiming to reproduce oxidative by-products found in naturally aged paper. In literature, much research has been carried out in the area of paper artificial ageing, especially as regards the simulation of hydrolytic damage of paper leading to the depolymerisation of cellulose.[3, 4] However, other mechanisms that proceed during the natural ageing of paper, such as oxidation and autoxidation reactions, can become predominant in certain cases and therefore render these systems more complex and difficult to reproduce in the laboratory.[5-8]

In the last few years, much work has been performed in order to shed light on this class of reactions and on the reactive species, which promote and catalyze them. Much evidence has been collected on the role of reactive oxygen species (ROS) in the cellulose natural oxidation reactions, on their ability to induce paper radical reactions and to produce radical species in ancient papers.[9-13] In general, nowadays serious and complete studies of paper radicals and, in particular, of their correlation with the paper oxidation by-products are not present in literature.

In this sense, they have been reported here the first steps followed towards the development of a specific method of artificial ageing, which implies the use of ozone as a trigger for the accelerated degradation of paper. A great effort has been dedicated towards the achievement of an ozonation protocol of paper, which could reproduce the formation of both the natural degradation by-products and the open-shell species and allow for a deeper study of their nature and their effect on the writing support. The continuous comparison between the data collected on ancient papers and on artificially aged papers is the only sensible way to develop and optimize new methods for artificial or accelerated ageing of

paper, able to simulate the natural degradation in cellulosic materials according to their chemical composition.

The third part of this research ("Logwood inks", Chapter 7) reports the results of the spectroscopic and analytical study on Logwood inks, carried out in cooperation with the Scientific Department of the Metropolitan Museum of Art, NYC. Fe and Cu/Fe - based Logwood inks have been synthesized following late 19^{th}recipes and they have been characterized using UV-VIS, IR, Raman, EPR and ESI-MS analyses. This multi-technique approach is aimed to shed light on the coordination environment of the metallic ions in the colorant matrix, in order to better understand the structure of the complexes responsible for the ink colors. The UV-VIS and FT-IR spectra confirm the complexation of the metallic ions by the coloring Logwood organic matter, the hematein (Hm) macromolecule, while the Raman spectra show that the aromatic rings, composing the molecule, are also involved in the interaction. The high-sensitivity of the EPR technique allows for a deeper study of the ink structure giving information about the coordination environment of the metal ions. It turns out, together with ESI-MS, as the only technique, among the applied ones, that can provide a unique outline for each ink. Unexpected results are obtained by the ESI-MS analyses: for the first time in literature, mass analysis of Logwood inks has demonstrated the breakdown of Hm molecules during the ink preparation, as just complexed cathecols and/or byciclic compounds were identified as the main component of the three inks. These chemical species are very similar to the ones which compose the iron gall inks: the Fe(II)/Fe(III)-pyrogallates.

ABSTRACT

Questo lavoro è finalizzato all'identificazione dei prodotti di degrado in carte antiche attraverso l'uso di analisi chimiche, spettroscopiche e cromatografiche e allo sviluppo di metodi innovativi di invecchiamento artificiale capaci di simulare la degradazione naturale di questi materiali. Per molti secoli la carta ha rappresentato il principale supporto scrittorio per tramandare la conoscenza e la cultura dell'intera umanità. La carta è un materiale incline al degrado: data la sua ampia diffusione, una particolare attenzione è stata dedicata alla preservazione e alla conservazione del patrimonio documentario cartaceo. È, infatti, ampiamente riconosciuto che è necessaria una profonda conoscenza delle reazioni di

degrado per progettare un efficace trattamento di conservazione. A questo scopo, una grande quantità di dati è stata raccolta dall'analisi di carte artificialmente invecchiate, ma solo alcuni lavori in letteratura riportano studi su materiale cartaceo naturalmente invecchiato, a causa dell'impossibilità di applicare tecniche di analisi distruttive e non distruttive su carte antiche di alto valore storico-artistico.

Nella prima parte di questo lavoro ("Analysis of degradation by-products in ancient papers", Capitolo 4) si propone, per la prima volta in letteratura, un protocollo globale che sfrutta la combinazione di un vasto numero di analisi spettroscopiche, chimiche e separative su materiale ottenuto dal lavaggio di fogli appartenenti a libri antichi. Infatti, i trattamenti di conservazione di libri antichi spesso prevedono il lavaggio dei fogli di carta per eliminare l'acidità e i composti bruni, che conferiscono la colorazione scura alle carte degradate. Se le acque contenenti questi prodotti "di scarto" vengono conservate anziché gettate, la loro analisi può fornire un'ampia e profonda conoscenza dei prodotti di degrado cartaceo insieme ad utili informazioni sullo stato di conservazione dei libri/documenti in esame e sulle reazioni di degrado avvenute sui fogli, che li costituiscono. In questo lavoro di tesi, il protocollo proposto è applicato alle acque di lavaggio ottenute dalle pagine di un libro a stampa risalente al sedicesimo secolo, il *De Divina Providentia*, e sul materiale estratto da fogli in differente stato di conservazione (da molto degradati a non degradati).

Il metodo qui descritto vuole proporsi come un *protocollo pilota* per lo studio dei processi di degrado in carte antiche e storiche: esso rappresenta il punto d'inizio per uno studio più ampio di carte antiche e storiche. La sua potenziale applicazione su un numero rilevante di libri e carte risalenti a varie epoche, di diversa origine e caratterizzati da vari stati di conservazione, permetterebbe la creazione del primo database dei prodotti di degrado indotti dall'invecchiamento del supporto scrittorio.

Nella seconda parte di questa ricerca ("Artificial ageing by ozonation", Capitolo 5), si propone un metodo di invecchiamento artificiale mirato a riprodurre i sottoprodotti di ossidazioni trovati in carte invecchiate naturalmente. In letteratura, molte ricerche si sono concentrate sulla simulazione del deterioramento idrolitico della carta, che causa la depolimerizzazione delle catene di cellulose. La carta, però, è anche soggetta ad altri meccanismi di degrado, quali l'ossidazione e l'autossidazione, che in certi casi diventano predominanti e rendono il sistema più complesso e difficile da riprodurre in laboratorio. Negli ultimi anni, molto lavoro è stato realizzato per studiare maggiormente questa classe di

reazioni e le specie reattive, che le promuovo e le catalizzano. Molti dati sono stati raccolti sul ruolo delle specie reattive all'ossigeno (ROS) nelle reazioni di ossidazione della cellulosa, sulla loro capacità di indurre reazioni radicaliche e di produrre specie radicaliche nelle carte antiche.

In generale, in letteratura non è ancora presente uno studio completo sui radicali della cellulosa e sulla loro correlazione con sottoprodotti di ossidazione cartacea. In questo senso, vengono qui riportati i primi passi verso lo sviluppo di uno specifico metodo di invecchiamento artificiale, che implica l'uso di ozono come agente di innesco della degradazione accelerata della carta. Un grande sforzo è stato dedicato alla realizzazione di un protocollo di ozonizzazione della carta, che potesse riprodurre la formazione dei prodotti di degrado naturale della carta e le correlate specie *open-shell* e che permettesse uno studio più approfondito della loro natura e del loro effetto sul supporto cartaceo.

Il costante confronto fra i dati raccolti direttamente su carte antiche e i dati ottenuti su carte invecchiate artificialmente rappresenta l'unico criterio ragionevole per lo sviluppo e l'ottimizzazione di metodi innovativi di invecchiamento accelerato o artificiale del supporto cartaceo, capaci di simulare la degradazione naturale dei materiali cellulosici, in base alla loro composizione chimica.

Nella terza parte di questo lavoro ("Logwood inks", Capitolo 7) vengono riportati i risultati dello studio spettroscopico e analitico di inchiostri a base di campeggio realizzato in collaborazione con il Dipartimento Scientifico del Metropolitan Museum of Art di NYC. Durante questo progetto, sono stati sintetizzati tre tipi di inchiostro a base di campeggio, due dei quali contenenti ioni Fe^{3+}/Fe^{2+} e un terzo contenente sia ioniFe^{3+}/Fe^{2+} che ioni Cu^{2+}, seguendo delle ricette del tardo ottocento, e sono stati caratterizzati tramite l'uso di tecniche UV-VIS, IR, Raman, EPR ed ESI-MS.

Lo scopo dello studio è quello di comprendere la natura e la struttura dei complessi responsabili del colore assunto dall'inchiostro. Gli spettri UV-Vis e IR degli inchiostri indicano l'avvenuta complessazione degli ioni metallici da parte del colorante organico estratto dal campeggio, l'emateina, mentre gli spettri Raman mostrano come gli anelli aromatici della molecola siano coinvolti nell'interazione con gli ioni metallici. L'elevata sensibilità della tecnica EPR ha permesso uno studio approfondito dalla struttura degli inchiostri, fornendo informazioni sull'intorno di coordinazione degli ioni metallici. Insieme all'ESI-MS, l'EPR risulta essere l'unica tecnica capace di fornire un profilo unico e identificativo per ciascun inchiostro.

L'applicazione dell'analisi ESI-MS ha fornito risultati inaspettati: per la prima volta in letteratura, gli spettri di massa degli inchiostri a base di campeggio hanno dimostrato come il processo di preparazione dell'inchiostro implichi la decomposizione della macromolecola di emateina. La colorazione dell'inchiostro non è data quindi da complessi metallo-emateina, ma da catecoli e/o composti biciclici, strutture costituenti la macromolecola, complessati agli ioni metallici aggiunti nella preparazione. Queste specie chimiche sono molto simili a quelle che sono alla base degli inchiostri ferrogallici: i pirogallati di ferro.

Chapter 1

1. Composition, structure and properties of cellulose and other paper components

1.1 Paper

The word “paper” is etymologically derived from Latin *papyrus*, which comes from the Greek πάπυρος (*papuros*), the word for the Cyperus papyrus plant. Papyrus is a thick, paper-like material produced from the pith of the *Cyperus papyrus* plant which was used in ancient Egypt and other Mediterranean cultures for writing before the introduction of paper into the Middle East and Europe. Unlike paper, papyrus and all the other materials used as writing support, such as clay, wood, bamboo and parchment, presented some disadvantages. For example, clay or wood tablets were heavy, awkward and unpractical.

The papyrus was not pliable enough to fold without cracking and a long roll, or scroll, was required to create large-volume texts. Papyrus had the advantage of being relatively cheap and easy to produce, but it was fragile and susceptible to both moisture and excessive dryness. On the other hand, parchment represented a highly resistant material: it was made from animal skins, often calfskin, sheepskin, or goatskin. Parchment was commonly cut in leaves, like papyrus but, unlike it, parchment sheets were not sewn in rolls, but they were folded and gathered in books, named *codices*.

However, parchment was really expensive: the production of sixteen small sized sheets required an entire sheepskin. The paper introduction provided a new light material, which was, at the same time, sturdier and cheaper than parchment. Rags, like cotton, hemp and linen, were used as paper raw materials: they were selected according to their structure, quality and color before being washed and bleached through a pure ash treatment (see the Appendix Section). Therefore, paper raw materials were vegetable fibers, whose main component is represented by *cellulose.*

1.2 Cellulose and its structure

Cellulose is the paper main component, an organic compound with the formula $C_n(H_2O)_m$, which represents the most abundant organic polymer on Earth. Indeed, it is an important structural component of the primary cell wall of green plants. Cellulose is a polysaccharide

consisting of a linear chain of several hundreds to many thousands of β(1→4) linked D-glucose units.

Cellulose is considered a polydisperse polymer as it is composed by several chains of different length, and therefore by a variable number of glucose units (Fig. 1).

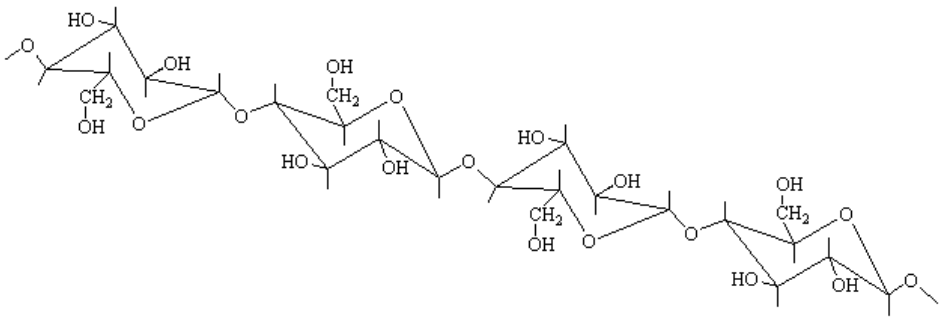

Figure 1: Polymeric chain composed byβ(1→4) linked β-glucose molecules, forming the cellulose macromolecule.

The average number of glucopyranosyl units per chain defines the *degree of polymerization* (*DP*), ranging between 300 up to 4000, according to the cellulose origin and the extraction process. The degree of polymerization can be strongly reduced (*depolymerization*) as a consequence of paper treatments and/or the presence of specific substances added to paper during its manufacturing. The depolymerization process involves the breakage of long cellulose chains into shorter chains, increasing the paper brittleness and reducing its durability.

Cellulose is a straight chain polymer: unlike starch, no coiling or branching occurs, and the molecule adopts an extended and rather stiff rod-like conformation, aided by the equatorial conformation of the glucose residues. The multiple hydroxyl groups on the glucose from one chain form hydrogen bonds with oxygen atoms on the same or on a neighbor chain, holding the chains firmly together side-by-side. These interactions can undergo specific reactions, which can modify their assessment, making the whole structure weaker. The so formed sheets of cellulose are held in staggered layers, one on top of another by Van der Waals force. The geometry of the short, carbon-hydrogen bonds minimizes the distance between layers and, therefore, Van der Waals forces (which are proportional to the inverse of the sixth power of the intermolecular distances) are maximized. These forces play a fundamental role in the maintenance of the structure: indeed, little variations of the intermolecular distance,

due to mechanical stresses, chemical reactions and/or humidity changes, are sufficient to delete these attraction forces or to convert them in repulsive interactions. This effect weakens the cellulose fibers, making them proner to degradation. The small units of cellulose formed through side-by-side hydrogen bonding and layered by Van der Waals forces are called *elemental fibrils*: these structures show a coexistence of more compacted and organized domains, called *crystalline regions*, and less-ordered and less-regular domains, called *amorphous regions* (Fig. 2).

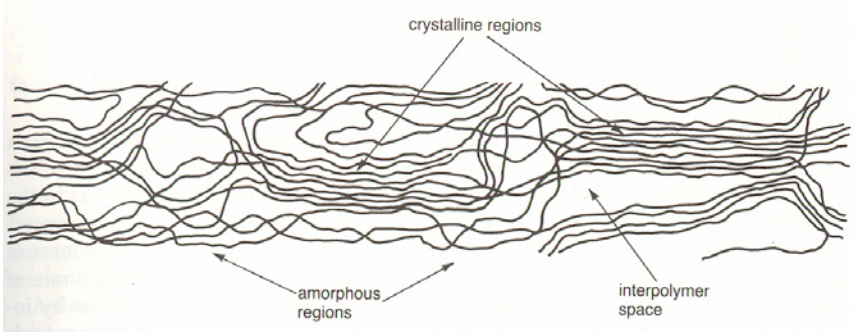

Figure 2: Amorphous and crystalline regions in a polymeric chain bundle.

Crystalline regions are hardly degraded due to their lesser accessibility to reactive species, which, conversely, can easily diffuse through the amorphous domains due to the local chain disorder. Thus, the degradation does not occur uniformly throughout the whole polymer but quickly and more easily in the amorphous regions.

Elemental fibrils pack together to form flat filaments, called *microfibrils* (Fig. 3). More microfibrils give rise to the fibrils, which in turn, once gathered together, form the fibers.

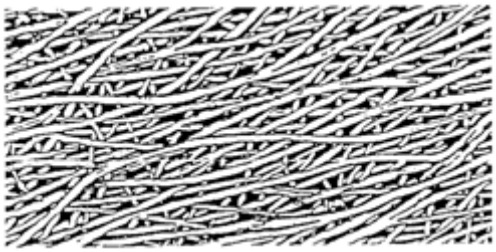

Figure 3: Microfibrils seen at an electron microscope.

Fibers of different length and size, braiding each other, form a paper sheets. Several paper features, like appearance, sturdiness, adaptability to different uses and durability, depend on specific characteristic of the cellulose matrix, i. e. the length of the cellulose fibers, the

respective percentage of crystalline and amorphous regions and the presence of residual substances deriving from cellulose extractive processes and/or from paper manufacturing.

1.3 Gelatin size and additives

Cellulose pure paper represents a strongly absorbing material: the multiple hydroxyl groups on the molecule side can easily interact with water through the formation of hydrogen bonds. The water-cellulose and cellulose-cellulose bond energies are of the same order of magnitude: therefore, water can penetrate among the paper fibers, slacken the hydrogen bonds among the cellulose chains. In this sense, since antiquity sizing materials were commonly used to improve the resistance of a sheet of paper to the sorption of water and to prevent the bleeding of the inks through or on cellulose sheets thus allowing for drawing and writing upon the surface. The mostly used sizes over the centuries were extracted by mammalian bones, sinews and gristles. The most pure glue size, introduced in the Italian papermaking in the 13th century and widely used all over Europe until the 19th century, was gelatin. It is derived from the partial either acidic or alkaline hydrolysis of collagen, which is the principal protein found in animal connective tissue, skin and bones. Glue sizes of animal origin are filmogenous, very hygroscopic substances, easily prone to biodeterioration and photoxidation. Since the first half of the 18th century, some additives have been added to improve sizing properties. In particular, the use of alum, $KAl(SO_4)_2 \cdot 12(H_2O)$, as a mordant, i. e. a substance able to strengthen the interaction between the sheet and the sizing cover, was widespread.

Moreover, over the centuries, multiple additives and fillers were added to the cellulose matrix in order to improve optical and superficial features of paper.

Therefore, paper is a heterogeneous material composed by:

− polymeric structures (cellulose, starch, gelatin), which supply consistency and resistance to degradation;

− organic (rosin) and inorganic (alum, carbonates, sulfates, optical brighteners) substances: some of them have a degradation effect on the paper, they were added to, while others exert a conservative action.

1.4 Inks

1.4.1 The history of ink

The invention of ink represents a milestone in the history of writing: its introduction in the III millennium B.C. completely revolutionized the writing and the art of calligraphy providing an easier writing medium than clay or wax tablets, definitely uncomfortable supports.

Many medieval miniatures testify the importance of ink at that time, since they depicted the devil trying to steal St John's ink, while the saint was writing the Gospel.

The word ink derives from the greek word "ἔγκαυστον",which means seared, encaustic. Then, the word was used to identify reddish dye used by the Byzantine emperors to issue letters and decrees. The oldest inks hailed from around 5000 years ago and their use was spread almost simultaneously by the Egyptian and Chinese people.

Formerly, inks were made by a simple mixture of pulverized wood-coal in water, which a thickening agent was added to, in order to bind the coal particles. Afterwards, the wood-coal was replaced by charcoal, an artificially originated product. Two mainly charcoal types were used:

• black resin, obtained by the combustion of conifer roots or by rosin calcinations;

•lamp black, coming from the combustion of substances that were used as fuel for lamps.

The coal ink and lamp black were preferentially used as they were not aggressive towards the substrate thanks to the chemical carbon inertness. Moreover, the ink particles did not alter over the time and did not fade to light. Nevertheless, the presence of moisture could cause the occurrence of stains and also the ink, which was not able to penetrate in depth in the writing support, could be removed from the support even by a simple abrasion.

In order to fix the ink easy removal, ferrous sulfate was added to the ink mixture: because of its high water-solubility, it penetrates deeply into the paper, producing brown incrustations, due to the formation of iron oxides, very difficult to be removed. However, the addition of this salt, if used in high amounts, entailed a superimposition of the brown iron oxides on the black coal particles making the color of the ink lighter. This drawback was overcome with the discovery of the reaction between tannins and iron salts: indeed, this reaction gave rise to dark black particles, obtaining a mixture of carbon black and iron gall ink.

This reaction has been known since antiquity: Pliny the Elder (AD 23/79) in his "*Naturalis Historia*" described an experiment, in which he treated a papyrus sheet, previously soaked in

a tannin solution, with an iron salt solution, with an immediate blackening of the originally cream-colored papyrus.

Although already known to the Romans, the use of metal-gall ink has started to spread since the Middle Ages, becoming the most common type at the Renaissance age. This ink has several advantages that contributed to its spread: the simplicity of preparation, the fluidity into the writing support and the difficulty to be removed from the surface it was applied on. The assertion of metal-gall ink was also facilitated by an increase in demand for ink to write.

In Europe, the first detailed description of the iron-gall ink recipe was left by the German friar Theophilus (XI-XII century) in his essay "Schedula Diversarum Artium", which stated that the raw materials to be used are the pulverized and dried bark of certain plants and the green vitriol (iron sulfate salt).

1.4.2 Iron-gall inks

Iron-gall ink has been undoubtedly the most important writing medium in the western history, and it was used, e.g., by Leonardo da Vinci, Bach, Rembrandt and Van Gogh. Since the fifteenth century, the use of iron gall inks has been introduced to the art of drawing by Rembrandt, Guercino and Lorrain.

The main ingredients of iron-gall inks are:

- Gall nuts: the galls are excrescences of various sizes and shapes, formed on the branches of some plants in consequence of insect bites. The insect bite introduces the eggs from which the larvae develop, inducing the plant to react enclosing the impact point with a wood swelling containing wood tannins. Tannins are organic substances, polyphenols, and can be divided into hydrolysable and condensed tannins. The first, the only usable in the preparation of inks, can be easily cleaved by enzymes and acids into their components, in particular, gallic acid and glucose. The complex formed from gallic acid and Fe(II), once oxidized by atmospheric oxygen, gives rise to pyrogallate ferric complexes responsible for the dark color of the ink.
- Ferrous sulfate (vitriol): it is the most important Fe(II) compound of natural origin. It is a light-green salt, which crystallizes with seven molecules of hydration water. In the ancient recipes of pigments and inks, it was called "green vitriol or copperas". Vitriol can be extracted from mines, can be obtained by evaporation of the ferrous soil

water, or, as it was common at the end of the 16th century, can be produced by treating ferrous nails with sulfuric acid.

- Binder material: over the centuries, the most used binder was Arabic gum. Arabic gum is a polysaccharide secreted by some African acacia species, in particular Senegal Acacia. In the ink preparation, its purpose is to stabilize the aqueous suspension of the ferric-pyrogallate particles, which have a tendency to aggregate and therefore to precipitate. The addition of the binder increases the medium viscosity allowing it to maintain the particles in solution. Moreover, it favors the ink adhesion to the writing support and avoids the ink bleeding on the paper. Besides arabic gum, egg white, sugar, gelatin, olive oil and honey were used as binders as well.
- Solvent: the common solvent was water. Rarely wine was added to the ink mixture, even if it has been found that the possible addition of alcohol provides some advantages, including the better tannin extraction from the vegetable matter, the slight increase in solubility of the tannic acid, the better penetration of the ink into the paper, the better preservation of arabic gum. Moreover, alcohol can act as a protection against molds and bacteria and promote faster drying of the ink applied on the writing support, although with a more rapid ink evaporation in the inkpots. Vinegar can be added as well: it acts more as antiseptic than as a solvent. The addition of vinegar, camphor, garlic clove or juice was intended to improve the ink conservation.

The recipes of an iron-gall ink began with the tannin extraction from the gall nuts, which were crumbled and macerated for several days up to one week, in a solvent (usually water) and then boiled. The heating lasted until the solution reached a third of the starting volume. Then vitriol was added: it reacted with the gall-tannic acid, forming a fine, black precipitate. At this point the binder was added, in order to stabilize the suspension consisting of particles of ferrous gallate, formed by the reaction. The freshly prepared ink, just applied on a support, although already black, appeared very clear and began to darken after a few seconds when exposed to atmospheric oxygen. Almost all the old recipes, in fact, suggested an exposure to a heat source prior to use, so as to partially oxidize the compound, or the addition of logwood inks, which bestowed the black color on the ink since its drafting.

1.4.3 Ink-induced degradation

Iron-gall inks, once applied on the writing support, can induce degradation reactions of multiple nature, which involve a loss of ink color and the deterioration of the support until the complete corrosion, thus undermining the integrity of the manuscript.

In the case of paper materials, the main causes of deterioration induced by iron-gall inks are due to two chemical compounds: sulfuric acid and ferrous sulfate. The sulfuric acid catalyzes the cellulose hydrolysis inducing the cleavage of the polymer chains. The shorter length of the cellulose chains reduces the paper strength, with a deleterious effect leading to its perforation. The acidity is undoubtedly the major cause of the deterioration and of the damages that occur on the printed material.

The acidity catalyzes the breakage of bonds between the glucose molecules of the cellulose chains, as well as the cleavage of the peptide bonds between the amino acids of gelatin-based size.

The excess of ferrous sulfate with respect to the quantity of tannins involves an excess of ions Fe(II), which can oxidize Fe(III) in the presence of oxygen and may catalyze cellulose oxidative degradation reactions, which occur through a series of chain reactions, the so-called Fenton reaction. The redox chain reaction involves the initial formation of superoxide radicals, $O_2^{-\bullet}$ (as a consequence of Fe(II) to Fe(III) oxidation). The $O_2^{-\bullet}$ species is not particularly oxidizing, but it has a long lifetime. This property allows the radical to easily spread in the cellulose fibers: inside the cellulose matrix it can firstly give rise to hydrogen peroxide and then, in the presence of the Fe(II)/Fe(III) couple, to the strongly oxidizing hydroxyl radical $OH^{\bullet}$, capable of triggering the oxidation reactions responsible for the degradation of the cellulose chains.

The oxidation reactions, i.e. loss of one or more electrons by an atom or group of atoms, can produce organic acids, which in turn catalyze the cellulose hydrolysis reactions.

Chapter 2

2. Paper degradation mechanisms

The principal reactions occurring on the cellulose structure, which can induce its alteration, are:

- Chemical degradation: hydrolysis, oxidation, photodeterioration;
- Mechanical degradation: fiber deformation;
- Biochemical degradation: biological deterioration.

2.1 Hydrolysis

Cellulose is particularly prone to hydrolytic processes, i. e. the breakage of the glucosidic bonds among the glucose units by means of cellulose-bound water molecules. The polymeric chains, composing the leaf fibers, shorten and weaken, increasing in this way the brittleness of the writing support. The hydrolytic reaction is strongly catalyzed by the presence of strong acids and bases: acid-catalyzed and basic-catalyzed hydrolysis occur with different mechanisms and induce the formation of different products.

2.1.1 Acid-catalyzed hydrolysis

The acid-catalyzed hydrolysis is the principal paper degradation pathway. It can be due to multiple factors:

- additives (i.e. alum in gelatin- or rosin-based size);
- environmental pollutants;
- writing media (i. e. iron-gall inks).

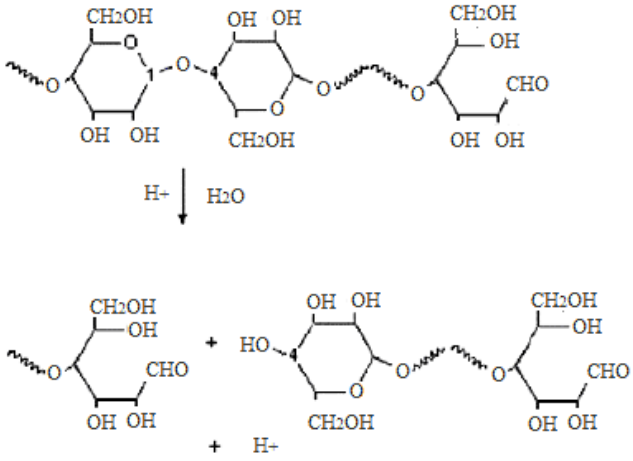

Figure 4: Acidic hydrolysis causes the breakage of the β(1→4) glycosidic bond and the consequent chain depolymerization.

Acidity catalyzes the cleavage of glucosidic bonds among glucose molecules, composing the cellulose chains (Fig. 4), as well as the peptidic bonds between the amino acids in the gelatin size. The progressive hydrolysis of cellulose reduces its DP: the cleavage of only one bond halves the DP. Theoretically, the acidic degradation could proceed up to the complete

demolition of the fibers, with the final formation of glucose. However, acidity can only affect the amorphous regions, while the crystalline domains are more resistant to the acidic attack. Therefore, the degradation slows down really fast once achieved the DP value (around 100 - 200), known as levelling-off DP (LODP), equal to the average length of the cellulose chains in the crystalline regions.

In the case of oxidized cellulose, its hydrolytic degradation gets even faster. Normally, cellulose oxidation occurs on the C_6 and the hydrolysis leads to the formation of uronic acids on the non-reducing chain end.

Uronic acids belong to β-oxyacid class, which, in a no-acqueous medium, can be degraded by the acidity (or by biologic agent enzymes), with the formation of hexenuronic acids, with a C_4 – C_5 double bond (Fig. 5).

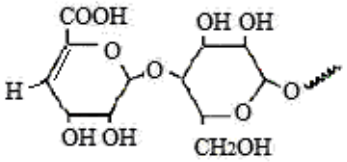

Figure 5: Hexenuronic acids.

In acidic medium, these acids, in turn, are hydrolyzed and easily degrade, with the formation of low-molecular mass furan-derivates. These compounds are in part responsible of the typical smell of oxidized and acidic papers.

2.1.2. Base-catalyzed degradation

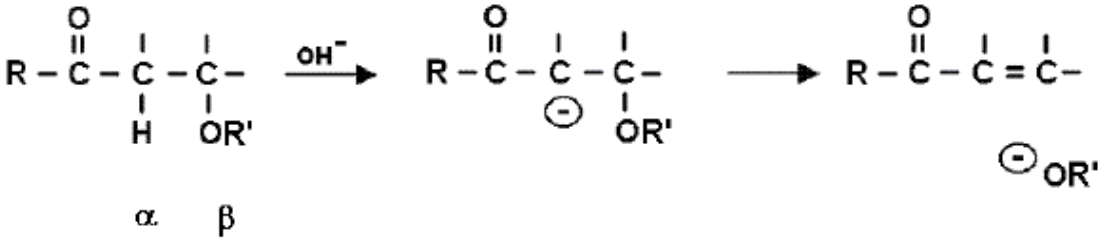

Figure 6: Simplified mechanism of the β-alkoxyelimination reaction.

In general, alkaline degradation is slower and less harmful than the acidic one, unless in the case of oxidized cellulose. Cellulose alkaline degradation mechanism is based on the *β-alkoxyelimination* (Fig. 6): an H atom, in α position with respect to a carbonyl group, is quite

acidic and it can be removed by a basic compound, leaving a negative charge on the α carbon. If a good leaving group is in β position (such as -OR'), the leaving group gets off with the negative charge, with the formation of a C=C double bond on the residue.

2.1.2.1 Alkaline degradation of oxidized cellulose

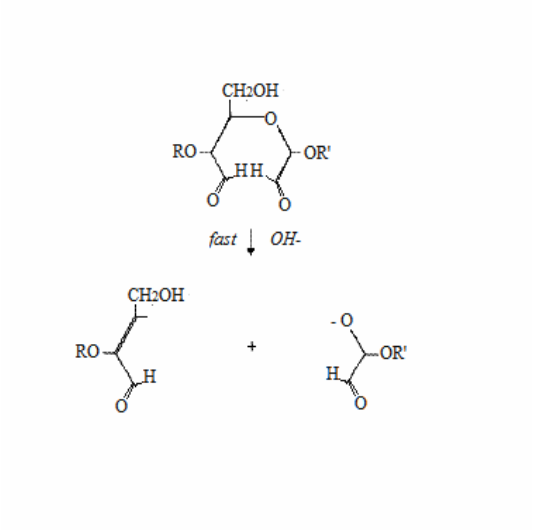

Figure 7: Alkaline degradation of oxidized cellulose in sodium periodate.

In the case of fully-oxidized cellulose, a carbonylic or carboxylic group can form in every position of the glucosidic ring by oxidation of a primary (C_6) or secondary alcoholic group (in particular C_2, C_3). In general, the β-alkoxyelimination can easily occur (at room temperature, in a short time, in slightly alkaline conditions) because a good leaving group is always present in β position.

The alkaline degradation of oxidized cellulose induces a chain cleavage, with a consequent DP decrease. However, if the initial oxidation occurs not in a random way, but in clusters, i. e. involving close glucosidic rings, it induces, together with the DP decrease, the formation of low-molar-mass acidic by-products (Fig. 7).

2.1.2.2 Alkaline degradation of unoxidized cellulose

The β-alkoxyelimination can occur in unoxidized cellulose as well, although in a slower way. Unoxidized cellulose does not have carbonylic groups, apart from the aldheydic group on C_1 on the reducing chain ends. This functional group has an H atom in α position, but no good leaving groups are present in β position: this conformation does not allow a fast β-alkoxyelimination. However, in an alkaline medium the reducing ends are prone to isomerization processes, which induce a migration of the carbonylic group along the glucosidic ring. In particular, the glucosidic ring can be transformed into a fructosidic end, which has a good leaving group in β position and which is therefore more prone to the alkaline degradation. This type of reaction is called *peeling*, as it induces the progressive elimination of the terminal glucosidic rings, with the formation of isosaccharin acid, which is soluble in the reaction environment (Fig. 8).

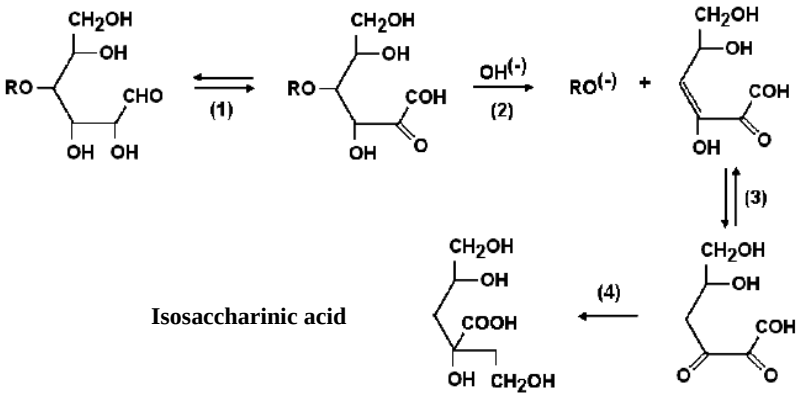

Figure 8: "Peeling" process of the reducing end of the cellulose chain.

In an alkaline medium, cellulose undergoes a progressive loss of weight. Theoretically, the peeling reaction should proceed up to the complete conversion of glucose into isosaccharinic acid.

However, this reaction is quenched by the presence of crystalline domains and by a simultaneously stopping reaction (Fig. 9), which stops the peeling reaction inducing the formation of carboxylic groups on the cellulose chain ends.

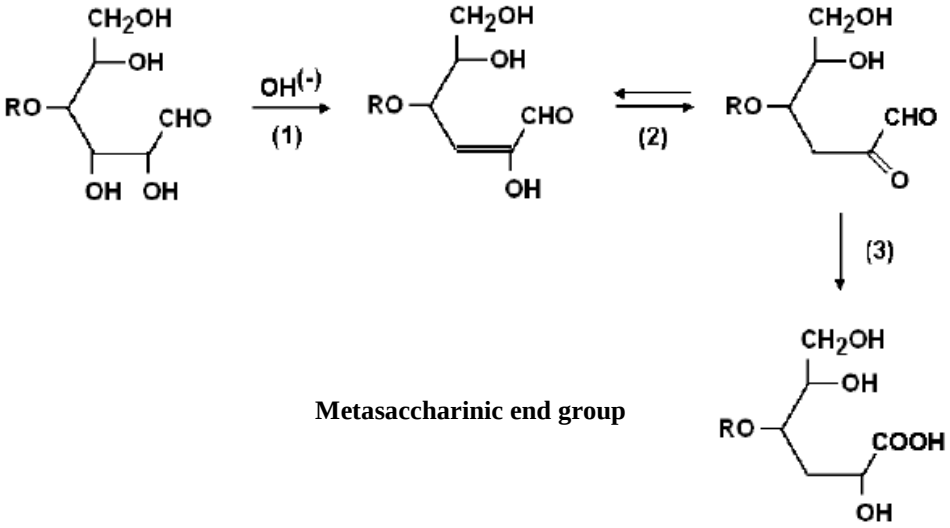

Figure 9: "Stopping" process of the reducing end of the cellulose chain.

2.2 Oxidation

Oxidation is the second main cellulose degradation mechanism. The oxidative degradation of cellulose can naturally occur (autoxidation) or can be artificially induced in presence of oxygen, light, various pollutants, such as nitrogen and sulfur oxides, or substances present in the paper matrix, such as transition metal ions, inks and dyes or specific chemical reagents.

The several primary and secondary hydroxylic groups present in cellulose structure are very sensitive to oxidative reactions: carbonyl (aldehydes and ketones) and carboxyl groups can form through oxidation. The formation of double and triple C-C bonds inside the ring is possible as well.

The primary alcoholic group of the pyranose unit is in C_6 position, which can be oxidized into aldehyde group and further into carboxyl group:

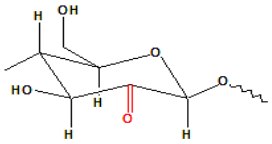

The secondary hydroxyl groups in C_2 and C_3 positions can be oxidized into ketons and if both the hydroxylic groups are involved in the oxidative process, a keto-enolic equilibrium sets up.

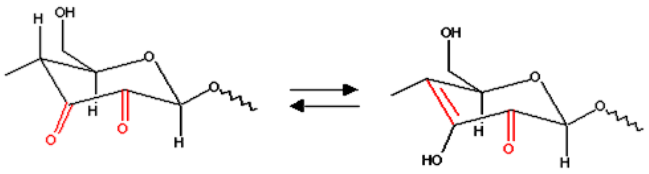

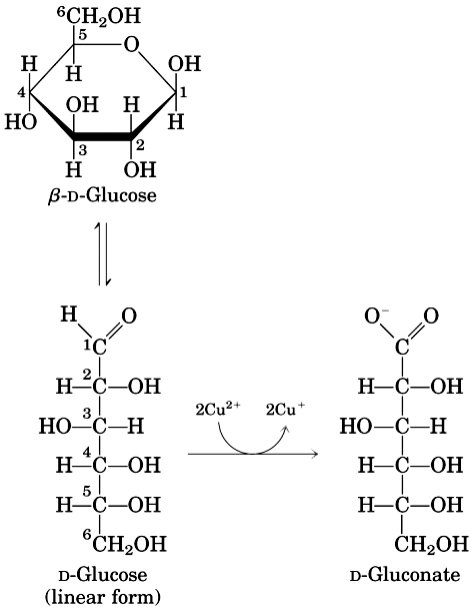

Figure 10: Example of reducing end group oxidation into carboxylate group.

Moreover, the reducing end groups can be oxidized into carboxylic groups (Fig. 10).

Cellulose oxidation can be due to different factors and therefore it can affect the polymer molecular structure in different ways with different effects on the paper support, e. g. bleaching or yellowing phenomena (generally called “discoloration”). In any case, it induces degradation and a loss of consistency of the sheet. Oxidation reactions, in turn, lead to the production of organic acids as well, which, therefore, can catalyze the hydrolytic cellulose reactions.

Both hydrolytic and oxidative degradation can be catalyzed by metal ions, such as iron and copper: these species can be present in the ink used as writing means, or they come from the water used in the papermaking or from fragments sloughed off the papermaking tools. Acidity and

alkalinity can catalyze dehydration reactions as well, giving rise to conjugations inside pyranose rings.

The synergy of the two main degradation reactions, hydrolysis and oxidation, makes extremely difficult and diversified the alteration process paper undergoes. Artificially ageing method of paper can just partially reproduce the naturally ageing mechanism. Indeed, it is necessary to bear in mind that cellulose is not the only paper component, that a book is not only made by paper, but that both paper and books are composite materials and every element is more or less prone to degradation processes.

2.3 Fiber deformation

The cellulose fibers, which compose the paper sheet, because of their several hydroxyl groups, can absorb water by the formation of hydrogen bonds. The water absorption leads to the transversal swelling of the fibers: this process causes the loosening, and ultimately the cleavage of the hydrogen bonds and London attractions among the cellulose chains. Therefore, the mechanical resistance decreases and, as the molecular structure is modified, its chemical-physical features change as well. Also in the crystalline domains, the fiber swelling makes the fiber weave more fragile. Fiber expansion, due to water absorption, induces an increase of the sheet size, with a simultaneous loss of flexibility and sturdiness. The breakage of the bonds among the cellulose chains and cellulose fibers can also be due to dehydration processes. The shrinkage of the fibers and the reduction of the space among them cause a higher stiffness, with a decrease of the paper mechanical properties and size. If the paper expansion and contraction occur in a short span of time, these phenomena lead to a collapse of the material.

Moreover, it is necessary to bear in mind that every change in paper size involves a strain on all the material it supports: e. g. inks, glue sizes, dyes undergo distortion, breakage and shedding.

2.4 Biodeterioration

When paper water content overtakes a threshold value (R. H. higher than 80%), it is very likely the formation of microorganisms. The most part of bacteria and fungi use paper as nutritional and breeding environment and their whole life cycle completely occur inside and upon this material. Most of paper alterations are due to the metabolic activity of the

microorganisms: the ones mainly present on paper are molds, whose paper species are about two hundreds.

These species can affect paper in these three ways:

- *mechanically*: the stringy structures of the fungi insert into the cellulose fibers, in particular in the amorphous regions, inducing paper weakening and breakages;
- *chemically*: the microorganism metabolism produces hydrolytic enzymes, able to break the bonds among the fibrils. The demolition of the fiber structure leads them to be “absorbed” by cellulose itself with a consequent glucose fermentation and the production of water-soluble intermediates;
- *aesthetically*: bacteria and fungi produce colored stains, which show different shapes and colors according to the species, the growth, the different ventilation and illumination, paper acidity or alkalinity.

Fungi species produce organic acids, which induce hydrolytic reactions with a further degradation of the paper material. Moreover, several fungi secrete particular polysaccharides with adhesive properties, which cause a welding between adjacent sheets.

Together with the microorganism, insects can find their nourishment and habitat inside paper as well, generally preferring darker environments. The number of insects affecting paper is around one hundred and the type of damage depends on the species they belong to. The most harmful insects belong to the *Coleoptera* order, in particular to the *Anobium punctatum* and *Dermestidae* families**,** commonly known as woodworms. These insects lay eggs in small holes inside wood or paper: the larvae, coming out from the eggs, quickly feed on these materials causing the characteristic pathways. Another typical insect is the *Lepisma saccharina*, commonly known as silverfish, deriving from the animal's silvery light grey and blue color plates, combined with the fish-like appearance of its movements. It causes irregular outline erosions on the paper surphace. The *Liposcelis divinatorius*, commonly known as booklice, is one of the smallest insects, living inside paper materials. The most harmful insect to paper is the *Kalotermes flavicollis*, a species of “Dampwood termites” belonging to the family Kalotermitidae, one of the most primitive families of termites. This species swam in colonies, far from light, and therefore it is very difficult to locate them and the damage they cause, because they keep intact the affected surface, damaging the inside.

In general, warm, humid and poorly ventilated environments represent suitable conditions for a biological attack.

The infection is naturally prone to extend to the organic materials, which paper is composed by or paper is in touch with, involving an interaction among the different deterioration processes.

2.5 Photodeterioration

Archival documents and works of art are sensitive to photodeterioration processes, induced by the lighting: natural and artificial light, according to its wavelength, power and exposition time, induces particular and complex degradation mechanisms, attributable to photolysis, photoxidation and photosensitization phenomena.

In particular, the energy of ultraviolet radiations can induce molecular electronic transitions, which lead to the scission of interatomic or intermolecular bonds, with the formation of radical species. These species are strongly reactive, forming new chemical bonds and therefore giving rise to new compounds. Paper components such as lignin, hemicelluloses and optical brighteners, can strongly absorb UV radiations, forming degradation intermediates that can react with cellulose as well as induce paper discoloration.

Artificial light is normally produced by incandescent or fluorescent lamps: the formers (wire filament or halogen lamp) emit a minimum amount of UV radiations, but, because of the IR high production, they heat up and therefore must be kept far from the works of art and strictly not used in narrow spaces, like showcases. Fluorescence lamps (neon tubes) are extremely dangerous because of the UV light emission, and, if used, they must be protected by means of proper filters. However, they do not produce IR radiations. Illumination for documents should not overtake the threshold value of 50 lux/hour and it should be void of ultraviolet radiation or at least UV radiation should not be higher than 75 μwatt/lumen.

2.6 Degradation causes

For the purpose of a proper renewal of the document material and in order to slow down the degradation processes, it is necessary to know deeply the chemical-physical reactions occurring on paper together with all the possible factors able to induce the development of such mechanisms.

A special attention has to be paid on:

- material nature;
- environmental conditions;

- use.

2.6.1 Material nature

The basic element of paper, the cellulose fiber twine, is naturally subject to a chemical-physical transformation according to its nature and the type of paper manufacture. Paper of different qualities undergoes different type of alteration. The technological process, prompted to seek for more economic and copious products, has led over the centuries to a decrease of the durability and quality of this material. This is particularly true after the introduction, in the second half of the XIX century, of wood-pulp instead of rag-pulp as the raw material used to form the paper sheet. Albeit cheaper than rag-pulp, wood-pulp is characterized by the presence of lignin, an acidic polymer of aromatic alcohols which strongly favors paper degradation reactions. The fiber deterioration became even more rapid with the introduction of paper machines, which produced shorter and less resistant fibers. Furthermore, in order to increase the whiteness of wood-pulp paper, bleaching and other paper treatments were applied, involving the use of oxidant and reducing substances, which induce strong alteration of the cellulose structure.

Additives like colors and fillers can interact in the normal degradation mechanisms of cellulose, enhancing the deterioration effects. Among the several fillers added to ancient papers, alum has been the most harmful one, as it generates sulfuric acid by hydrolysis. Also $CaCO_3$, added as alkaline reserve able to neutralize the paper acidity, can reduce the mechanical properties of paper, if used in excessive amount.

Some making processes can leave residues among the cellulose fibers: among them, the most dangerous are metal ions, such as iron, copper, zinc, aluminum, which can catalyze hydrolytic and oxidative paper degradation reactions, with the consequent formation of stains and discoloration effects. Inks, waxes, colors can be composed by chemical compounds, able to damage paper more or less seriously.

2.6.2 Environmental conditions

The physical conditions of a paper document depend strongly on the place in which it is stored.

During the conservation of documental and archival materials, a special attention has to be paid on the following environmental factors:

- climate;
- lighting;
- atmospheric pollution;
- atmospheric particulate.

The climate is the most incisive external factor in the alteration of works of art: temperature and humidity are among the main causes of degradation and destruction of innumerable documents and works of art. Paper hygroscopy induces a strict dependence between the sheet water content and the external humidity: besides inducing the hydrolytic degradation of paper, water causes deformation and physical weakening of the fibers. Moreover, the water absorption over threshold values leads to a microorganism attack. Temperatures higher than 18°C can facilitate the metabolism of microorganisms and insects. Temperature rise normally accelerates all the chemical processes: if the temperature does not overtake 40°C (what normally occurs) it does not affect the chemical nature of the paper support. However, differences in temperature affect the relative humidity (R. H.), i.e. the ratio of the air vapor concentration to the maximum vapor concentration at a specific temperature and pressure value (saturation value). For example, if the indoor temperature is lower than the outdoor, the room R. H. tends to increase, because the temperature gradient between the two environments drives the vapor inwards. In this way, the lower temperature of support surfaces, with respect to the room temperature, can cause water condensation and damage the works of art set on them.

Paper should be stored in environments with a R. H. ranging from 45% to 65%, avoiding sudden temperature and humidity changes, which could affect the cellulose structure. Temperature should be between 16 and 20°C, but, if the temperature is out of this range, temperatures below 16°C rather than above 20°C are better in order to hamper the spread of microorganism infections.

Several pollutants can act as degradation factors of paper materials: among them, nitrogen oxides, sulfur oxides, chloric acid, sulfurous and sulfuric anhydrides. In the presence of water, the most part of the pollutants coverts into acids, with a more harmful action on paper. Also in this case, modern papers are more susceptible to deterioration: chemical-pulp papers can absorb a quantity of pollutants ten times higher than rags or cotton papers, while wood-pulp leaves can absorb a quantity twenty-five times higher. The presence of atmospheric particulate in the air results really harmful for documents and books: the particulate, laying

down on the leaf surface, can cause a serious chemical and biological degradation. The particulate particles are strongly absorbent and, when they fall on the paper surface, tend to concentrate in a narrow space high amounts of pollutants, aqueous vapor, microorganisms and insects.

2.6.3 The use

Consultation, photo reproduction, exposition, document transfer activities involve a series of mechanical stress, environmental changes, light exposition, which, in the long period, can cause a degradation of the work of art.

2.7 Foxing

Foxing is a term describing the age-related brown-reddish, brownish or yellowing spots, of small size with more or less regular outlines. Several stains are fluorescent, if excited with UV radiations. The mechanism of foxing formation has been studied since 1930s but, so far, the real cause of this phenomenon has not been found yet. Indeed, some spots show the presence of bacteria or fungi, others the presence of iron and/or copper. Investigations performed at the Istituto Centrale di Patologia del Libro (ICPL, now ICPAL) on authentic and artificially induced foxing stains revealed that the process is always coupled with a strong oxidation of the cellulose chain, which is characterized by a high number of carbonylic groups, double and triple C-C bonds.

Chapter 3

3. Analysis of degradation by-products in ancient paper: experimental

3.1 Material description

"*De Divina Providentia*" is a medieval printed book, written by Domanino Lattanzio, a Mantuan Carmelite friar, and published by the editor Francesco Osanna in 1592. At the end of the 16th century, paper-making technology in Italy was mature. Renowned paper mills produced good-quality paper sheets with an outstanding uniform basis weight (about 80–100 g m^{-12}), carefully gelatin-sized in order to waterproof the paper and to prevent the spread of ink within. The sources of cellulose were rags, widely available at that time, subjected to a slow process of maceration and beating with wooden hammers. Accordingly, the leaves of "*De Divina Providentia*" are of excellent quality and composed of flax fibers.

The book belongs to the Mantua Biblioteca Comunale Teresiana, but other copies of it are hedged in many Italian libraries. The ink used for the printed book is lamp black.

Aqueous extracts were obtained by washing very degraded (Extract 1), slightly degraded (Extract 2) and not degraded (Extract 3) leaves of "*De Divina Providentia*".

The leaves were washed in bidistilled water at 60 °C during a routinely conservation workshop and then were left to soak until the water temperature decreased to room temperature. This allowed for the extraction of the water-soluble low-molecular-mass fractions formed in the leaves as a result of cellulose and other paper components degradation reactions and induced by natural ageing. The extracts were collected in 50 mL plastic bottles and were divided into three categories according to the level of degradation of the leaves (Table 1, Fig. 11).

Figure 11: Frozen wash waters of the three Extracts (left) and freeze-fried powders of the three Extracts (right).

The extracts were stored in freezer (-20 °C) in aliquots until use. For the analyses, small frozen amounts were melted and then quickly freeze-dried to obtain powders (numbered 1,2,and 3 for the respective extracts). It has been estimated that around 25 mg of powder can be obtained from 1 g of paper for the all three sample solutions.

Table 1. Properties of the Extracts.

Sample	Origin	pH	Color
Extract 1	Very degraded leaves	4.64	very brown
Extract 2	Slightly degraded leaves	5.92	light brown
Extract 3	Not degraded leaves	7.67	yellowish

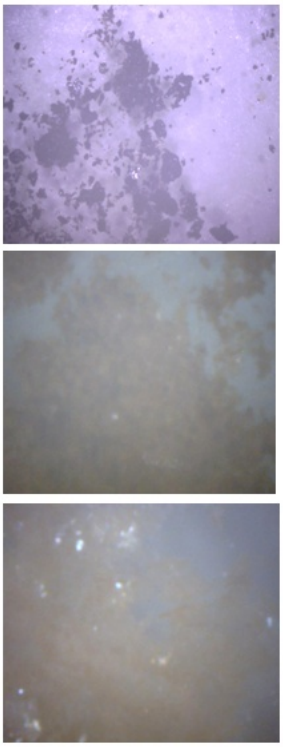

Figure 12: Microscope image of the sample powder.

Extract 1 powder shows a sticky consistency, a very dark color and it is characterized by white microcrystals.

Extract 2 powder shows a sticky consistency and a very dark color as well, without any white microcrystals.

Extract 3 powder shows a bright yellowish color, a sticky consistency and several white microcrystals.

Extract 1 underwent two different treatments aimed at better investigating the natural by-products, dissolved in it.

An aliquot of this sample was acidified by addition of 6MHCl up to pH 1.13 and its powder (called Sample AP) was analyzed by means of UV-Vis and IR spectroscopy.

Another portion was dissolved in methanol and subjected to catalytic hydrogenation (Pd/C catalyst) for 6 h under stirring in order to prevent the sample precipitation, as it is only slightly soluble in methanol. At the end of the reaction, the solution completely lost its original light yellowish color. The residue obtained by evaporation of the solution appeared as a white film (Fig. 13), slightly silver due to the incomplete removal of the catalyst (called Sample HP). Sample HP was characterized by FTIR-ATR and UV-Vis analysis.

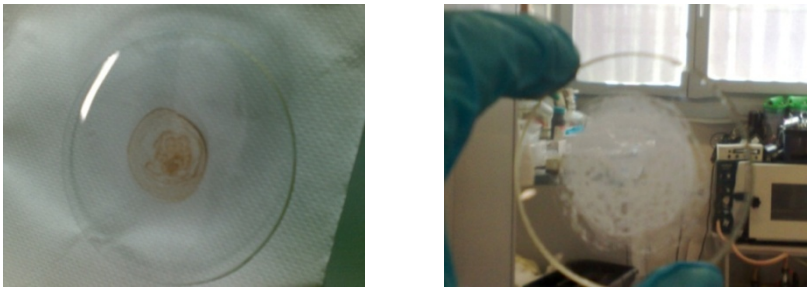

Figure 13: Evaporated Extract 1 before (left) and after (Sample HP, right) the catalytic hydrogenation.

3.2 Chemical and microchemical analysis

3.2.1 CHNS microanalysis

Thermo Scientific Flash 2000 was used for CHNS microanalysis: it was constituted by a primary combustion column at 950°C, where few mg of sample were introduced in a separation column for the combustion gases and a TCD detector. Calculations and analytical procedures were carried out using a specific software tool (Flash 2000 Eager Xperience), which provides for the use of K-Factor as a method of calibration and of BBOT2,5-Bis-(5-tert-butyl-benzoxazol-2-yl)-thiophen as standard.

3.2.2 ESI-ToF spectrometry

Mass spectra (electrospray ionization source, ESI-ToF) of Extract 3 were carried out by operating in positive-ion mode by means of PerSeptive Biosystem Mariner instrument (Framingham, MA). The sample was prepared by dissolving 0.2 mg of Extract 3 powder in 250 µl of a solution 1:1 acetonitrile-water. The mobile phase used was a 1:1 acetonitrile-water solution added with 0.1% formic acid.

The mass spectra were run in two different mass ranges, from 100 to 4000 Da and from 100 to 1000 Da. As most of the peaks fell in the lowest mass range, only the lower mass range was deeply studied.

3.2.3 Solubility tests

The solubility of Extract 1 has been evaluated in solvents of different polarity; it was very soluble in water, slightly soluble in methanol and ethanol and insoluble in diethyl ether.

3.2.4 pH measurements

The pH of three extracts (Table 1) was measured by using a standard pH meter (Inolab, Sigma Precision S.r.l.).

3.3 Spectroscopic analysis

3.3.1 UV-Visible Spectroscopy

The UV-Visible spectrophotometry, together with IR, is an absorption spectroscopy, i.e. it deals with light absorption phenomena in the region of the electromagnetic spectrum belonging to the visible (350-700 nm), near ultraviolet (200-350 nm) and far ultraviolet range (10-200 nm). In the latter case, it operates under vacuum or in inert gas atmosphere, because atmospheric oxygen absorbs at those wavelengths.

The molecule absorption of this type of radiation induces electronic transitions involving the valence electrons.

The most common types of electronic transition are:

1. Transitions involving electrons in charge transfer

The coordination compounds of transition metal ions, such as MnO_4^- and CrO_4^{2-}, and molecular complexes, as I_2 in benzene, exhibit very intense colors because the absorption spectrum in the visible region is associated with electronic charge transfer transitions, inducing large changes of the dipole moment, related to high values of the molar extinction coefficient. Such types of systems are called charge-transfer complexes. In order for a complex to show these features, it is necessary that an electron-donor species is linked to an electron-acceptor one: the radiation absorption induces an electron transfer from a molecular orbital, mainly localized on the donor, to an empty orbital, mainly localized on the acceptor.

2. Transitions involving *d* and *f* electrons

In coordination compounds, the interaction between the metal center and its ligands causes a separation between the five *d* orbitals (or the seven *f* orbitals, in the case of lanthanides), that, in the absence of the ligands, would all have the same energy. The absorptions corresponding to the transitions between *d* (or *f*) orbitals fall often in the visible region, because the separation energy is relatively small. Consequently, the coordination compounds of transition metals with electrons in *d* orbitals or of lanthanides with electrons in *f* orbitals often appear colored. Although this *d-d* transitions are formally forbidden, the coupling

between electron transitions and nuclear vibrations (vibronic coupling) makes these transitions weakly allowed.

3. Transitions involving *π*, *σ* e *n* electrons

As regards the organic molecules, the UV-Vis absorption is the main characteristic of the functional groups called *chromophores* and of the molecules containing such functional groups, which have valence electrons (π, σ e n) at low excitation energy. The spectrum of a molecule, which contains a chromophoric group, is quite complex: the absorption bands are very extended due to the overlap of rotational and vibrational transitions within the single electronic transition. The main electronic transitions, involving the electrons of organic molecules are reported in the following energy diagram:

Electronic transition	Radiation wavelenght necessary for the transition
σ → σ*	110 – 135 nm
π → π* n → σ*	160 – 255 nm
n → π*	> 285 nm

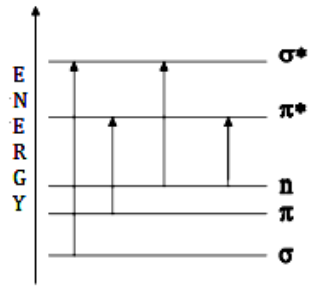

The σ → σ* transitions, typical of hydrocarbons, are transitions involving σ type electrons, i.e. electrons consisting of an electronic cloud thickened along the union axis of the nuclei of the atoms involved in the bond. When the molecule absorbs the incident radiation, electrons are excited from a bonding orbital (σ) to the corresponding anti-bonding orbital (σ*). The required energy to bridge the energy gap between the two orbital is high: the required wavelength of the radiation is between 110-135 nm. This type of transition cannot be detected by normal spectrophotometers and therefore it is necessary to resort to *in vacuum* recording techniques.

The n → σ* transitions are typical of saturated compounds containing heteroatoms such as O, N, S, equipped with "lone pair" (*n* electrons), i.e. not shared electron pairs. These transitions generally require less energy than the σ → σ* ones and they are promoted by radiation between 150-250 nm. Only the halides have an absorption wavelength at 255-260 nm and therefore are visible with conventional spectrophotometers. The organic compounds, that can give rise to these transitions, are: amines, alcohols, thioalcohols, ethers, thioethers.

The π → π* transitions are typical of unsaturated compounds: they involve π electron type, consisting of electron pairs, whose highest electron density is located outside the union axis of the nuclei.

Finally, the n → π*transitions are characteristic of the compounds containing unsaturated chromophores with one heteroatom (e. g. carbonyl or iminic bonds). The absorption bands are not very intense, because such transitions are not allowed by the selection rules, due to the unfavorable geometry of the involved orbitals.

3.3.1.2 Experimental tools and methods

The UV-Vis spectra were acquired on a Cary 5 double beam UV-Vis-NIR spectrophotometer. The measurements were made on dilute solutions of all samples (20 μg of powder in 2 ml of bidistilled H_2O). The UV / Vis spectrum of Extract 1 was acquired in methanol before and after the catalytic hydrogenation.

3.3.2 Infrared spectroscopic analysis

3.3.2.1 Theoretical aspects

Infrared spectroscopy (IR) analyzes the absorption of infrared radiations by the material: IR electromagnetic radiations are characterized by a wavelength between 700 nm and 1000 microns. This radiation has enough energy to cause oscillations and vibrations of the material atoms. For a single non-linear molecule, 3N-6 are the possible vibrational normal modes, which represent collective motions of the atoms with respect to the center of mass. The normal vibrational modes are the correct way to represent molecular vibrations, because they are mutually independent and correspond to the molecular symmetry, but at the same time they are difficult to be detected, and therefore their decomposition into mode types, involving two atoms or two groups of atoms of the molecule, is preferred.

These motions are classified as:

- *Stretching modes*, due to a stretching of the interatomic bond along the axis, resulting in an increase and decrease in the interatomic distance;
- *Bending modes*, due to a variation of the angle between two consecutive bonds or, more generally, to a movement of a group of atoms compared to the rest of the molecule that does not change the bond length.

The motions of bending are divided in turn into:

- *in-plane* vibration modes (scissoring and rocking);

- *out-of-plane* vibration modes (wagging and twisting).

The IR radiation is absorbed by the molecule if at least one vibrational mode induces a change in the electric dipole moment of the molecule. In this case, this vibrational mode is called *IR active*.

Many important molecular functional groups have the IR absorption at well-defined frequencies, slightly influenced by the rest of the molecule. This peculiarity allows the analyst to recognize such groups, even without a full identification of the analyzed substance. Indeed, the IR spectrum may indicate the presence of double or triple bonds, carbonyl and carboxyl groups and then allow one to understand and predict the behavior of the molecule under particular experimental conditions.

Infrared spectroscopy is therefore a valuable diagnostic and analytical method in the field of Cultural Heritage: taking advantage of the information collected by the IR spectrum, it is possible to assess the conservation state of a document or in general a work of art and to study the processes that may have caused its degradation and ruin.

This technique also makes possible the collection of information relating to the individual constituents of the work of art: specific signals in the paper IR spectrum, for example, allow for the identification of matrix cellulosic material, the type of ink, the presence of size and/or additives in the artifact.

3.3.2.2 Experimental tools and methods.

The IR spectra of the samples were recorded by means of the instrument Bruker Equinox 55 FT-IR, equipped with a diamond ATR module and MCT detector. The analysis in Attenuated Total Reflectance is based on the propagation of a IR radiation through a material (Internal Reflection Element or IRE) with a high refractive index (n_e) and on its total reflection at the interface between this IRE material and the medium placed over it, in this case the sample itself (n_{sample}). Two requirements are necessary to get a total internal reflection:

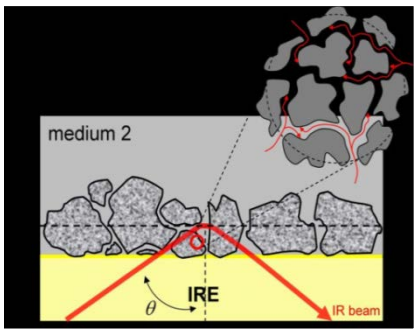

- the incidence angle of the IR radiation must be greater than the critical angle of the IRE material;

- n_e must be greater than n_{sample}.

When these conditions are satisfied, the wave emitted by the source passes through the IRE and arrives at the interface, where it undergoes an internal reflection. Due to the wave nature of radiation, at the interface between IRE and sample the radiation is not confined within the IRE, but penetrates into the sample by a thickness comparable to its wavelength and dependent on the n_e/n_{sample} ratio: this effect is named *evanescent wave*. The evanescent wave is partly absorbed by the sample so that the totally reflected beam is attenuated at frequencies corresponding to the IR absorption of the sample. The reflected beam is then sent to the detector for recording the IR spectrum. This mode of analysis is very useful as it allows the spectrum to be recorded directly on the sample by simply placing it on the material (IRE diamond, in our case) of the module ATR, avoiding the preparation of tablets with KBr and the consequent loss the sample.

3.3.2.3 IR data processing

A deconvolution method was applied to the band at 1630 cm^{-1} observed in the IR spectra of Extract 1, Sample AP and HP, as this band is highly diagnostic for degradation. To this purpose, the three spectra were baseline corrected and normalized with respect to the highest band in the fingerprint region (1023 cm^{-1}) attributed to the cellulose C-O primary alcohol stretching modes.

The method is based on the assumption that the IR spectrum can be represented as a sum of Gaussian and Lorentzian functions. Each of these functions is defined by three parameters: *height*, *width* and *average value*. In the experimental IR spectrum, the overlap of signals in a very narrow frequency region can lead to the formation of a single broad band, where the partially solved signals emerge as shoulders, local minima or maxima. A partially resolved band can still be mathematically decomposed into a sum of individual signals. Obviously, the number of deconvolution peaks is completely indeterminate, because a signal can be considered as the sum of an arbitrary number of Gaussian or Lorentzian peaks with values of height, average and width selected to minimize the variance between the sum and the experimental curve.

However, the imposition of specific limits on the used parameters, defined by the knowledge of the involved chemistry and by the comparison of different samples, allows for a good identification of the functional groups that give rise to the final spectrum.

The deconvolution of the FTIR spectra was performed on the normalized IR spectra as a sum of twelve Lorentzian curves, according to a well-defined procedure.[14-17] The calculated parameters were the peak height (in absorbance units), the peak area (in absorbance units * cm^{-1}), the full width at half height and the center of the peak (both in cm^{-1} units). The data processing algorithms were carried out by using the OriginLab software version 8.1, which allowed for a deconvolution by a non-linear curve fitting method. In order to avoid the finite size effects due to the strong absorbance below 1550 cm^{-1}, calculations were performed between 1250 and 1850 cm^{-1}. The width at half height of the deconvoluted bands was always set initially to a wavenumber values below 80 cm^{-1}. However, in some instances broader deconvoluted bands have been accepted and interpreted from a chemical standpoint. In order to evaluate the number and the rough initial position of the bands, the spectra of all the samples were overlapped and their common features (e.g., shoulders or small peaks) were considered for the initial frequency guesses (Fig. 14). It should be underlined that the utilized deconvolution procedure is well defined for high-molecular-weight cellulosic compounds, with evident shoulders due to relatively small and partly overlapped peaks, whereas our samples show strong and broad bands that may limit the reliability of the deconvolution algorithm.

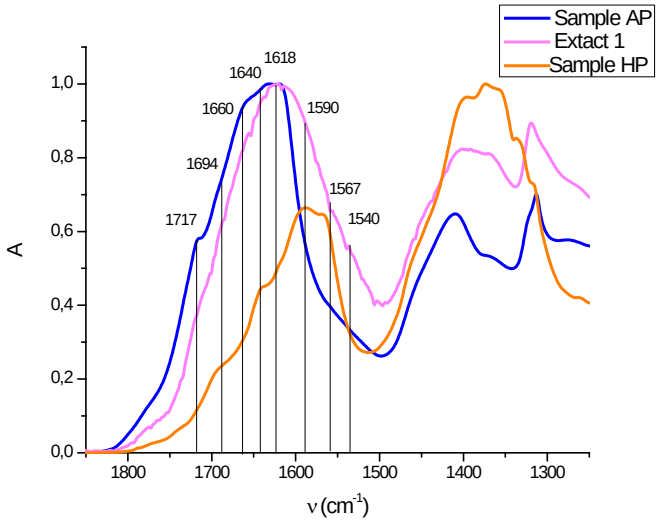

Figure 14: Extract 1 (pink), Sample AP (blue) and Sample HP (orange) IR spectra.

3.3.4 EPR spectroscopy

3.3.4.1 Theoretical aspects

EPR (Electron Paramagnetic Resonance), also called ESR (Electron Spin Resonance), is a spectroscopic technique suitable for the study of paramagnetic centers like organic radicals, compounds of transition metal ions, solids with electronic localized defects, systems with triplet state, biradicals and systems with conduction electrons. The EPR experiment consists in the irradiation of a sample, immersed in a magnetic field, with a radiation at an appropriate frequency. The paramagnetic centers, present in the sample, are characterized by spin states that, in the presence of the magnetic field, separate in energy levels. The separation between levels is directly proportional to the magnitude of the magnetic field. In the experiment, the frequency of the radiation is kept fixed, while the magnetic field slowly varies. When the energy separation between the levels is equal to the radiation energy, the absorption of the radiation takes place (*resonance condition*). The spectrum resulting from the EPR experiment is therefore an absorption curve, whose maximum falls at the field value, at which the resonance condition is reached. Since the EPR lines are basically wide and with a low signal-noise ratio, the technique resorts to the modulation of the applied magnetic field: through the use of a small alternating magnetic field at a fixed frequency at about 100 KHz, the resonant signal is made oscillate with the same phase and frequency. A phase sensitive band-pass filter (lock-in) extracts the signal components that oscillate with the same frequency and phase of the modulation field, eliminating a large part of the noise (which has instead random phase and frequency). The method, which significantly increases the signal-to-noise ratio, involves the registration of an EPR signal as the first derivative of the absorption signal. The EPR spectrum in absorption could be recovered through digital integration of the experimental EPR spectrum, but routinely the EPR spectrum is kept in its first derivative form, as the spectral resolution is better. The spectrum of a paramagnetic species is characterized by parameters useful for the identification of the species. The main parameter is the *g tensor*: the g tensor is a parameter, which depends upon the molecular surrounding of the electron and which can be considered as the analogue of the *shielding constant* in NMR. If the paramagnetic species is subject to a fast reorientation motion (e. g. in solution), the g tensor is mediated to a scalar, the *g-factor*, which determines the position of the signal in the spectrum (as much as the chemical shift in NMR). For a free electron, the g-factor has a value of 2.0023. For an EPR line, the larger is the *g*-factor, the lower is the

resonance field. Another important parameter is the *hyperfine A tensor*. If the interaction of the electron with the magnetic field caused only the separation of the energy levels, all the EPR spectra would consist of a single line, and the only information would derive from the *g* value. The hyperfine interaction arises from the interaction between the spin magnetic moment of the electron and the spin magnetic moment of the adjacent nucleus (^{1}H, ^{13}C, ^{14}N). This interaction is described, for each nucleus, from the corresponding *hyperfine coupling A tensor*. If the paramagnetic species is subjected to a fast reorientation motion (e. g. in solution), *A* is mediated to a scalar, the hyperfine constant. The hyperfine interaction causes the splitting of the single-line spectrum of the electron in (2 *I* + 1) lines, with *I* the momentum quantum number of the spin of the nucleus. Lines are separated by the *A* constant (similar to the *J* constant in NMR).

3.3.4.2 Experimental tools and methods

The continuous-wave EPR spectra have been acquired on a Bruker ER200 instrument, equipped with a TE102 probehead. Microwave frequency was about 9.5 GHz, modulation amplitude 0.2 mT and microwave power 2 mW.

3.3.5 Raman spectroscopic analysis

3.3.5.1 Theoretical aspects

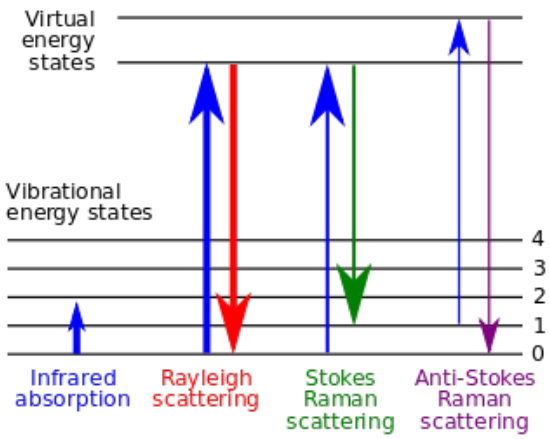

Figure 15: Energetic chart showing the excitation-relaxation phenomenon responsible of the Raman Rayleigh, Stokes e anti-Stokes scattering.

The basic principle of Raman technique is the diffusion of a monochromatic radiation impinging on the sample: the photons interact with the polarizable electron density and the bonds of the molecule in the phase and environment where the molecule is located.

The photon can be backscattered in two ways:

- if the diffusion occurs by elastic interaction, i.e. without a net energy transfer, the photons composing the scattered radiation have the same energy as the incident ones: this phenomenon is known as *Rayleigh scattering* and it represents the most likely event;

- if the diffusion is a consequence of an inelastic interaction, with an energy transfer from the photon to a particle or vice versa, the scattered photons have an energy respectively greater or lower than the incident one: this phenomenon is named *Raman scattering* and is quite unlikely.

Both in elastic and inelastic interactions, if the incident photon has a hv_0 energy, the molecules is expected to be excited to a virtual energy quantum state hv_0 above the ground state, then decaying by emitting photons, as illustrated in Fig. 15.

In the case of inelastic interactions, the molecule decays from the virtual state to an excited hv_1 vibrorotational state emitting a photon with a hv_0-hv_1 energy, smaller than the incident photon one, or, if the molecule is already in an excited state hv_1, it can decay from the virtual state to the ground state by emitting a photon with energy equal to hv_0+hv_1, larger than the photon incident one.

The Raman spectrum of a molecule irradiated by a monochromatic light is then characterized by three types of signal:

- *Rayleigh radiation*, the most intense of the spectrum, having the same wavelength as the incident radiation;
- signals corresponding to the inelastic interactions, in which photons are emitted at an lower energy than the incident radiation, called *Stokes lines*;
- signals corresponding to the inelastic interactions, in which photons are emitted with a higher energy than the incident one (hv_0+hv_1), called *Anti-Stokes lines*.

At room temperature, the fundamental vibrational level is more populated, the Stokes lines are therefore more intense than the anti-Stokes ones.

The almost entire information of a Raman spectrum of a molecule derives from the Stokes lines. The Rayleigh radiation does not provide any information because it has the same energy in each sample, while the intensity of the anti-Stokes lines is too low to be detected.

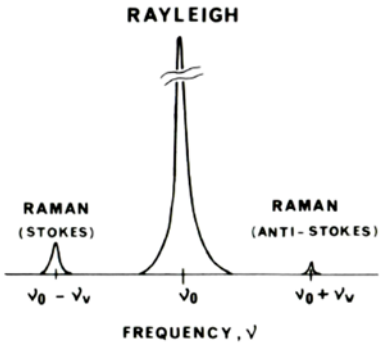

Since molecular vibrorotational excited states are involved in the formation of the Stokes lines, the Raman shift, given by the difference between the frequency of the incident radiation and the frequency of the Stokes line, provides the vibrorotational frequency of a molecular mode. The Raman spectrum, therefore, is related to the vibrational modes of the molecule, like the IR spectrum, and therefore it can be used in a similar way for the identification of molecular functional groups.

The Raman signals corresponding to the various groups approximately fall in the same spectral range as in an IR spectrum, except for small differences due to *selection rules*, different for the two spectroscopies.

Indeed, in the IR spectroscopy, the energy absorption from the radiation is due to molecular dipole moment variation, while in the inelastic light scattering in the Raman technique it is induced by molecular polarizability variation. As a consequence, some vibrational modes may be active in IR and not in Raman, or vice versa.

In the field of Cultural Heritage, there are several advantages deriving from the application of the Raman technique:

1) The Raman instrument can be very compact, allowing for *in situ* investigations, that represents a very important aspect in this field;

2) It prevents the direct contact between the sample surface and the probe, that is necessary in ATR-IR technique;

3) Water and glass do not cause interference in the Raman spectrum;

4) The use of the VIS-NIR light allows one to browse only the surface (just a little interference of the substrate);

5) The Raman peaks are usually narrower than the corresponding IR peaks and therefore easily attributable;

6) The spectral range is wider, allowing one to study particularly the low-frequency IR region (between 200 and 600 cm^{-1}), useful for the identification of mineral pigments;

7) It is usually combined with a microscope, which allows for the selection of few square micrometer areas.

One of the Raman limits deals with the fluorescence emitted by some samples, once excited, which easily covers the Raman spectrum. This problem is typical of degraded papers, in an advanced oxidative state: their Raman spectra exhibit a strong baseline distortion due to the strong fluorescence emitted by electronic polyconjugated compounds, formed by the

degradation reactions. In literature, multiple approaches have been adopted in order to eliminate the fluorescence influence and in this way to record the Raman spectrum of ancient papers. One of the most common procedure implies the sample irradiation with near infrared (NIR) laser at 785-1064 nm, which provides a higher definition and a lower fluorescence in the region between 1100 to 2500 cm^{-1}.[18, 19]

The use of NIR lasers reduces the fluorescence phenomena, because their application reduces the probability of spontaneous emission (which declines with the cube of the emitted photon frequency), resulting much lower for the electronic transitions in the NIR than in the visible region. An effective method to increase the Raman signals above the background fluorescence is SERS (Surface Enhanced Raman Scattering). SERS allows one to obtain an increase in the Raman effect, thus minimizing the fluorescence interference and therefore allowing for the recording of the Raman spectra of strongly fluorescent materials (usually organic materials).[20]

This technique takes advantage of the surface amplification of the Raman scattering by molecules adsorbed on a metal wrinkled surface.

There are two theories, one related to each other, trying to explain the exact mechanism of the SERS amplifying effect.

The former is named "*the electromagnetic theory"*: this theory is based on the formation of surface plasmons (electromagnetic waves that propagate along the surface parallel to the metal/dielectric interface), which form when the incident light excites the electron clouds of the metal surface. When the adsorbed molecule is located in proximity to the plasmon, it experiences an electromagnetic field and produces an amplified Raman diffusion.

The field induced amplification gets higher when the plasmon frequency is in resonance with the radiation. Moreover, in order for the adsorbed molecules to cause a light scattering, the plasmon oscillations must be perpendicular to the surface. Metal rough surfaces or nanoparticles arrangements are commonly used in the SERS technique, since this type of surfaces provides the suitable area for the plasmons generation, necessary to achieve the signal amplification. The choice of the metal surface or the type of the metal nanoparticles depends on the resonance frequency of the respective plasmon: silver and gold are the typical metals used in the SERS experiments, since the resonance frequency of their plasmons falls in the visible and NIR region, allowing for the maximum amplification of the radiation with wavelengths in this range.[21, 22]

The second theory, not supported by scientific data, is the *chemical theory*, according to which there would be a charge transfer between the chemisorbed species and the metal surface at the base of the amplification effect.[23, 24]

3.3.5.2 Experimental tools and methods

A Renishaw in Via Raman microscope was used to perform measurements on all the sample powders. This system is equipped with a laser source at λ=633 nm and an optical microscope. The Raman measurements of the samples were carried out with a 5x objective, 100% laser power (15 mW), five accumulations and 15 s scan time on a considered area of hundreds of square micrometers. All the spectra showed a strong fluorescence band, which completely covered the Raman signals. As it was not possible to set the laser excitation source to a lower frequency to avoid the fluorescence, we used instead the SERS technique, based on the interaction of the materials to be analyzed with gold nanoparticles.

These latter were produced by LASiS, a laser ablation of bulk gold under water with 9 ns pulses at λ=1064 nm. This technique gives nanoparticles of about 20 nm of diameter and with a free surface, not covered by stabilizing molecules, because the particles have been already charged when they were produced.[25] This property allows a good interaction of the nanoparticles with the substrate, a condition essential to observe the SERS effect. For the purpose of the present analysis, 40 ml of the gold nanoparticle solution (3 nm) were mixed with 10 ml of sample and the obtained mixtures were left to evaporate on a slide. The obtained "stains" showed a large amount of powder at the edges, decreasing inward. The spectra were acquired directly on various parts of the stain by using a 50x objective, 5% laser power (0.75 mW), five accumulations and 30 s scan time on a considered area of few micrometers square. All spectra were normalized with reference to the maximum.

3.3.6 NMR spectroscopic analysis

3.3.6.1 Theoretical aspects

The nuclear magnetic resonance spectroscopy (NMR) measures the absorption of radiofrequencies by molecules immersed in a strong magnetic field. This absorption only occurs in presence of nuclei with a nuclear spin, i. e. an intrinsic angular momentum. The spin of each particle depends on the quantum number *I*, specific for the type of particle. A nucleus with a non-zero *I* has an angular momentum *J*, to which a magnetic dipole moment μ

is associated; μ is proportional to J through a constant, the gyromagnetic ratio γ, characteristic for each nucleus:

$$\boldsymbol{\mu = \gamma * J}$$

In the presence of a magnetic field B_0, J, and therefore also μ, can assume only specific orientations: in particular, the projection of J along an axis can assume only certain values, defined by the quantum number m, ranging between $-I$ and $+I$, with increments of one unit. Therefore, m can assume $2I+1$ different values.

The nuclear magnetic moment can be meant as a small magnet, whose direction changes according to the main magnetic field. The field exerts a torque on the magnetic moment, forcing the magnetic dipole to perform a precession motion around the field axis with an angular velocity $\omega_0 = -\gamma B_0$. The rotation frequency, at the same magnetic field, is therefore characteristic of each nucleus, and it is called the *Larmor frequency*. The energy associated with this motion is given by the following equation:

$$\boldsymbol{E = -\mu B_0 = -\gamma \hbar m B_0}$$

For a proton, such as for every nucleus with spin $I = ½$, two are the possible energy states, characterized by a different energy: the state with $m = + ½$, called *α state*, where the magnetic moment component along the field and the field have the same direction, and the *β state*, with $m = - ½$, where the magnetic moment component is opposed to the field; the *α* state has a lower energy than the *β* state. In a macroscopic system containing N spins, the populations of the two energy levels are different and defined by the Boltzmann distribution. The resultant of the magnetic moment vectors (microscopic) of the different nuclei, constituting the sample, is the macroscopic *magnetization* M_0. In thermal equilibrium, M_0 is aligned with the magnetic field (conventionally indicated as z axis), because the α state is more populated than the β state. However, since the energy difference is quite small, the nuclei population in the two states is virtually identical with a very small prevalence for the state at low energy: at room temperature, the excess population is of an order of magnitude of 100 ppm. This little population difference is responsible for the low NMR sensitivity.

The energy difference between the two α and β states is $\boldsymbol{\Delta E = \gamma \hbar B_0}$. It is therefore possible to induce the transitions between the two energy levels using photons of energy $\boldsymbol{\hbar \gamma B_0}$, i.e. radiation at the Larmor frequency $\boldsymbol{\omega_0 = \gamma B_0}$.

In the experiment, the radiation magnetic field B_1 oscillates along an axis perpendicular to z (e.g. along the x axis) and causes a rotation of M_0 around B_1, that lasts as long as the

radiation is applied. At the end of the pulse, M_0 is no longer aligned with the static magnetic field B_0, which therefore exerts on M_0 a torque. The magnetization, under the action of this torque, starts to rotate in the *x*,*y* plane at the Larmor frequency and its projections (components) along the *x* axis (M_{0x})and along the *y* axis (M_{0y}) get oscillatory.

In a solenoid displaced, e.g., along the x axis, oscillating M_{0x} induces an alternating voltage in the solenoid, detectable as a signal of sinusoidal form. The acquired NMR signal in the time domain is called FID (free induction decay). In order to convert this time-domain signal into a frequency-domain signal, which is the NMR spectrum, a mathematical function, the *Fourier transformation*, has to be applied to the FID. The NMR spectrum can provide information about the structure of chemical species in the analyzed sample.

The first factor considered in the NMR spectrum is the *chemical shift* (δ), i. e. the exact position of the resonance of each nucleus that is strongly affected by the surrounding chemical environment. Nuclei in different chemical environments proceed at different frequencies as they are affected by the action of local fields, higher or lower than the applied B_0, generated by the orbital motion of electrons around the nuclei. In this way, each nucleus is shielded by an electron cloud, whose density depends on the surrounding atoms. The effective field has intensity equal to:

$$\mathbf{B_{eff} = B_0 (1-\sigma)}$$

where σ is the screen constant.

The value of effective resonance frequency is then:

$$\mathbf{\nu_{eff} = (\gamma/2\pi)\, B_0 (1-\sigma)}$$

The chemical shift *δ (ppm)* measures the effect of the screen, by quantifying the shift of the resonance frequency with respect to a reference compound frequency:

$$\mathbf{\delta = [(\nu_0-\nu_{rif}) / \nu_{rif}] * 10^6}$$

A second, very informative parameter is the integral (area) of a NMR signal, which is proportional to the number of protons giving rise to that signal.

The *coupling factor J* (or spin-spin coupling constant) is a measure of the interaction between magnetic moments of nearby nuclei. Most of this interaction is not through space but occurs via bonding electrons. The interaction of a nucleus with another of spin *I* induces the splitting of the resonance line due to the former nucleus in *2I + 1* lines, separated of the *J* coupling constant (measured in Hz).

NMR spectroscopy has emerged in recent years as the most powerful and fastest technique for the identification of reaction products or unknown organic compounds, starting from the resonance frequency of the active nuclei. The most common NMR active nuclei are ^{1}H, ^{13}C and ^{15}N.

3.3.6.2 Experimental tools, methods. Literature references

The ^{1}H NMR spectra and the ^{1}H-detected heteronuclear multiple quantum coherence (HMQC) spectra were obtained on a Bruker Advance DMX-600 spectrometer, equipped with a three-axis gradient TXI probehead (measurement parameters in Table 2). The spectra were obtained at room temperature on solutions of the three samples in D_2O.

Mono-dimensional spectra of multi-component samples show a spectrum characterized by several crowded overlapping signals, preventing their attribution to specific functional groups.

In two-dimensional NMR spectra (or 2D), the resonances are dispersed on a plane rather than on a line and the resultant signals are a function of two frequencies, drastically reducing the overlap probability between two resonances. The 2D technique takes advantage of pulse sequences, which allows one to perform different types of experiments in order to get information about the correlation between the homo- or hetero-nuclei, interacting by scalar coupling (COSY, TOCSY, HSQC, HMQC, HMBC) or by dipolar coupling (NOESY and ROESY).

Since the results of the multiple analyses indicated that the samples are mainly composed by oxidized and/or partially dehydrated oligomers, HMQC turns out to be the most suitable technique for investigating them. This NMR technique is particularly suited for the determination of directly linked ^{1}H-^{13}C pairs. The two-dimensional spectrum is characterized by an X-axis, the proton chemical shifts (0 - 12 ppm), and a Y-axis, the ^{13}C chemical shifts directly bound to the protons (0 - 240 ppm). Each peak corresponds to a particular ^{1}H-^{13}C couple in a particular chemical environment.

The parameters set to obtain the highest possible resolution of the spectrum are:

Table 2: HMQC set-up parameters

Experiment number	150
Scansion number	900
Acquisition spectral window	10 ppm
Evolution spectral window	240 ppm

The HMQC experiment does not provide information about coupling constants of not directly linked ^{1}H-^{13}C, necessary to investigate the presence of carboxylic and carbonyl groups in the cellulose chains of the sample. The HMBC experiment, meant to detect coupling constants of not directly linked ^{1}H-^{13}C, however, is less sensitive than the HMQC and requires highly concentrated sample, conditions that cannot be satisfied in the case of our samples.

3.3.7 ICP-MS analysis

3.3.7.1 Theoretical aspects

Inductively Coupled Plasma Mass Spectrometry or ICP-MS is an analytical technique used for elemental determinations. An ICP-MS combines a high-temperature ICP (Inductively Coupled Plasma) source with a mass spectrometer. The ICP source converts the atoms in the sample to ions. These ions are then separated and detected by the mass spectrometer.

With respect to other elemental analysis techniques such as atomic absorption and optical emission spectrometry, including ICP Atomic Emission Spectroscopy (ICP-AES), ICP-MS has many advantages, including:

- Detection limits for most elements equal to or better than those obtained by Graphite Furnace Atomic Absorption Spectroscopy (GFAAS);
- Higher throughput than GFAAS;
- The ability to handle both simple and complex matrices with a minimum of matrix interferences due to the high-temperature of the ICP source;
- Superior detection capability to ICP-AES with the same sample throughput;
- The ability to obtain isotopic information.

In the ICP source, argon gas flows inside the concentric channels of the ICP torch. The RF load coil is connected to a radio-frequency (RF) generator. As power is supplied to the load

coil from the generator, oscillating electric and magnetic fields are established at the end of the torch. When a spark is applied to the argon flowing through the ICP torch, electrons are stripped off of the argon atoms, forming argon ions. These ions are caught in the oscillating fields and collide with other argon atoms, forming an *argon discharge* or *plasma*. The argon discharge has a temperature of around 6000-10000 K and therefore it is an excellent ion source. The sample is typically introduced into the ICP plasma as an aerosol, either by aspirating a liquid or dissolved solid sample into a nebulizer or using a laser to convert directly solid samples into an aerosol. Once the sample aerosol is introduced into the ICP torch, it is completely desolvated and the elements in the aerosol are converted first into gaseous atoms and then ionized towards the end of the plasma. Once the elements in the sample are converted into ions, they are then brought into the mass spectrometer. The interface region in the ICP-MS transmits the ions traveling in the argon sample stream at atmospheric pressure (1-2 torr) into the low pressure region of the mass spectrometer (<1 x 10^{-5} torr). Once the ions enter the mass spectrometer, they are separated by their mass-to-charge ratio. The most commonly used type of mass spectrometer is the quadrupole mass filter. The ions formed by the ICP discharge are typically positive ions, M^{+} or M^{+2}, therefore, elements that prefer to form negative ions, such as Cl, I, F, etc., are very difficult to be detected by ICP-MS. The detection capabilities of the technique can vary with the technique of sample introduction used, as different techniques will allow different amounts of sample to reach the ICP plasma.

ICP-MS has some limitations as to the amount of total dissolved solids in the samples.

Detection capability will vary with the sample matrix, which may affect the degree of ionization occurring in the plasma or allow the formation of species that may interfere with the analyte determination.

3.3.7.2 Experimental tools and methods

ICP analyses were performed on an ICP-MS Agilent 7700, equipped with a fragmentation chamber in a helium stream and a signal correction system based on the use of internal standards. Before the analysis, the three Extracts underwent a specific matrix digestion protocol. 0.5 ml of sample were added to 3 ml of 65% HNO_3 and the solution was heated for two hours at 200 °C. At the end of the treatment, the digested solution was limpid and

transparent and its volume was around 2 ml. Once cooled down, the solution was diluted with MilliQ water in a 100 ml volumetric flask.

3.3.8 XRF analysis

3.3.8.1 Theoretical aspects

X-ray fluorescence (XRF) is the emission of characteristic "secondary" (or fluorescent) X-rays from a material that has been excited by bombarding with high-energy X-rays. The phenomenon is widely used for elemental analysis and chemical analysis, particularly in the investigation of metals, glass, ceramics and building materials, and for research in geochemistry, forensic science and archaeology.[26] It is in principle applicable to all elements except the first two (H and He) of the periodic system, thereby covering an energy region from about 50 eV to 100 keV. However, many light elements are difficult to measure and require advanced instrumentation, which often limits practical work to atomic numbers above 13 (Al).

An electron can be ejected from its atomic orbital by the absorption of a photon of sufficient energy. The energy of the photon (hv) must be larger than the binding energy of the electron in the atom. When an inner orbital electron is ejected from an atom, an electron from a higher energy orbital will “fall” to the inner orbital, filling the hole left behind. During this transition a photon is emitted from the atom (atomic fluorescence). The energy of the emitted photon will be equal to the difference in energies between the two involved orbitals. As the energy difference between two specific inner orbital shells, in a given element, is always the same (i.e. characteristic of a particular element), the emitted photon will always have the same energy. Therefore, by determining the energy (wavelength) of the X-ray light (photon) emitted by a particular element, it is possible to determine the identity of that element.

Neither the frequency nor the intensities of the fluorescence lines is noticeably affected by the chemical state of the analyzed atoms (except for very long wavelengths and very light elements) so that no destructive dissolution and/or atomization by a flame, arc, spark or plasma is required, as it is generally the case in optical emission (and absorption) methods. Homogenization may become an issue as many objects of art and archaeology are rather inhomogeneous by nature, and a question may arise of the extent, to which the results from a limited analyzed volume represents the whole artifact.

The method is ideally suited to analyze, for example, cross-sections of paints or element distributions at surfaces.

3.3.7.2 Experimental tools and methods

The powder of the three Extracts underwent XRF measurements, carried out on a XRF system constituted by an X-rays tube with Mb anode (operated at 20 kV and 1.2 mA in helium stream). The measurement time was set at 300 s.

3.4 Chromatographic analysis

High Performance Liquid Chromatography (HPLC) is used for the analysis of non-volatile or thermally stable compounds. It is one of the most widely used instrumentation for the analysis of pharmaceutical products, isolation of natural products, petrochemical industry, and compounds of environmental interest, among others.

3.4.1.1 Theoretical and instrumental aspects

The instrument is normally equipped with a diode array detector (DAD),which can measure simultaneously wavelengths in the UV-Visible range, thus providing more information than traditional fixed wavelength detectors. In order to be suitable for the analysis, the sample must absorb radiation in the UV-Vis range (usually organic compounds must contain double bonds).The system can also be operated with a Mass Spectrometric (MS) detector, suitable for identification and quantification experiments. The ElectroSpray Ionization (ESI-MS) is the common used MS detector, as it accomplishes ionization from solution and is carried out at atmospheric pressure, therefore the column effluent can be directly interfaced to the ion trap mass spectrometer. The column effluent is passed through a metal capillary held at a high voltage in order to separate charged analyte molecules from their counter ions.[27] The mass spectra obtained with positive ion ESI-MS consist primarily of the protonated molecular ions (MH^+) of constituents of the solution. Salt clusters can also be detected in the negative ion mode. ESI is a soft ionization technique, causing little fragmentation, so that identification of the molecular ion is usually possible. This helps one to determine the mass of the various analytes, a key element in the process toward their identification. Further structural information on the single analytes can be achieved by tandem mass spectrometry (MS-MS) analysis. A MS-MS spectrum is obtained by selecting and fragmenting the molecular

ion of interest. The resulting scan gives a mass spectrum of the product ions resulting from the decomposition of the molecular ion.

3.4.1.2 Experimental tools and methods

LC/quadrupole-time-offlight (LC/QTOF)-MS analysis was performed with an UHPLC system (Agilent Series 1200; Agilent Technologies, Palo Alto, CA, USA), consisting of a vacuum degasser, an auto-sampler, a binary pump and a column oven coupled to both a diode array detector (DAD) and a QTOF mass analyzer (Agilent Series 6520; Agilent Technologies). The UV detection wavelengths were recorded over the λ=190–800 nm range and for the analysis of Extract 1 specific values were chosen according to its UV absorption features: λ=250 and 350 nm.

The analytical column was an Alltima HyPurity 3.0 mm C-18 (150 mm x 2.1 mm i.d., Grace, IL, USA) coupled to a 5 mm C-18, 7.5 x 2.1 mm i.d. guard cartridge, thermostated at 30°C. The injected sample volume was 5 µl. The mobile phase components A and B were acetonitrile and water, respectively, both added with 5 mm ammonium acetate. The eluent flow rate was 0.2 mL min^{-1}. The mobile phase gradient profile was as follows (*t*in min): t_0 A=0%, t_{20} A=100%, t_{24} A=100%, t_{25} A=0%, t_{34} A=0%. The QTOF system was equipped with an electrospray ionization interface (ESI), operating both in negative and positive acquisition, with the following operation parameters: capillary voltage = 3500 V, nebulose pressure = 35 psi, drying gas = 8 L min^{-1}, gas temperature = 350°C, fragmentor voltage = 100 V, skimmer = 65 V. Full scan mass spectra were recorded as centroid over the range m/z=50–3000 with a scan rate of two spectra per second. Mass spectra acquisition and data analysis were processed with Masshunter Workstation B 04.00 software (Agilent Technologies). Aqueous standard solutions of glucose, xylose and glucuronic acid at a concentration of 10^{-5} M were injected into the LC-MS system under the same experimental conditions.

3.4.2 CE analysis

The capillary electrophoresis (CE) is one of the analytical techniques that meets the conditions normally required for the performance of chemical analyses on ancient papers or in general on ancient and high-value works of art. Indeed, CE is a micro-destructive tool and it requires just a minute amount of sample (1-10 nl) allowing for a miniaturisation of the sample size (microscale applications) which is a considerable advantage in Cultural Heritage

applications, where the available sample amount is an issue. Easy sample handling, short analysis time (few minutes), very small reagent consumption and the possibility of quantitative analysis are the other major advantages of CE.

In the last year, a collaboration with the *CRCC* (Centre de Recherche sur la Conservation des Collections) at the *Muséum National d'Histoire Naturelle* of Paris was started. At this research center, CE-UV has been applied in order to investigate and recognize the individual paper degradation by-products in the extraction solutions obtained from the leaves of the 16th century book, "*De Divina Providentia*", which were previously deeply and broadly analyzed by means of spectroscopic analyses. The obtained results, combined with the spectroscopic data collected in last two years, provided useful information for a more complete characterization of these compounds.

3.4.2.1 Theoretical and instrumental aspects

Electrophoresis is a process for separating charged molecules based on their movement through a liquid under the influence of an applied electric field. If the solutes have different electrophoretic mobilities, the separation will usually occur.

The electrophoretic mobility is dependent upon the charge *q* of the molecule, the viscosity $\boldsymbol{\eta}$, and the hydrodynamic radius *r*, according to the equation

$$\mu_{EP} = q / f = q / (6\pi\eta r)$$

where *f* is the frictional coefficient.

The velocity at which the particle moves is directly proportional to the applied electric field through its mobility:

$$v = \mu_{EP} * E$$

the greater the field strength is, the faster the motion is. Of course, neutral species are not affected, only ions move under the electric field. According to the above equations, ionic species are separated depending on their hydrodynamic radius and charge.

Electrophoresis, where the ionic species flow through a submillimeter capillary, is the Capillary Electrophoresis, used predominantly because it gives quick results and provides high resolution separation.

A typical CE system consists of a high-voltage power supply, a sample introduction system, a capillary tube, a detector and an output device. The capillary is made of fused silica and is sometimes coated.

The positive and negative poles of the power supply are connected to electrodes, respectively anode and cathode. The anode and one side of the capillary tube are dipped in a vial containing an electrolytic solution or a buffer, the cathode and the other side of the tube dipped in another similar vial. The background electrolyte (BGE), the carrier electrolyte or simply the run buffer maintains the requisite pH and provides sufficient conductivity to allow for the passage of current, necessary for the separation. Additional materials are added to the BGE to adjust the resolution of the separation through the generation of a secondary equilibrium or to allow for a better detection sensitivity. Moreover, the BGE can maintain the solubility and prevent the interaction of the solutes with the capillary wall.

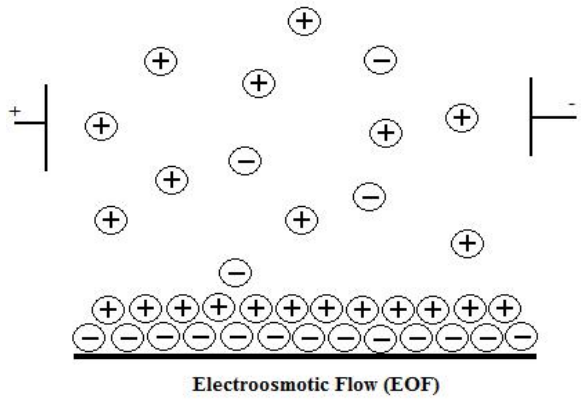

Figure 16: Electroosmotic Flow due to Applied Voltage.

Application of a high voltage to the electrodes results in an electric field in the solutions, generating an electroosmotic flow (EOF) through the tube. The EOF occurs when the buffer running through the silica capillary has a pH greater than 3 and the SiOH groups lose a proton to become SiO^- ions. The capillary wall then has a negative charge and, attracting cations, develops an electrical double layer near the wall (Fig. 16). This double layer is dense and stationary near the wall, becoming less dense and free to move toward the center of the capillary. Due to the negatively charged capillary walls, an excess of cations is present in the tube center: the applied electric field causes the free cations to move toward the cathode creating the EOF.

The electroosmotic velocity is governed by the following equation:

$$v_{EOF} = \varepsilon / 4 \pi \eta * E \zeta$$

where ε is the dielectric constant of the solution, η is the viscosity of the solution, E is the field strength, and ζ is the zeta potential. The EOF is better with a large zeta potential between the cation layers, a large diffuse layer of cations to drag more molecules towards the cathode, low resistance from the surrounding solution, and buffer with pH of 9, so that all the SiOH groups are ionized.

Some instruments include a temperature control device to ensure reproducible results and to dissipate the heat generated by Joule effect through the capillary tube. This is because the

separation of the sample depends on the electrophoretic mobility and the viscosity of the solutions decreases strongly as the capillary temperature rises. Two type of detection are mainly used in CE: UV and MS detection.

For a CE-UV measurement, a small window near the cathodic end of the capillary is present to allow UV-VIS light to pass through the analyte as it travels through it in order to measure the absorbance.[28]

This is the most commonly used detection mode in CE and its use requires a specific method created for a family of compounds depending on their UV-VIS features.

3.4.2.2 Experimental tools and methods

Electrophoretic separations were performed by means of P/ACE MDQ capillary electrophoresis instrument (Beckman Coulter). The system operation and the data acquisition were performed using 32 Karat 5,0 software (Beckman Coulter). A bare fused silica capillary of 75 µm internal diameter and 65 cm length was used. The protocol used for the measurement is the "acides_110711.met": prior to the sample injection, the capillary was rinsed by flushing 2 min with NaOH 0,1 M and 2 min with deionised water. The third step involves the conditioning of the capillary for 3 min with the running buffer.[29, 30]

The buffer was prepared with 2,6-pyridinedicarboxylic acid (PDC 99%, Aldrich) 5 mM as background electrolite (BGE) and Cetyltrimethylammonium bromide (CTAB, Aldrich) 0,5 mM at pH 5,6, adjusted with NaOH 1 and 0,1 M.

The injection was made in the hydrodynamic mode by applying a pressure of 0,7 psi for 4,5 s. A separation voltage of -25kV was applied to the anodic end. The resulting current was 20,1-20,5 µA.

For the organic acids the indirect UV detection at 350 nm was used with reference at 200 nm and a bandwidth of 20 nm with a photodiode array.

Five model low molar mass organic acids (LMMOA), commonly found as cellulose degradation by-products, were used as references: acetic (A), formic (F), glycolic (G), lactic (L) and succinic (S).

The separation method is really fast: the five acids are separated within little more than 3 minutes. The complexity of the sample matrix affects slightly the migration time (t_m) of the different acids in consecutive runs, but it does not affect the selectivity and the sensitivity of the method.

3.4.3 HPIC analysis

High Performance Ion Chromatography is designed to resolve a large number of inorganic anions and organic acid anions from a single sample injection in one run using hydroxide eluent systems. In combination with an optimized elution protocol, it can allow for the identification of multiple organic and inorganic monovalent, divalent and trivalent anions, which can be eluted in a single run and in less than 35 minutes, providing chromatogram peaks sharp, intense and easy to be attributed to specific species.

In Fig. 17 the chromatogram of a standard solution is reported as an example of the high-efficiency and high-selectivity of the column. In sequence, it is possible to clearly identify the single analytes: F^-, Ac, Cl^-, NO_2^-, NO_3^-, Succ, Tar+Mal, SO_4^{2-}, Ox, PO_4^{3-}.

3.4.3.1 Theoretical and instrumental aspects

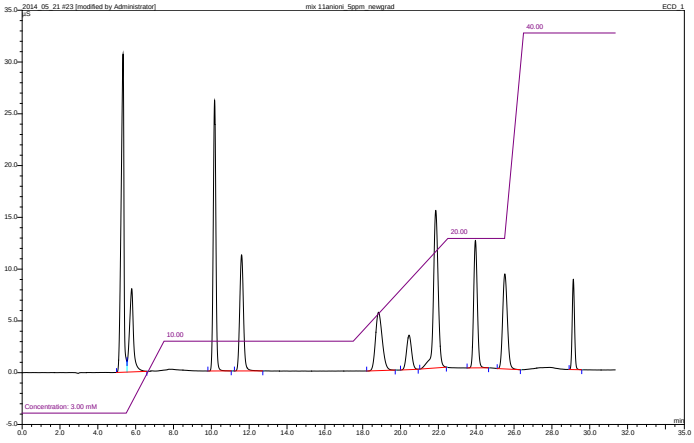

Figure 17: Ionic Chromatogram of a 5 ppm standard solution: in sequence the peaks are attributed to F^-, Ac^-,Cl^-, NO_2^-, NO_3^-, Succ, Tar+Mal, SO_4^{2-}, PO_4^{3-}.

The Ion Chromatographic System is basically composed by an ion-chromatographic system with suppressor.

Eluent is pumped by an eluent pump through an injection valve, where exactly reproducible sample volumes are injected for continuous regeneration. The sample ions are carried by an eluent flow to a separation column, where interaction with fixed ions of opposite charge (i.e., positive) take place. The ions are thereby slowed down to an extent characteristic of each ion and arrive separated at the "suppressor", where the eluent and analyte ions are transformed before they reach the detector. The detector measures the electrolytic conductivity of the eluate and the function of the suppressor is both to reduce the background of the eluent and to increase the sensitivity for the sample ions.

The most common type of elution is *isocratic*, where the eluent has a constant concentration and composition during the entire run. Another possibility of elution is a *gradient*, where the eluent concentration is changed in a reproducible way in each run. The reason for using

gradient elution is that ions with widely different retentions can be separated in the same run with good separation efficiency and reasonable retention time. After each gradient run the column must be equilibrated with the start concentration of the eluent before the next sample can be injected: it is important to choose eluents that produce a minimum shift in baseline conductivity during the run, as well as a fast equilibration time from one run to the next.

3.4.3.2 Experimental tools and methods

The Thermo Scientific™ Dionex™ IonPac™ AS11-HC-4µm anion-exchange column was used for the analysis of the samples described in Section 2.2.3. The column is composed by supermacroporous polyvinybenzyl ammonium polymer cross-linked with divinylbenzene. The functional groups involved in the analyte separation are alkanol quaternary ammonium. The elution and separation of the several organic acids and inorganic anions has been performed in gradient mode using NaOH as eluent. Indeed, the use of NaOH for a gradient elution allows: 1) strongly retained trivalent ions, such as phosphate and citrate, to be efficiently eluted in the same run; 2) baseline resolution of the weakly retained monovalent anions, as sodium hydroxide is converted to water in the suppressor with a negligible effect on background conductivity.

Table 3: Measurement Gradient Elution Program

Time (min)	NaOH Concentration (mM)
0-3	3
5	10
15	10
20	20
23	20
24	40
35	40

The optimized elution program, i. e. the one, which allowed for the best separation of the searched analytes, is reported in Table 3.

The above-described gradient made possible the elution of weakly retained monovalent anions like F^-, Ac^- and Cl^- and of strongly retained trivalent anions like PO_4^{3-} in a single run and in less than 35 minutes.

In combination with an effective gradient elution program, the analysis protocol involved an easy but proper sample preparation as well. The sample was diluted 1:2 in order to reduce the matrix effect and the t_R shift, induced by the high amount of strongly retained analytes on the previously eluted ones. The sample was filtered by the use of a 0,22 μm filter before the injection, in order to avoid organic material (fibers) to stick into the column.

For performing quantitative measurements, a special attention was paid on the column cleaning. Before every measurement section, the column was rinsed for one hour with 60 mM NaOH flow, in order to completely clean the column from every impurities and/or sample traces left from the previous runs. After this treatment, MilliQ water was injected three times in the column, following the sample elution protocol, in order to ensure the removal of every impurity.

The equilibration time, suitable for the eluent concentration reset and for starting a new measurement, was 8 minutes.

In order to obtain a minimal background conductivity level, a new hydroxide eluent was prepared every day, filling the water tank of the eluent generator with freshly tapped MilliQ.

The calibration curve, used for the specie quantitation, was established using six levels of concentration solutions (0.5, 2.5, 5, 10, 25 ppm) for each model analyzed species. Each calibration point corresponds to two injections.

The identification of the different species was not possible just by the t_R comparison, because, as already seen in the CE measurements, small difference in pH and different matrix effects affect the t_R reproducibility and do not allow for a sure attribution.

Therefore, we resorted to the “spiking method”, preparing two spiking solutions and adding one at a time to the sample solutions.

Chapter 4

4. Analysis of degradation by-products in ancient paper: results and discussion

The three sample solutions respectively obtained by very degraded, slightly degraded and non-degraded leaves of "*De Divina Providentia*" showed an intense color, indicating the high capacity of water to extract degradation by-products from the paper leaves. Every single solution has been analyzed by means of a wide range of spectroscopic techniques: studying the relationship between the paper conditions and the by-products formed during its natural ageing is fundamental to provide an outline of the degradation reactions, which ancient and historical books could undergo.

4.1 Extract 1

The UV-Visible spectrum of Extract 1 is shown in Fig. 18a. In literature, the UV-VIS spectra of artificially aged papers have been recorded by diffuse reflectance in the visible region (Fiber Optic Reflectance Spectroscopy, FORS) at a R. H. of 50% at room temperature.[11, 31, 32] The absorption spectra are then obtained from the reflectance spectra by means of *Kubelka-Munk transformation*.

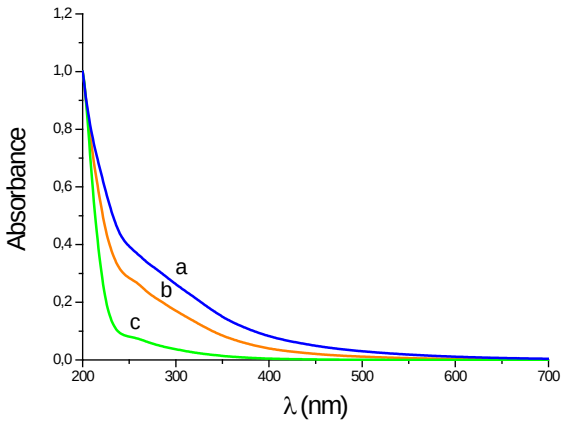

Figure 18. UV-Vis spectra of the Extract 1 (a), the Extract 2 (b) and the Extract 3 (c).

The UV-Vis spectra reported in the literature for degraded cellulose show very intense bands in the region between 280-360 nm and sometimes a long tail in the visible. The bands in the near-UV region, whose intensity slowly decreases in the visible range, are attributed to n-π*

and π-π* transitions in conjugate ketones and their tautomers, enols, formed on the cellulose chain as a result of a hydrolysis and oxidation combined action.[11, 31, 32] The yellowing and/or browning of the degraded paper can be attributed to the presence of this long tail of overlapping bands in the absorption spectrum.[31, 32]

The UV-VIS spectrum of Extract 1 presents features similar to the UV-VIS spectra of degraded cellulose: it is characterized by an intense absorption in the ultraviolet range and a slow decrease in the visible range up to 700 nm. A broad shoulder between 250 nm and 350 nm, related to carbonylic and carboxylic n-π* transitions, can be also observed. The appearance of the long tail in the visible range suggests the presence of conjugated systems in the degradation products dissolved in the wash extracts.[9, 32]

The FTIR spectrum of Extract 1 is reported in Fig. 19a.In literature, the FTIR analysis of a large number of paper samples have revealed that the most easily degradable component in paper is cellulose,[33] and that its weakest points are represented by hydroxyl groups and by the C_1-O-C_4 glucosidic bond. The FTIR technique is not able to report a decrease in the degree of polymerization as a result of hydrolytic scissions, as the structure of the cellulose chains, closely linked together by hydrogen bonds with neighboring chains within the fibers, clogs those vibrational movements of the glucosidic bond, hampering their detection through IR.

Instead, the synergic effect of oxidation and dehydration generates small but significantly intense FTIR signals. In particular, it is observed a very well centered signal around 1630 cm^{-1} in the IR spectra of highly-degraded papers.[11, 16]

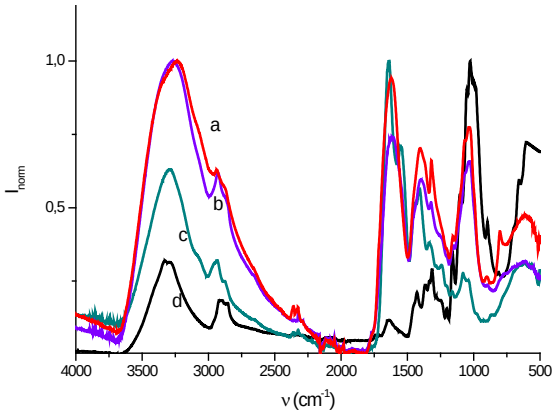

Figure 19. FTIR spectra of the Extract 1 (a), the Extract 2 (b), the Extract 3 (c) and cellulose (d).

This band represents a convolution of signals related to various functional groups, which formed on the cellulose chain as a result of oxidation, auto-oxidation and dehydration reactions.[34-36]

Since the band at 1630 cm^{-1} is highly informative, in literature a deconvolution procedure is often applied to this band to determine the entity of the various contributions, which are reported in Table 4. Details of the method are reported in the section 3.3.2.3.

Table 4. IR frequency attributions

Frequency (cm^{-1})	Functional groups
1540 - 1567	Conjugated and unconjugated carboxylates complexing trivalent metal ions (Fe^{3+}, Al^{3+})
1590	Free carboxylates, i. e. complexing monovalent or divalent metal ions (Na^{+}, Ca^{2+})
1618	Conjugated C=C
1640	Water and simple C=C
1660	α,β unsaturated carbonyl
1694	α,β unsaturated carboxyl
1717	Simple carboxyl

In the Raman spectrum of Extract 1, acquired by means of SERS technique (Fig. 20a), a strong and broad peak at 1575 cm^{-1} is visible. Oxidized papers exhibit Raman spectra quite different than non-degraded papers, especially in the region below 1800 cm^{-1}, whereas hydrolyzed papers and not degraded papers present similar spectra. This difference is because degradation reactions usually induce chemical and structural changes in the cellulose chains, while hydrolysis processes cause the breakage of the cellulose chain but do not change its chemical structure.

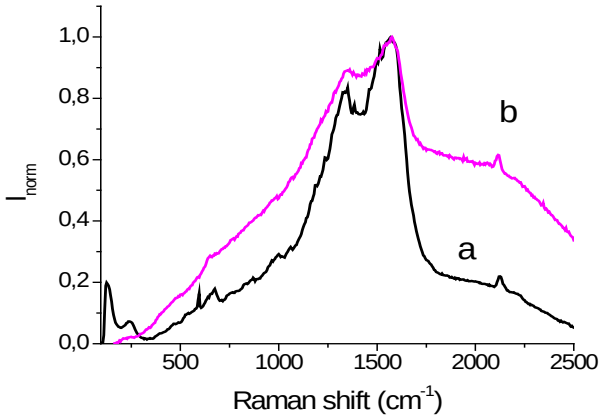

Figure 20. Raman spectra of the Extract 1 (a) and of the Extract 2 (b).

Raman spectra of oxidized leaves are always characterized by a band centered at 1577 cm^{-1}, which is considered a "marker" of the oxidative processes.[19] The band, as the one at 1630 cm^{-1} of the IR spectrum, is a convolution of multiple Raman peaks belonging to oxidation-induced

functional groups, falling in this narrow region: the stretching of isolated and conjugated C=C and asymmetric stretching of carboxylates.

Moreover, due to oxidative attacks, multiple adjacent carbonyl groups can form on the glucose ring of the cellulose chains, which can give rise to keto-enol tautomerism and therefore to the formation of C=C-O groups, whose stretching also occurs in this region. The carbonyls are not easily detectable in the Raman spectrum, since the intensity of their bands is low because of the selection rules. The presence of conjugated C = C groups, as one of the components of the band at 1577 cm^{-1}, is confirmed usually by the presence of signals at 634 cm^{-1} (C=CH wagging), while a confirmation of C=C-O is provided by signals at 636 cm^{-1} (O=CO bending in plane) and at 1444 cm^{-1} (carboxylate OC-O symmetric stretching).[19]

The strong signal at 1575 cm^{-1} that we observe in Fig. 20a is therefore in agreement with the literature: it is related to the band at 1630 cm^{-1} observed in the FT-IR spectra, in that the same species giving rise to the IR band contribute to this Raman peak. The maximum in the Raman spectrum is shifted to lower wavenumbers with respect to the IR band due to the above-mentioned different selectivity of the Raman, enhancing signals from conjugated double bonds and carboxylates.[9, 19]

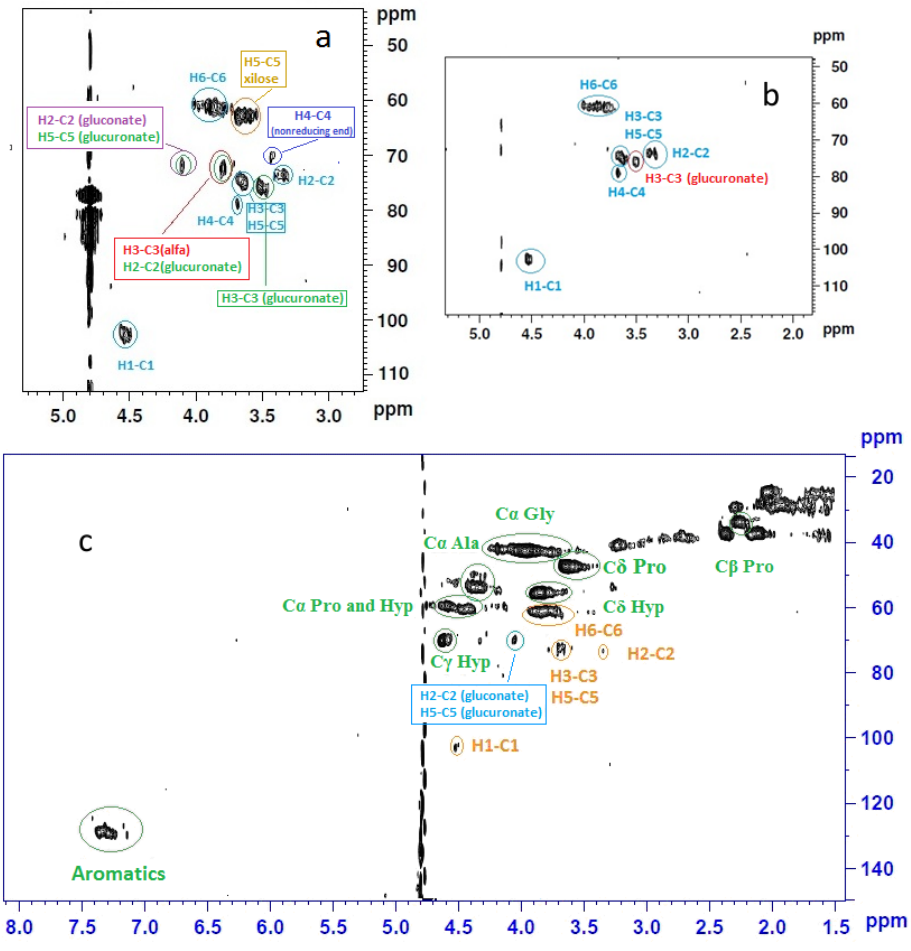

Figure 21. HMQC of the Extract 1 (a), of the Extract 2 (b) and of the Extract 3 (c).

The presence of the carboxylate groups, detected by the FTIR and Raman spectra, is in agreement with the relatively high pH value of Extract 1 (Table 1): it indicates that the carboxylic groups are mainly present in their

deprotonated form, accounting for the high solubility of Extract 1 only in a high polar solvent like water.[35] Carboxylate species could arise from low molecular mass organic acids (LMMOA), whose study in ancient and historical papers has been widespread in literature, and/or from oxidized glycosidic units of cellulose chain or, as in this case, oligomers. In Fig. 21a the HMQC spectrum of Extract 1 is reported. In the literature, no relevant data have been collected on NMR spectra of ancient paper: many works deal with the analysis of spin-lattice relaxation times in order to determine the degree of crystallinity of the cellulose chains [36] or to calculate the amount of water bound to the polymer,[37] and this is done essentially to relate these data with the sample degradation state. Mostly damaged papers show, in fact, an extended dehydration and a strong increase of the amorphous cellulose component.[36, 37] In literature no deep NMR studies on cellulose are present, the most of the published articles deals with the analysis of I_α and I_β allomorphous polymers and with artificially oxidized cellulose.[38, 39] Several spectra are instead recorded by means of ^{13}C CP-MAS NMR and ^{13}C NMR, as they turn out to be excellent tools for the study of the conformations assumed from polysaccharides both in solid state and in aqueous solution,[40] or for the identification of the functional groups, generated on the cellulose chain due to aging and/or degradation processes.[38, 39]

The HMQC spectrum in Fig. 21a shows signals at 3.5-77 ppm and 4.1-71 ppm, which can be attributed respectively to the H_3-C_3 and H_5-C_5 spin systems of glucuronic acid or its salt glucuronate,[41-43] verifying the formation of oxidized glucose derivatives. This latter signal (4.1-71 ppm) can be due also to the H_2-C_2 spin system of gluconate.[44]

The degradation of cellulose oligomers seems to proceed to the further step of decarboxylation, as pointed out by the peak at 3.42–62 ppm attributed to xylosic units (H_5-C_5).

The decarboxylation processes, giving rise to xylosic units, are commonly observed in carbohydrate samples upon ozone treatment and for this reason they represent a reliable proof of oxidative paths occurring on cellulose.[45, 46] In this case, it is unlikely that the xylosic rings are attributed to the presence of hemicellulose, as the paper sheets, from which the sample was extracted, are composed by pure linen (rag pulp, the only used in the Middle Age to form the paper leaves, consists of pure cellulose, whereas wood pulp contains also hemicellulose, whose structure embeds xylosic units).

Finally, the correlation peak at 3.8–73 ppm can be assigned to α-glucose (H_3-$C_{3(alfa)}$): this species only occurs if single molecules of glucose are present in the degradation by-products. Its detection provided a further proof of the occurred acidic hydrolysis on the cellulose chains of the book leaves.

The presence of glucose and cellobiose inside the sample is confirmed by the HPLC analysis as well and their amounts have been estimated (0.2 and 1.3 ppm, respectively). The chromatograms of Extract 1 (Fig. 22) are characterized by a series of not well-defined peaks, indicative of a broad distribution of oligomeric compounds. In particular, the analysis was focused on the chromophoric compounds, which show a significant absorption within the λ=200–350 nm range: the related mass spectra show the evidence of oligomers of MW greater than 2 kDa, indicating that the chromophoric units are part of polymeric chains, likely oligosaccharides.

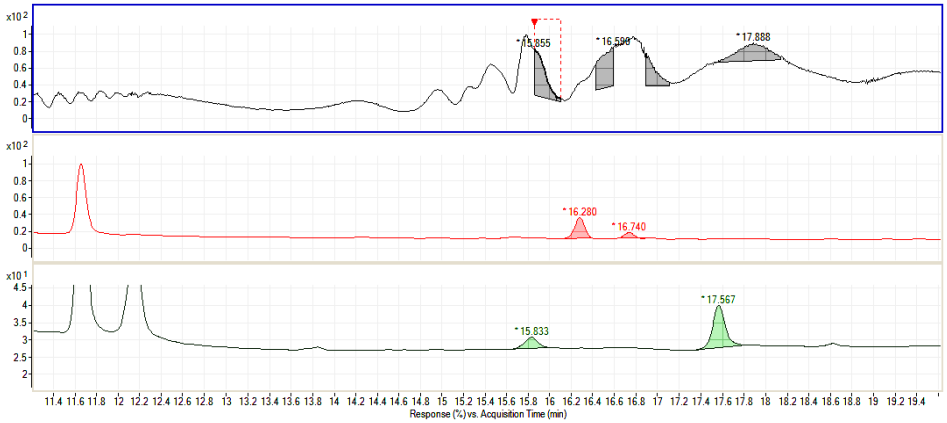

Figure 22. HPLC-DAD-MS chromatograms of the Extract 1: total ion current in positive or negative ESI acquisition (top panel) and HPLC-DAD chromatograms recorded at λ=250 (middle) and at 350 nm (bottom).

Low molecular mass organic acids (LMMOA), such as glycolic, formic, succinic, lactic and acetic acid, considered as common paper degradation by-products, were identified and quantified by means of CE-UV (their amount in 1,5 ml of Extract 1 solution are reported in Table 5). For comparison purposes, the CE-UV results of the three samples were paralleled with those of the aqueous extracts from 18th (so-called "SE") and 19th century (so-called "OC") books, obtained using the same analysis protocol followed here (methodology which had been developed then), and reported in a previous work.[29] The choice of these two books as basis for the comparison was based on the composition of their sheets, factor that directly affects the degradation pathways and kinetics: indeed, as "*De Divina Providentia*" they are made with rags.

In different conservation conditions the two books showed different LMMOA yields: higher for SE, which is in relatively degraded state, and lower for OC, which is visibly in good conservation conditions. If a true quantitative comparison cannot be done here, the relative abundance of the various acids in the extracts of SE and OC was slightly different from that in the 16th century book extracts. In both SE and OC, formic acid was by far the most abundant LMMOA followed by glycolic acid, while succinic acid was the least abundant.

Table 5. Quantitation of LMMOA in the three samples through CE.

	Amount (ppm)	**t_m(min)**	**Amount (ppm)**	**t_m(min)**	**Amount (ppm)**	**t_m(min)**
LMMOA / Extract	**1**		**2**		**3**	
A (ppm)	4,55 ± 0,26	3,1393 ± 0,0023	4,19 ± 0,22	3,1347 ± 0,0029	6,35 ± 0,22	3,2053 ± 0,0023
F (ppm)	2,59 ± 0,26	2,5670 ± 0,0040	2,23 ± 0,30	2,5540 ± 0,0040	4,03 ± 0,30	2,6040 ± 0,0000
S (ppm)	0,818 ± 0,059	2,8317 ± 0,0023	0,64 ± 0,10	2,8447 ± 0,0023	1,63 ± 0,10	2,8947 ± 0,0023
G (ppm)	7,41 ± 0,091	3,0290 ± 0,0040	5,28 ± 0,25	3,0210 ± 0,0040	8,20 ± 0,25	3,0933 ± 0,0023
L (ppm)	3,199 ± 0,021	3,2303 ± 0,0046	2,93 ± 0,10	3,2263 ± 0,0023	4,64 ± 0,10	3,3113 ± 0,0029

Conversely, in Extract 1 the succinic acid is clearly the most abundant, only followed by acetic acid, while glycolic acid is the least abundant.

The origin of the rag paper (linen, cotton, hemp, etc.), the presence of additives such as gelatin sizing and alum, but also the likely impact of the conservation history of the books and the extraction conditions used to obtain this type of samples are the reasons that can explain the differences in the LMMOA content.

HPIC analyses were performed, in order to widen the study performed by CE-UV technique towards the detection of multiple organic acids and the identification of inorganic ions.

Among the spectroscopic and analytical techniques used, this analysis turned out to be the only one, which has allowed for an unambiguous detection of oxalate species in ancient papers.

Oxalates are common organic degradation by-products and in literature they are considered a sort of “marker” of an occurred oxidative deterioration: their detection could provide specific information about the type and the mechanism of the biological/chemical degradation reactions, which has led to their formation and therefore to the work of art deterioration.[47-51]

In literature, the identification of these compounds in ancient papers has been quite difficult. In the FT-IR and Raman spectra of ancient and oxidized papers, the oxalate features are

completely covered by the peaks of the oxidation-induced functional groups.[5, 52, 53] Moreover, oxalate do not show particular UV-Vis features, therefore spectroscopic techniques turns out to be not suitable for the identification of those species.

Table 6: Type and amount of the species detected by means of HPIC.

	Amount (ppm)	t_R (min)	Amount (ppm)	t_R (min)	Amount (ppm)	t_R (min)
Extracts	**1**		**2**		**3**	
Quinate	8,14 ± 0,23	4,777 ± 0,006	6,59 ± 0,36	4,49 ± 0,060	0,402 ± 0,044	4,28 ± 0,18
Fluoride	2,62 ± 0,31	5,120 ± 0,010	0,950 ± 0,015	5,01 ± 0,14	1,470 ± 0,041	4,80 ± 0,13
Lactate	3,23 ± 0,11	5,183 ± 0,021	0,38 ± 0,04	5,09 ± 0,15	1,445 ± 0,067	5,11 ± 0,15
Acetate/Glycolate	0,97 ± 0,24	5,450 ± 0,017	0,67 ± 0,20	5,35 ± 0,16	2,58 ± 0,16	5,34 ± 0,16
Formate	1,4 ± 0,21	6,560 ± 0,053	<LOD	-	5,10 ± 0,18	6,41 ± 0,22
Chloride	2,32 ± 0,13	9,953 ± 0,015	2,28 ± 0,10	9,85 ± 0,14	14,28 ± 0,26	9,84 ± 0,14
Nitrite	<LOD	-	1,31 ± 0,19	11,20 ± 0,17	<LOD	-
Nitrate	2,14 ± 0,18	18,013 ± 0,081	0,54 ± 0,09	17,86 ± 0,25	17,51 ± 0,25	17,69 ± 0,25
Succinate	3,42 ± 0,31	19,07 ± 0,22	<LOD	-	8,80 ± 0,49	18,96 ± 0,19
Tartrate-Malonate	3,36 ± 0,36	20,36 ± 0,19	2,52 ± 0,17	18,33 ± 0,12	2,08 ± 0,28	19,93 ± 0,20
Sulfate	5,86 ± 0,20	22,59 ± 0,17	5,55 ± 0,20	19,70 ± 0,26	6,91 ± 0,13	22,59 ± 0,22
Oxalate	71,2 ± 1,9	24,04 ± 0,19	<LOD	22,32 ± 0,26	6,22 ± 0,31	23,88 ± 0,80
Phosphate	5,31 ± 0,26	28,903 ± 0,045	3,042 ± 0,087	23,96 ± 0,26	2,34 ± 0,17	28,930 ± 0,056

The CE-UV protocol did not allow for their detection as well, as the oxalate peak fell in the broad inorganic ion peak at the beginning of the electropherogram.

Unlike the above-quoted techniques, in the HPIC chromatogram, the oxalate peak is well-separated from the other analytes and can be easily identified: it falls immediately after the sulfate peak with an average t_R of 24 minutes.

From the HPIC results, the huge amount of oxalates in Extract 1 chromatogram emerged, if compared with the amount of the other species and the amount of the same analyte in the other two samples. On the other hand, although the spectroscopic analyses suggested that the degradation state of Extract 2 is very close to Extract 1 one, its oxalate amount is quite low.

In general, HPIC measurements have provided a very good separation of inorganic and organic low molar mass acids with a pattern of well-separated, sharp and therefore easily identifiable peaks. Moreover, the column showed a high reproducibility in term of retention time and intensity of the signals.

There is not a full conformity between the amounts of the same species detected by CE-UV and HPIC chromatographic techniques: indeed, as reported in Table 5 and 6, in some cases the amount of LMMOA detected by CE-UV is higher, although in the same order of magnitude (ppm).

Further investigations have to be pursued in this sense: it is necessary to record an electropherogram of the blank in order to check its possible interference in the species quantitation. As a matter of fact, CE-UV allows for a good separation and identification of the LMMOA such as lactic, acetic, glycolic, succinic and formic acids, which are not completely separated in CI chromatogram.

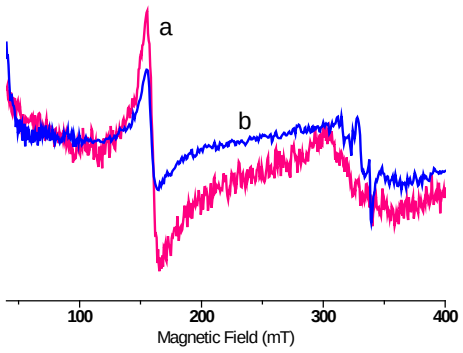

Figure 23. EPR spectra of Extract 1 (a) and Extract 2 (b).

Therefore, the combination of the two techniques is fundamental to get a clearer and more complete overview of the pattern of the organic and inorganic acids formed during the degradation of ancient, historical and artificially aged papers.

A deep study of the metal content of the sample has been performed as well: a strong effort has been dedicated on the detection and quantification of metal ions, with a particular attention on Fe(II)/Fe(III) and Cu(II) species. These paramagnetic centers have been well known to catalyze paper degradation reactions. The former one can catalyze oxidation reactions of cellulose, through a redox chain reactions mechanism, while the latter has been recognized as an efficient catalyst of both oxidation and hydrolysis of biomaterials. EPR, ICP-MS and XRF analysis were carried out on Extract 1 in order to probe the type, the coordination and the amount of metal ions.

In literature, in several works the EPR technique has been used to investigate the presence of paramagnetic impurities inside degraded ancient and modern papers.[37, 54-56]

These species primarily consist in:

- Transition metal ions (Fe^{3+}, Cu^{2+}, Mn^{2+}) present in different environments and symmetries;

- Organic radicals, common in modern papers, generated by photoexcitation of the lignin present in the wood pulp, used for the paper manufacture since the second half of the nineteenth century.

The EPR spectrum of ancient papers shows intense signals of the high-spin Fe^{3+} and Mn^{2+}. The signals related to organic radicals are normally absent in this type of paper.

In the three samples, the Fe^{3+} ion is present in two different chemical environments and gives rise to two different EPR signals:

- the first is a signal at g≈2 or B≈3500 Gauss, typical of Fe^{3+} in a pseudo-octahedral coordination;[37, 54]
- the second signal is a well-defined sharp line at g≈4.3 or B≈1500 Gauss, typical of Fe^{3+} in a rhombic environment. It represents a different metal symmetry from the axial one, which corresponds to complete inequality of the three main magnetic axes. The EPR spectrum in this case is unique, but not its symmetry and therefore it is not possible to accurately determine the chemical surrounding of the metal ion.[37, 54]

The high-spin Mn^{2+} signal is superimposed to the octahedral Fe^{3+} EPR line and consists of a sextet generated by the separation of the spin transition -½ → + ½ because of the hyperfine interaction between the electron spin magnetic moment and the ^{55}Mn nuclear spin I=5/2.[37]

The Cu^{2+} EPR signal, unlike for Fe^{3+} and Mn^{2+} ions, is detected only in a third of the degraded papers analyzed in literature.[54] Copper contains an unpaired electron and gives rise to a typical anisotropic spectrum, which shows mainly axial symmetry or small rhombic distortions. The spectra of samples of ancient paper containing Cu^{2+}show two types of signal, indicating that the metal ion can be found in two different chemical environments. Indeed, Cu^{2+} is either coordinated to the cellulose backbone or simply absorbed on paper and in this latter case, its EPR spectrum is similar to the spectrum of the hydrated Cu^{2+}ion.[54]

The investigation of these paramagnetic species is due their active role in the cellulose degradation processes: it has been found that the Fe^{3+} ions in a rhombic symmetry and the Cu^{2+} ion act likely as catalysts of the hydrolysis and oxidation reactions.[55, 56] The role of copper is crucial in the deterioration of the samples containing this ion (a phenomenon known as “Kupferfrass”). On the other hand, deteriorated or damaged ancient papers could

not contain copper, but in these cases the EPR spectrum shows often a very intense signal of Fe^{3+} in rhombic symmetry.

The presence of the ion Fe^{3+} in a pseudo-octahedral coordination as well as of the ion Mn^{2+} does not seem to affect the conservation status.[55, 56]

In general, the EPR characterization can gather important and unique information about the preservation state and the tendency to degradation of paper materials.[15, 55]

The EPR spectrum of Extract 1 (Fig. 23a) is characterized by a sharp line around 150 mT and by a weaker broad line, between 300-350 mT, resolved in six hyperfine lines. According to the above discussion, we can assign the sharp line to Fe(III) complexes in rhombic sites, attributed generally to Fe(III) strongly bound to the cellulose matrix. The six lines between 300-350 mT can be assigned to Mn(II) bound to cellulose. [37, 55, 56] No Cu(II) or pseudo-octahedral Fe(III) signals are observed. The significant presence of Fe was also confirmed by XRF and ICP-MS (Table 7 and 8), which, unlike EPR, allowed the detection of Al species. Al(III) ions in the wash solutions could indicate the use of alum during the sizing procedure of the sheets, from which Extract 1 was obtained. Alum is recognized as a paper degradation agent, due to its catalytic action on hydrolysis, and its presence could explain the higher degradation level of these leaves.

Table 7. Results of XRF analyses.

Extract 1	Al	Si	P	Cl	K	Ca	Cr	Mn	Fe	Cu
Extract 2			P	Cl	K	Ca			Fe	Cu
Extract 3			P	Cl	K	Ca			Fe	

Table 8. Results of ICP-MS analyses.

	Al (ppm)	**Fe (ppm)**	**Zn (ppm)**
Extract 1	66.6 ± 1.7	8.8 ± 2.5	74 ± 24
Extract 2	24.0 ± 1.7	5.3 ± 2.5	8 ± 24
Extract 3	37.1 ± 1.7	2.9 ± 2.5	47 ± 24

However, the very low amount of detected sulfur (Table 10) suggests that Al might derive from alternative sources, e.g. from rags maceration.

4.1.1 Sample AP

The UV-Vis spectrum of the Sample AP shows a better defined shoulder at 280 nm (Fig. 24Ab), suggesting that the treatment with HCl brought about a carboxylate – carboxyl shift, giving rise to a closer and more intense UV absorption band in this region.[11, 16, 31, 52] In literature, it has been shown that a n-π* transition between 260 – 300 nm is typical for dicarboxylic acids, particularly oxalic acids, whose carboxylate – carboxyl shift has a profile change like that shown in Fig. 24Aa – 24Ab.[57, 58] The IR spectrum of the Sample AP (Fig. 24Cb) exhibits an intensity increase and shape change of the band at 3000 cm^{-1} with respect to Extract 1. This band (due to OH stretching) could derive from an increase of the amount of carboxyl groups and/or to the formation of new H-bonds among the regenerated –COOH groups.

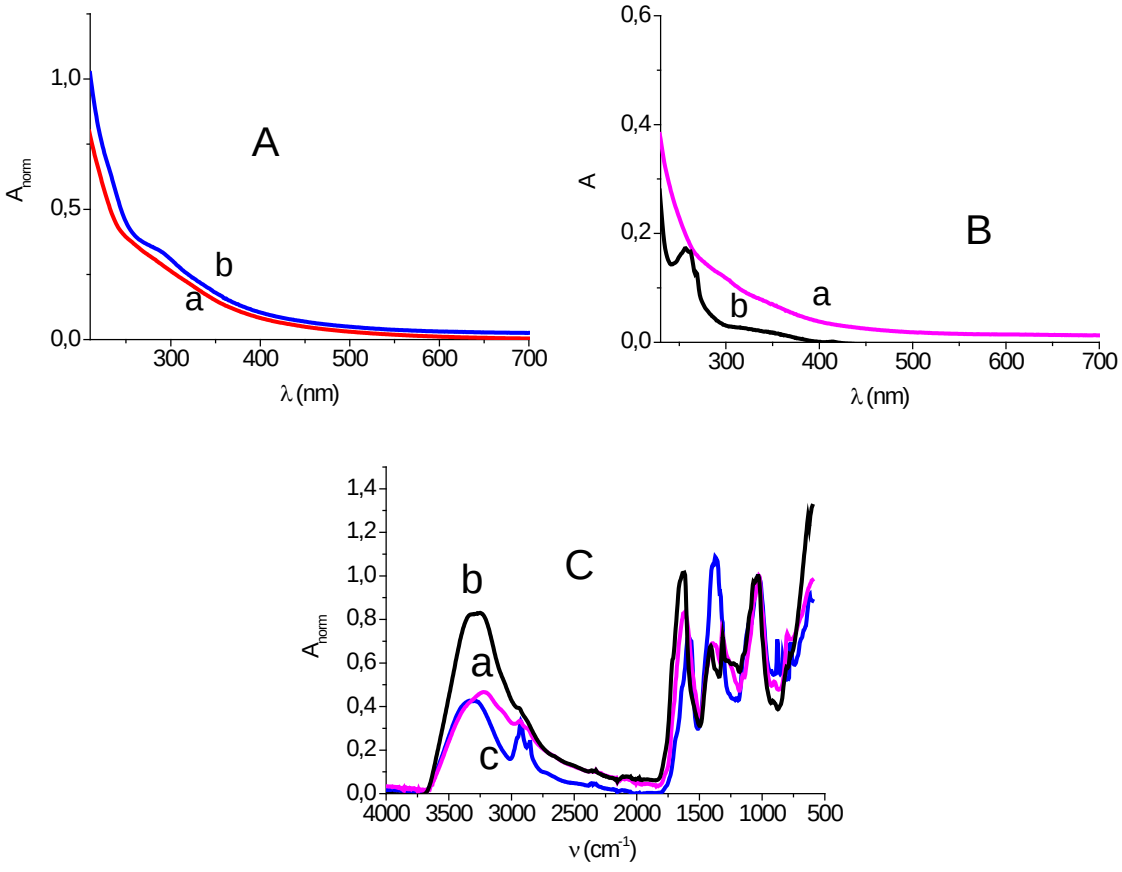

Figure 24.A. UV-Vis spectra of the Extract 1 (a) and the sample AP (b); **B.** UV-Vis spectra of the powder obtained by the Extract 1 dissolved in methanol (a) and of the sample HP in methanol (b); **C.** FTIR spectra of the Extract 1 (a), Sample AP (b) and Sample HP (c).

The band at 1630 cm^{-1} moves to higher frequencies. This is the consequence of the strong reduction of the carboxylate bands at 1550-1610 cm^{-1} and the increasing of the carboxyl

bands at 1720 cm^{-1},[14, 15, 34, 53, 59] as determined by deconvolution analysis (Table 9). The area of the band at about 1540-1550 cm^{-1}reduces a little after acidification and this finding could suggest that this band is due to conjugated carboxylates participating to pretty stable metal complexes.

4.1.2 Sample HP

The UV-Vis spectrum of the methanol solution of the Sample HP (Fig. 24Bb) shows a sharp absorption band at 260 nm, while the long tail in the visible range, present in the UV-VIS spectrum of Extract 1 in the same solvent (Fig. 24Ba), is lacking.

The absence of absorbance in the visible region is pretty evident even in the marked discoloration of the Sample HP with respect to Extract 1 (see Fig. 13, (b) and (a) respectively).

The FTIR spectrum (Fig. 24Cc) shows an overall decrease of the broad absorption between 3250 and 1800 cm^{-1}, particularly of the signal attributed to CH stretching (sp^2); an increase of the CH absorption in the 3070-2870 cm^{-1} region; and finally a strong intensity increase of the peak between 1300 and 1450 cm^{-1}. This latter effect can be attributed to the formation of alkane –C-H group vibrational modes such as bending, rocking and wagging. The band at 1630 cm^{-1} moves toward lower frequencies, showing an intensity decrease of the components of the band attributed to unsaturated carbonyl groups. We studied the effects of hydrogenation in detail through the deconvolution of this latter band (Table 9), which shows a substantial decrease of conjugated structures and the persistence of saturated groups.

Table 9: Deconvolution peaks of the Extract 1, Sample AP and HP in the frequency range between 1500–1850 cm^{-1}.

	assigned to	Esters	COOH and CO	C=C-COOH	C=C-CO	H_2O	C=C	COO^-	$C=C-COO^-$
Extract 1	center	1773	1717	1692	1665	1633		1596	1547
	width	20	24	41	52	65		82	79
	height	0,03	0,18	0,37	0,56	0,68		0,88	0,32
	area	1	7	24	46	70		113	40
Sample AP	center		1722	1670		1634		1613	1543
	width		39	108		107		30	80
	height		0.29	0.91		0.88		0.43	0.20
	area		12	155		148		20	26
Sample HP	center	1740	1696		1671	1643	1622	1592	1562
	width	12	44		55	35	13	79	31
	height	0,01	0,14		0,12	0,25	0,03	0,87	0,33
	area	0,19	10		10	14	1	108	16

In the literature the browning of ancient paper is indeed attributed to the presence of chromophores like carbonyl and carboxyl groups, often considered as conjugated, produced on the degraded cellulose chains in neutral to acidic environment.[9, 16, 18, 19, 31, 32, 52] However, to our knowledge not definite proofs of this assumption have been presented so far. In this work the catalytic hydrogenation, selective for C=C bonds, was utilized to verify their presence inside the sample and to understand how the presence of these groups affects the color of the degraded paper. The hydrogenation caused indeed a strong discoloration of Extract 1, as can be observed by comparing its UV-Vis spectrum with the HP one, see Fig. 24B.

From the comparison of the deconvoluted spectra of Extract 1 and Sample HP, it is evident the decrease of the band at 1540 cm^{-1} (conjugated carboxylates) and the appearance of a new band at 1560 cm^{-1}, while the area of the band at 1590 cm^{-1} before and after the hydrogenation has not changed.

The hydrogenation of unsaturated carboxylates could have given rise to a group of saturated ones, slightly different from that generating the band at 1590 cm^{-1}. The frequency difference between the two carboxylate bands could be accounted for by a different position of the –OH group respect to the carbonyl group or a different charge.[59] As pointed out in the above discussion about the IR spectrum of AP, the unsaturated carboxylates could chelate strongly iron ions, and therefore the hydrogenation of these compounds could result in the formation of iron-binding saturated carboxylates, whose IR stretching frequency occurs at 1560-1570 cm^{-1}.[15]

These results confirm the presence of a large amount of conjugate groups on Extract 1 and indicate that water-soluble and widely conjugated carbonyl or carboxyl compounds are the main chromophores responsible of the discoloration.[32, 60] It is likely that a cluster attack to the surface amorphous regions of cellulose fibers follows a pathway leading to these compounds, but their amount is low.

4.2 Extract 2

Extract 2 shows a similar composition of Extract 1. However, the lower intensity of IR signals (Fig. 19b), the lack of NMR peaks attributed to α-glucose and to xylose (Fig. 21b), the lower intensity of the band at 280 nm in the UV-VIS spectra and the shorter tail in the visible range

of the absorption (Fig. 18b), the slightly lower amount of LMMOA and oxalates (Table 5 and 6) and of the metal ions (Fig. 23b and Table 7 and 8) indicate that Extract 2 underwent milder hydrolysis and oxidation reactions than Extract 1.

This assumption has been also confirmed by the elemental analysis results (Table 10).

Table 10. Results of elemental analyses.

	Extract 1	**Extract 2**	**Extract 3**
C	38,14%	37,67%	38,97%
H	5,08%	5,19%	5,76%
N	4,53%	3,93%	10,19%
S	0,16%	0,26%	0,34%

The average formulas of compounds in Extracts 1 and 2 are respectively: $C_{3.18}H_{5.09}N_{0.32}O_{3.26}$ and $C_{3.13}H_{5.19}N_{0.28}O_{3.31}$. We must point out that, on the base of the analyses of Extract 1, we expect that Extracts 1 and 2 are mainly constituted by cellulose oligomers. Indeed, IR and UV-VIS spectra are very similar to that of oxidized cellulose, HPLC shows that oligomers are mainly present, and CE-UV and HPIC analysis state that small species, like LMMOA, amount to just few ppm. Thus, considering sugars and glucose-derivates as exclusive components of the two samples (therefore neglecting the N content), the empirical formulas rounded to the least integer numbers are approximately: $C_{64}H_{102}O_{65}$ and $C_{63}H_{104}O_{66}$. The calculated degree of unsaturation for Extract 1 is 4, while for Extract 2 it is 2. Then compounds in Extract 1 show one unsaturation every 2.5 pyranose rings, while in Extract 2 they bear one unsaturation every 5 rings. This result confirms that Extract 2 arises from paper with a lower degree of degradation than Extract 1 does. Furthermore, since the O ratio of

the two samples is almost the same, while the H ratio is lower in Extract 1 than in Extract 2, the compounds in Extract 1 contain likely a higher number of carbonyl groups and C=C double bonds.

4.3 Extract 3

The UV-Vis spectrum of Extract 3 (Fig. 18c) does not show the long tail in the visible range, and its carbonyl and carboxyl band is less intense.

The FTIR spectrum of Extract 3 powder (Fig. 19c) presents an intense doublet at 1630 cm^{-1} and 1540 cm^{-1} (more visible in the FTIR spectrum of the powder obtained by simple evaporation of Extract 3, not reported here): it is typical of "amide I" and "amide II" vibrational modes, and it is indicative of the presence of peptides, most likely the gelatin used for sizing.

These results have been supported by the HMQC data (Fig. 21c): the NMR spectrum is characterized by a large amount of peaks, mostly assigned in the literature to the amino acids typically present in the collagen structure, i.e. glycine (33% in animal gelatin), alanine (10%), proline (12%) and hydroxyproline (10%.) residues.[61, 62]

Table 11. Results of ESI-MS in positive mode of Extract 3.

Observed Mass	Type	Calculated Mass	Hypothetic Composition
173,0939	$[M+H]^+$	173,09987	1 Gly, 1 Pro
203,5651	$[M+H+Na]^{2+}$	203,0941925	3 Gly, 2 Pro
211,5511	$[M+H+Na]^{2+}$	211,09165	3 Gly, 1 Pro, 1 Hyp
224,0763	$[M+2H]^{2+}$	224,114395	3 Gly, 1 Ala, 1 Trp
232,0645	$[M+H]^+$	232,14061	3 Ala
270,1667	$[M+H]^+$	270,15626	1 Gly, 2 Pro
317,2212	$[M+H]^+$	317,160615	2 Gly, 1 Ala, 1 Hyp
354,1328	$[M+Na]^+$	354,157085	2 Gly, 3 Ala
362,1012	$[M+2H]^{2+}$	362,1933325	6 Gly, 1 Ala, 3 Pro
365,1322	$[M+Na]^+$	365,15821	2 Gly, 1 Ala, 1 Pro
391,2826	$[M+H]^+$	391,176265	2 Gly, 1 Pro, 1 Phe
401,2001	$[M+H]^+$	401,20023	5 Gly, 1 Pro
489,6904	$[M+H]^+$	489,23153	4 Gly, 1 Pro, 1 Phe
533,2515	$[M+Na]^+$	533,25534	2 Gly, 2 Ala, 1 Pro, 1 Hyp
570,1923	$[M+H]^+$	570,27775	4 Gly, 1 Pro, 2 Hyp
618,2118	$[M+H]^+$	618,27775	6 Gly, 1 Ala, 1 Trp
698,2758	$[M+H]^+$	698,34358	2 Gly, 5 Ala, 1 Pro, 1 Hyp
748,4337	$[M+Na]^+$	748,356825	3 Gly, 3 Ala, 1 Pro, 2 Hyp

Some cellulose signals are present, as well, while the correlation peak at 7.3-129 ppm could indicate the presence of aromatic species, probably phenylalanine (~ 1.4%) and tyrosine (~ 0.5%).[63, 64]

An ESI-MS characterization study was performed in order to more deeply investigate the nature of the oligopeptides present in Extract 3. As the spectroscopic results have shown the presence of protein in Extract 3 and, in particular, they have identified hydrolyzed gelatin (collagen) as the main component of the sample, all the ESI-MS m/z values, reported in Table 11, were attributed considering the collagen structure and amino acids composition.

Unlike for the first two samples, the ESI-MS results (Table 11) together with the IR (Fig. 19c) and NMR (Fig. 21c) spectra of Extract 3 point to hydrolyzed collagen as its main component.

Extract 3 shows the highest N ratio among the three samples (Table 10), confirming its high content of protein. The N ratio calculated from collagen molecular formula is about 15%. The N ratio of Extract 3 is lower (10%) because of the presence of a small amount of cellulose oligomers, as suggested by the NMR analysis. The Raman spectrum of Extract 3 (Fig. 25) is characterized by an intense signal at 1610 cm^{-1} (amidic O=C-O asymmetric stretching, C=C stretching and "amide I" bending), a broad peak at 1430 cm^{-1} (cellulose and amino acid CH_2 bending, COH bending, aromatic rings C-C stretching), two medium bands at 1215 cm^{-1} (C-N stretching) and at 1002 cm^{-1} (glycosidic bond C-O stretching), and two narrow and strong signals at 242 and 123 cm^{-1} (iron and sodium oxalates reticular modes).[49]

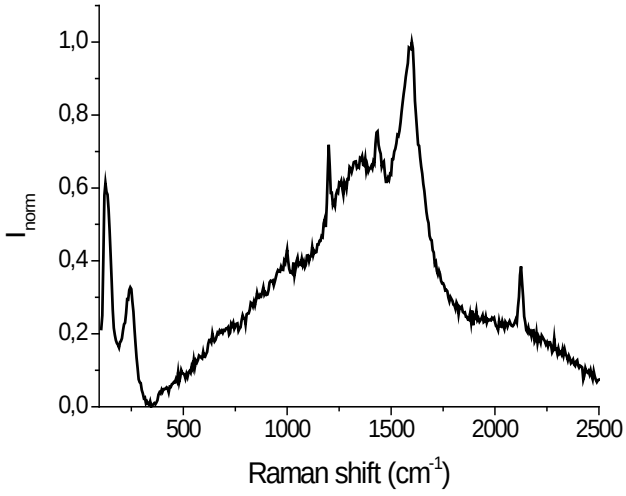

Figure 25. Raman spectrum of the Extract 3.

Therefore, the spectroscopic and chemical analyses have indicated that the cellulose structure of the leaves, from which Extract 3 was obtained, is almost undamaged, as cellulose degradation by-products were not found to be the main components in the wash water of this leaves. As found by other authors,[63-65] the presence of gelatin in the leaves seems to be connected to a lower extent of degradation. A hypothesis that has been put forward to account for this result is that the gelatin, by permeating the paper fibers, is more directly in contact with air and polluting agents, and thus can somewhat protect the fibers from oxidation and acidic hydrolysis by acting as a sink for the reactants.

It is also possible to deduce that these leaves belonged to a different paper ream than the leaves, from which Extracts 1 and 2 were obtained.

The CE quantization (Table 5) shows that the aqueous extracts obtained from the book sheets in good conservation condition (Extract 3) have the highest yield in total LMMOA degradation products. This unexpected result could be due to the different pH of the three samples (Table 1): given the pKa of the LMMOA, it is likely that in the paper the equilibrium was shifted to the deprotonated form in Extract 3 more than in the other two extracts.

Carboxylates are largely nonvolatile as opposed to carboxylic acids. Acids in Extracts 1 and 2 may have off-gassed continuously from the leaves upon their production even before the paper was washed, whereas in Extract 3, being the carboxylate ions predominant, they could stay in situ and could thus be extracted during the washing. In agreement with this hypothesis, in Table 6 we see that the most volatile LMMOA, formic acid, is present in larger amount in Extract 3 than in Extract 1 and 2; the acetic acid, not so volatile like formic acid, is present in an intermediate amount between Extract 1 and 2; quinate, largely nonvolatile, is present in lower amount in Extract 3 than in Extract 1 and 2.

The EPR spectrum of Extract 3 (not reported) does not present signals assignable to Fe(III) or Cu(II), while the ICP-MS values (Table 8) show that the total metal concentration lowers when comparing the most degraded (Extract 1) to the least degraded leaves (Extract 3).

The low amount of metallic centers, which catalyze the paper degradation reactions, and the high quantity of gelatin could have cooperated in order to preserve the cellulose chain of the leaves, from which Extract 3 was obtained.

Another hypothesis could suggest that the gelatin has protected the cellulose chain from the oxidation,[65] avoiding the formation of carboxylate groups: indeed, these latter are able to form stable distorted complexes with Fe(III), allowing it to act as a catalyst of the degradation reactions.

As well, these results are consistent with the measured pH values, as the most degraded leaves, showing a more acidic pH, dissolve in the extract solution a larger amount of metal ions than the least degraded leaves.

Chapter 5

5. Ozonation artificial ageing

5.1 Introduction

Most of the published articles, dealing with the degradation mechanisms in paper and more often in pure cellulose, propose artificial ageing methods, which involve the use of ventilated stoves at standard conditions of 80 - 100°C, in presence or in absence of humidity (see ISO standards 5630-01, -02 and -03) and UV irradiation (see ASTM standard 6789-02).These methods enhance the hydrolytic degradation, but underestimate the oxidation, while the results presented in the first part of this work provide enough evidence that long-term natural aging leads to many oxidation by-products, like oxalic and acetic acids. While hydrolytic reactions are now quite well understood, the synergy between hydrolysis and oxidation is still a debated matter. For these reasons, in the last few years the study of the paper degradation has been focusing particularly on the oxidative degradation reactions, and specifically on the role of the hydroxyl radical OH•.

In the troposphere, the hydroxyl radical is by far the most important oxidizing species: it is extremely reactive and able to oxidize most of the chemicals found in the troposphere - in spite of its short lifetime - by radical propagation reactions which interconvert the hydroxylic and the hydroperoxylic (HO_2•) radicals. The radicals OH• form from the decomposition of the ozone molecule: indeed, the O-O bond cleavage gives rise to the excited atomic oxygen, which can promote the formation of hydroxyl radicals, by the reaction with water or, as in this case, carbohydrates. In literature, products from long time ozonation of gluconic acid, glucose, cellobiose and cellulose have been investigated by means of HPLC chromatography, followed by NMR spectroscopical analysis of the fractions.[46, 66, 67]

Oxidation of C1, giving gluconic acid and its lactones, was the favored pathway for ozonation of glucose, but glucuronic acid, arabinose and carbon dioxide were also formed.[46, 66-71]

The origin of small molecules such as tartaric, erythronic and oxalic acids, whose presence is very common in naturally aged paper, is also apparent.[46, 67, 69, 72]

As the ozone attack on the sugars seems to produce by-products similar to those found in naturally aged samples, we decided to complement the study of naturally aged paper with paper artificially aged by means of ozonation, comparing the results obtained by the

analyses of the treated samples with the ones collected by authentic samples in order to improve the method. Here we present the early part of this study, involving the calibration of the ozonator, the building up of the ozonation chamber, and the first tests on paper samples.

5.2 Ozonator calibration

The used ozonator was an*A2Z 3GLAB* model using a Corona Discharge tube to produce ozone from air or oxygen. The discharge voltage could be adjusted nominally from C = 0% to 100% in order to provide from a minimum to a maximum level of ozone production. Maximum ozone production corresponded, according to the manufacturer's indications, to 1 g/h of ozone at 5 l/min oxygen input. Several tests were performed in order to detect and quantify the actual amount of ozone emitted by the ozone generator (ozonator).

Initial tests were performed using air as feeding gas. After unsuccessful tests for detecting ozone directly in the output gas, the gas was bubbled in water: in literature, works report that ozone dissolves easily in water and its concentration can be determined from the absorbance of the strong ozone band at 260 nm.[66]

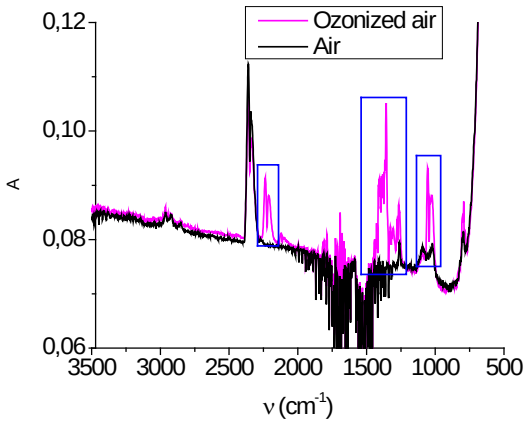

Figure 26: FTIR spectrum of ozonized air.

The presence of dissolved ozone was monitored by recording the UV-Vis spectrum of the water solution for different setting of the discharge voltage and different ozonation times. In all the tests, the UV-Vis spectrum showed a weak absorption at 300 nm and an intense band at 230 nm, but no band at 260 nm, indicating that, in the limit of UV-sensitivity no ozone was present. The bands at 300 nm and 230 nm indicate the occurrence of nitrogen oxides, therefore suggesting that ozone was consumed to produce NO_x species.[73]

In order to assess the actual ozone production, the FTIR spectrum of the output air was recorded, because of the increased sensitivity of IR to ozone concentration with respect to UV-VIS spectroscopy.

The IR spectrum of ozonized air (Fig. 26) shows peaks that could be attributed to the vibrational modes of ozone.[66]

This indicates that ozone was produced but interfering NO_X species were largely generated.

In order to avoid the production of nitrogen oxides and to increase in this way the amount of ozone produced by the ozonator, pure oxygen was chosen as feeding gas.

With oxygen as feeding gas, the UV-Vis spectrum of the bidistilled water, in which the output gas was bubbled, shows a clear band at 260 nm (Fig. 27).

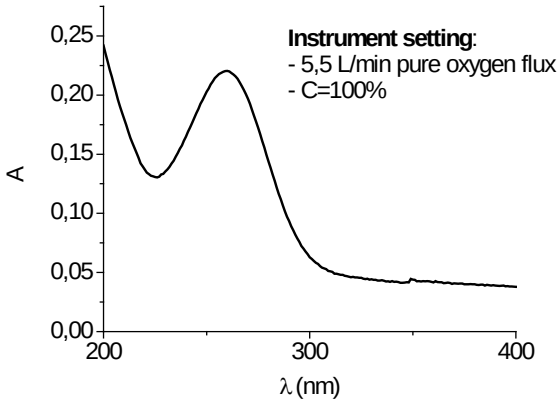

Figure 27: UV-Vis spectrum of the water solution, in which ozone was bubbled for 5 minutes.

Multiples tests were performed setting different discharge voltages.

The graph (Fig. 28) shows that the amount of ozone produced by setting C = 0% is approximately the same as the one produced at C = 50%. Otherwise, turning from C = 50% to C = 100%, the amount of ozone approximately doubles.

Other tests were carried out by bubbling ozone for different times in water bidistilled in order to calculate the ozone half-life time in water.

The amount of ozone dissolved in water increases with increasing ozone bubbling time (Fig. 29).

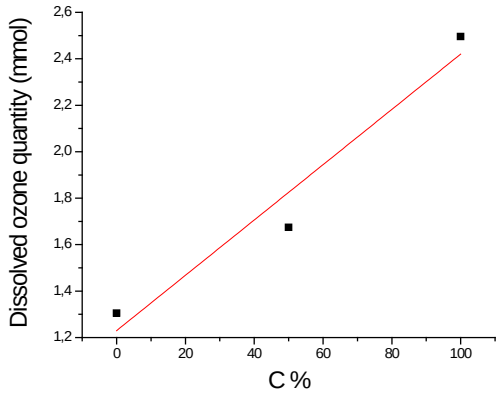

Figure 28: Quantity of ozone dissolved in water (mmol) VS set ozone concentration.

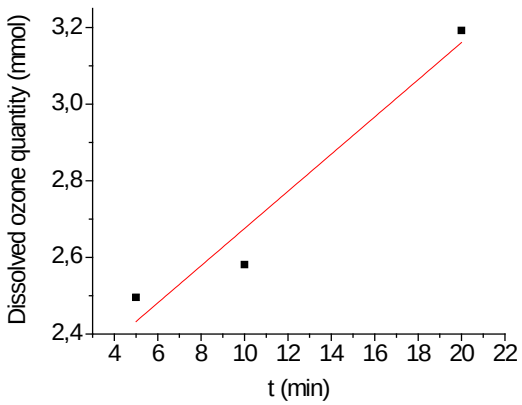

Figure 29: Dissolved ozone quantity in water (mmol) VS ozone bubbling time.

The ozone lifetime in water was calculated as well. Once recorded the UV-Vis spectrum of the water solution, in which ozone was bubbled for 10 min at maximum discharge voltage (100%), UV-Vis spectra of the same solution were collected at different times leaving the open cuvette exposed to the air.

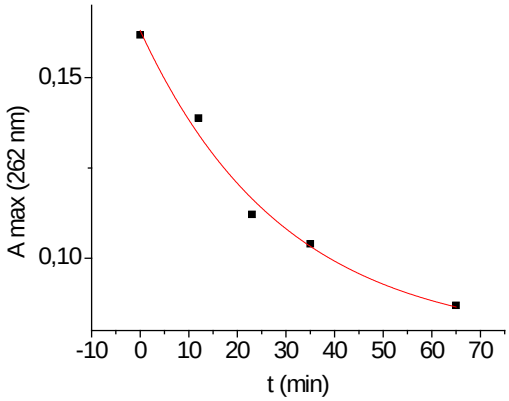

Figure 30: Absorbance decreasing of the band at 262 nm VS time.

In Fig. 30 it is shown the absorbance of the band at 262 nm as a function of the elapsed time between the first and the *n* measurement. The calculated ozone half-life is 20.50 minutes, matching very well the literature half-life value of 22 minutes. By means of the previous tests, the value of produced ozone grams per hour, corrected by a factor taking into account the ozone decay in water, was calculated. The value matches, within the experimental error, the one indicated in the ozonator handbook number (1000 mg / h).

5.3 Ozonation Chamber

The ozonation chamber (Fig. 31) is a stainless steel box (30 cm*10cm*20 cm) designed to host the paper samples to be ozonized. The choice of the material was based on the ozone high oxidative power. Stainless steel, Teflon and glass are the only type of materials that are inert towards ozone. The box is divided in two sections, one of which has a quartz window on the wall, which allows for the irradiation of the samples during the ozonation aging treatment. On the bottom of the box, two computer fans were installed in order to keep the ozone concentration constant and well-spread in the whole box. Two holes were created for the inflow of ozone and the outflow of non-reacted ozone and possible volatile by-products of the paper ozonation.

The cover of the box is a stainless steel lid: inwards, six hooks, made by stainless steel as well, were placed in order to hang the paper samples during the artificial aging.

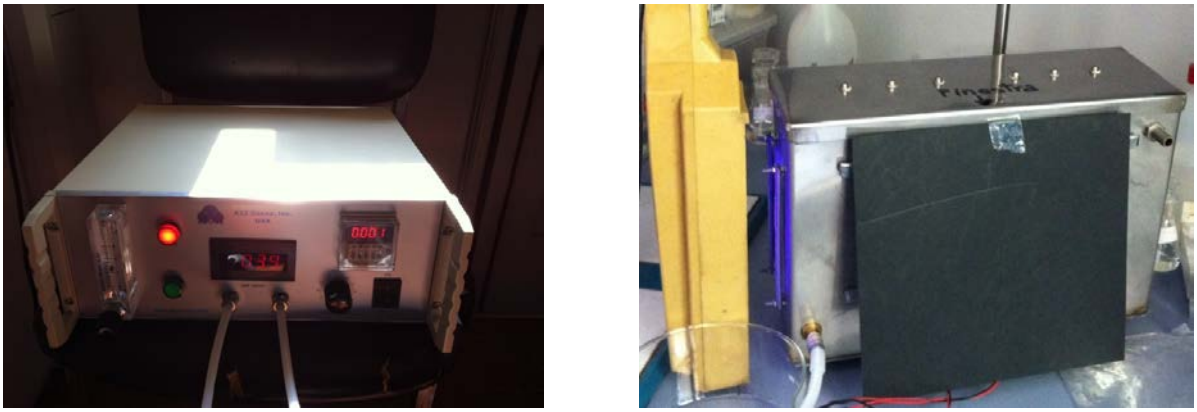

Figure 31: Ozonator (left) and ozonator chamber (right).

5.4 First tests

5.4.1 Sample description

Ozonation tests have been performed on two different types of samples:

- Whatman pure paper;
- Whatman pure paper covered by four layers of iron-gall ink.

Four paper strips were washed for two hours in MilliQ water, in order to wipe the impurities out, and they were left drying overnight. Two of them were painted with four layers of an Iron-Gall ink (natural iron-gall ink from oak galls, from Zecchi, Firenze) and let them dry overnight.

Before the treatment, a little piece of each sample was cut out to be used as reference.

The ozonation was performed in the ozonation chamber: a paper strip and a painted paper strip were hung in front of the quartz window, in order to expose them to UV light during the ozonation, while two others were hung in the other section of the chamber, far away from the lamp. The two parts of the ozonation chamber were divided by a black cardboard.

The set-up parameters are shown in the following table:

Table 12: Ozonation setting parameters.

Ozonation time	4 h
Oxygen flow	4 L/min
Lamp wavelength	366 nm

Table 13: Treatments and samples.

Treatments	Paper Sample names	Painted paper sample names
No treatments	Reference	Reference
Ozonation	Ozone	Painted paper ozone
Ozonation+irradiation	Ozone UV	Painted paper ozone UV
Ozonation+oven	Ozone oven	Painted paper ozone oven
Ozonation+irradiation+oven	Ozone UV oven	Painted paper ozone UV oven

After the treatment, each strip was divided in three pieces: one was kept in freezer, another one was placed in the oven at 105°C for one day and the last one has been exposed to the air at room temperature. In this way, 12 samples were obtained corresponding to all the possible combinations of treatment (Table 13) and were analyzed by means of EPR, FORS, ATR-IR and Raman measurements.

5.4.2 Spectroscopic analyses and results

5.4.2.1 UV-VIS fiber optic reflectance spectroscopy (FORS) results

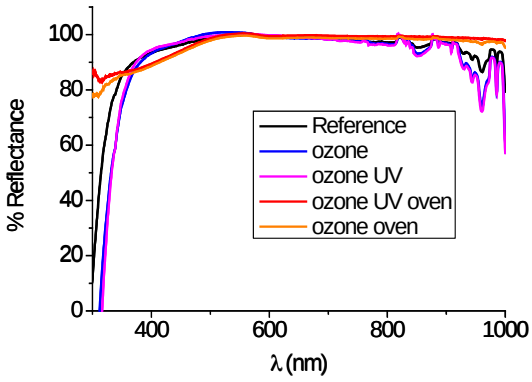

Figure 32: FORS spectra of Whatman paper before (black) and after the ozone (blue), ozone UV (pink), ozone oven (orange), ozone UV oven (red) treatments.

The ozonation and the synergistic action of ozone-UV seem to produce the same effect on the paper: both the FORS spectra show a depleted reflectance around 300 nm, which indicates the formation of carbonyl and carboxyl functional groups (Fig. 32). These groups could form on the cellulose, through oxidation at the carbons C_2, C_3 of the glucose ring, giving carbonyl groups, or through oxidation at the carbon C_6, to give carboxylic group. Also, strong oxidative degradation could result in the formation of LMMOA, also absorbing around 300 nm. After the oven treatments, a broad absorption band, more shifted towards the visible region, appeared. The reflectance decreases around 300 nm. The increased absorption in the visible suggest that the dehydration of the ozonized paper led to the formation of conjugate systems from the pure carbonyl and carboxyl groups already present on the oxidized papers. Furthermore, the

thermal treatment could induce decarboxylation or loss of LMMOA, decreasing the reflectance at 300 nm.

The dehydration in the oven induces changes in the UV-Vis absorption, reducing the reflectance around 300 nm (Fig. 32).

No differences can be appreciated from the comparison between the FORS spectra of painted paper ozone and painted paper ozone-UV samples (Fig. 33). In this case, the presence of ink prevents the observation of paper browning, and the visible region is not too much affected by the heating treatment (Fig. 34).

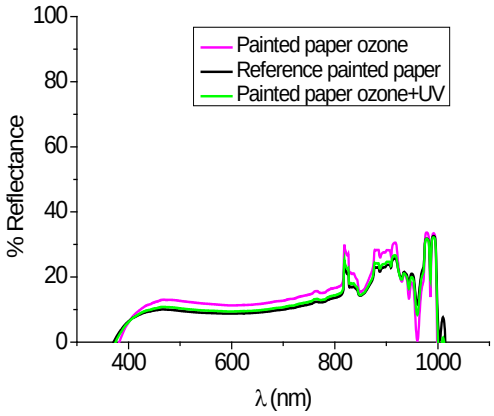

Figure 33: FORS spectra of painted paper before (black) and after the ozone (pink) and ozone UV (green) treatments.

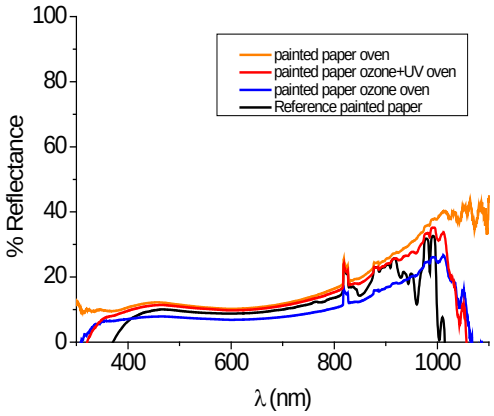

Figure 34: FORS spectra of painted paper before (black) and after the ozone oven (blue), oven (orange) and ozone UV oven (red) treatments.

5.4.2.2 IR results

The main differences in the IR spectra of the ozonized paper compared to the untreated fall in the 1500 –1800 cm^{-1} region (Fig. 35).

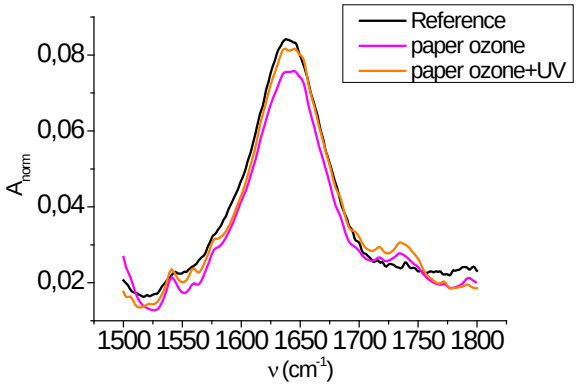

Figure 35: IR spectra of paper before (black) and after the ozone (pink), after ozone UV (orange) treatments.

A small peak at 1730 cm^{-1} is ascribed to COOH and CO groups, while the peak at 1536 cm^{-1} is assigned to conjugated carboxylates. Two small peaks at 1578 cm^{-1} and 1559 cm^{-1} are visible and attributable to carboxylates and α-hydroxyl-carboxylates.

The IR spectrum of the UV-ozonized paper shows the same bands we found in the simply ozonized one. After the treatment in oven, all the features produced by the ozonation and the irradiation disappeared or strongly decreased, as a result of decarboxylation and/or loss of LMMOA (Fig. 36). This is in agreement with the FORS data.

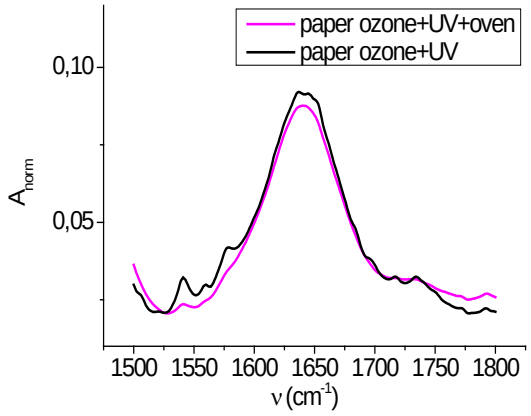

Figure 36: IR spectra of ozone UV (black) and ozone UV oven (pink).

Painted paper samples exhibit IR spectra with a strong signal around 1710 cm^{-1} attributable to carboxylic groups of the gall ink. All the IR spectra of the multiple samples show the growth of a band at 1538 cm^{-1} (Fig. 37), indicating the formation of conjugate carboxylates after ozonation. The strong bands at 1710 cm^{-1} and 1610 cm^{-1} also increases compared to the cellulose band at 1444 cm^{-1}, indicating formation of new carboxylic and carboxylate groups after ozonation in the various treatments. It is quite interesting to notice that after oven treatment no sensible change in the IR spectra is observed.

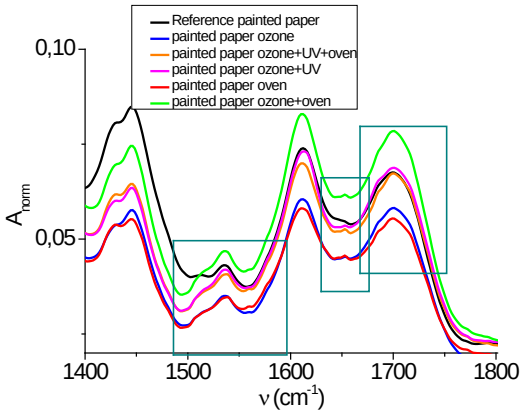

Figure 37: IR spectra of painted paper before (black) and after the ozone (blue), ozone oven (blue), oven (orange) and ozone UV oven (red) treatments.

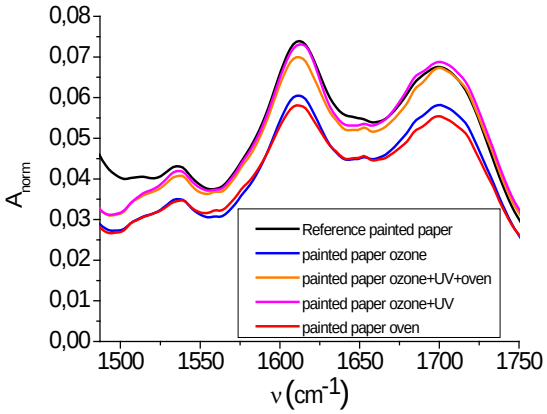

Figure 38: Zoomed section of the IR spectra of the multiple painted paper samples.

5.4.2.3 Raman results

All the treatments on paper samples gave rise to four different Raman signals at 1260, 1296, 1338 and at 1534 cm^{-1} (Fig. 39).The signal at 1338 cm^{-1} was present also in the reference paper, whereas the other signals increase after ozone treatment. The signal at 1534 cm^{-1} indicates the formation of C=C double bonds and/or carboxylates on the cellulose chains (Fig. 39). The other three peaks could be attributed to COH bending and Out-of-phase CCO stretching modes. Some differences could be identified in the comparison between the Raman spectra of *ozone UV* and *ozone UV oven* but they are not as great as the ones we found comparing the IR spectra of the two samples (Fig. 40). No differences have been shown by comparison of the Raman spectra of *ozone painted paper* and *ozone-UV painted paper* with the reference one (not reported here), but a further proof of the formation of conjugate structures on painted paper after the oven treatment could be found because all the samples of painted paper heated in oven show a high fluorescence, which is normally attributed to conjugate structures.

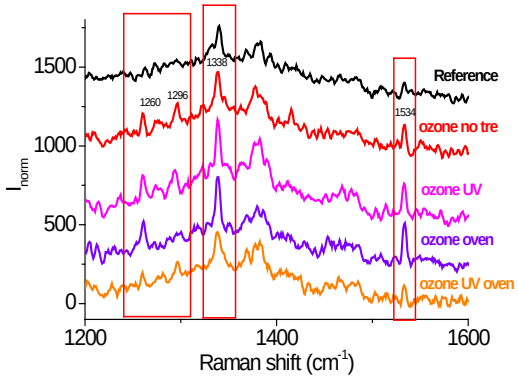

Figure 39: Raman spectra of the several samples.

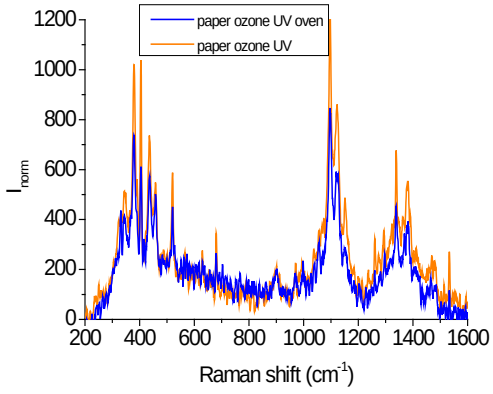

Figure 40: Raman spectra of ozone UV (blue) and ozone UV oven (orange).

5.4.2.4 EPR results of painted paper samples

The comparison between the EPR spectra of the painted paper before and after ozonation allows one to better understand the role of the oxidation in the type of iron complexes that formed. In Fig. 41A, the painted paper EPR (black) shows a weak signal of Fe(III) in rhombic site (around 1550 G) and a signal of Fe(III) in octahedral site (broad line around 3500 G), with a six-line Mn(II) superimposed signal. The octahedral component appears more relevant than rhombic one, suggesting that the Fe(III) form weakly coordinated complexes in the cellulose. After the ozonation, the EPR spectrum (red) shows an increased octahedral Fe(III)

component, probably due to the conversion of Fe(II)/Fe(III) by oxidation, but the rhombic Fe(III) signal does not increase. As previously explained, rhombic Fe(III) signal is assigned to strongly bound cellulose-Fe(III) complexes, and this suggests that ozonation does not lead (at least immediately) to the formation of this type of complexes. As a result of the simple heating treatment (Fig. 41B, black), the spectrum of the painted paper shows an increase in the component octahedral and perhaps a slight increase in the rhombic component, with respect to the untreated paper (Fig. 41A, black), using the Mn(II) signal as intensity reference.

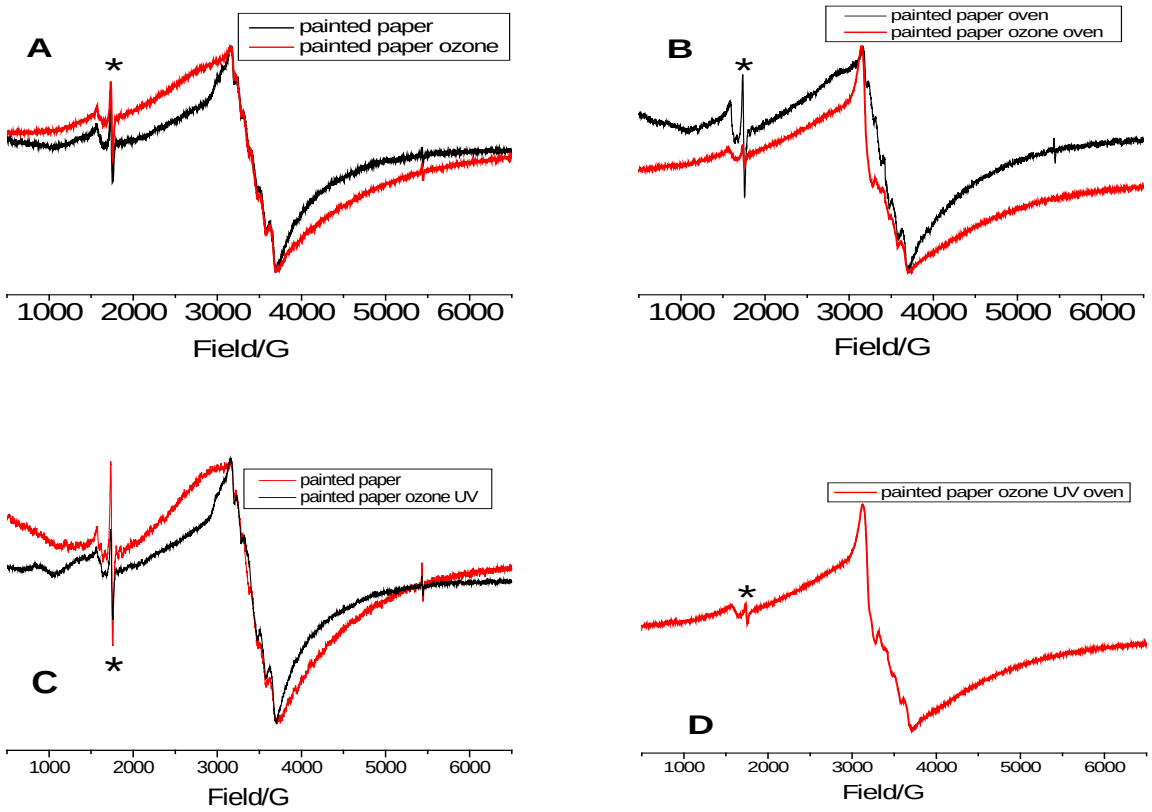

Figure 41: Comparison between EPR spectra of painted paper reference and painted paper ozone (A), of painted paper oven and painted paper ozone oven (B), painted paper reference and painted paper ozone UV (C) and EPR spectrum of painted paper ozone oven UV (D).The asterisk * indicates a background signal due to the probehead.

The spectrum of the ozonized painted paper after oven treatment shows a significant change in the spectral profile, with the appearance of a line rather narrow around 3100 G. This line, rather close to a g = 2.2, it is very likely attributable to small superparamagnetic particles of iron(III) oxide-hydroxide. Therefore, the ozonation combined with thermal heating led to the formation of these species. The ozonation could have led to the formation of ketons-Fe(III) complexes: these compound are known to be inclined to the cleavage or to the

decarboxylation once undergone to a heating treatment, causing the precipitation of minute particles of iron oxide (III) (hematite, limonite or other). To verify the formation of these species, a series of measurements on this material at lower temperatures should be run. After treatment with ozone and UV, the painted paper shows an EPR spectrum very similar to that obtained by simple ozonation (Fig. 41C), with an increase in the Fe(III) octahedral signal, and after oven treatment (Fig. 41D) a spectrum similar to that observed in Fig. 41C is observed. Therefore, also according to EPR, UV irradiation does not seem very effective.

5.4.3 Discussion of the results

The first ozonation tests have provided useful indications about ozone effect on paper: in particular, multiple analyses run on ozonized samples confirmed that ozone treatments induced the formation of several oxidation functional groups (carboxylates, α,β unsaturated carboxylic acids, α- or β-diketones, ketones and carboxylic acids), although the ozone treatment was not very effective, at least in the time span used (4 h). FORS suggests that a change of color occurs, indicating that unsaturated species formed on the cellulose chains, although this color change cannot appreciated visually. The action of ozone and UV rays produced the same effect as the simple ozonation on both Whatman paper and painted paper: probably the lamp (366 nm) used in this first test is too weak to break the O-O bonds of the ozone molecule. A decomposition of the ozone molecule and the consequent production of hydroxyl radicals could represent a key brick in the attempt of simulating the natural degradation of paper.

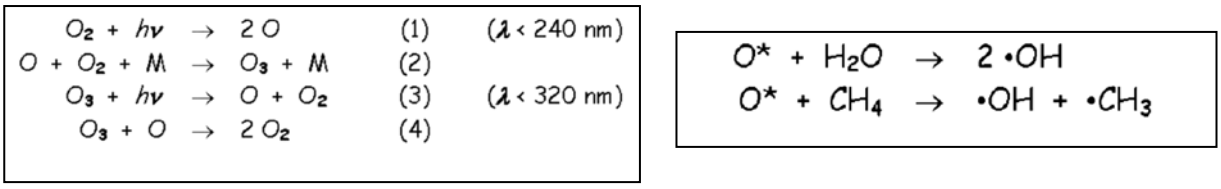

Figure 42: Mechanism for atmospheric ozone formation and destruction from oxygen species suggested by Chapman (left) and formation reactions of the OH• radicals (right).

The mechanical properties of the paper seemed not to change after the multiple treatments, while the painted paper were getting even more brittle after the sequential treatments.

The results suggest that the four hour-long ozonation and the one day long heating in the oven are not able to reproduce the effects of the natural paper aging reactions.

For the first time in literature, EPR spectra of iron-gall painted paper were acquired before and after ozonation and thermal treatments, in order to investigate the change in the Fe(III) signals. Just small changes were observed, and the degradation induced after the various ozone and thermal treatments did not seem to affect very much the Fe(III) rhombic signal, considered a marker for degradation, although paper was brittle and fragile. This prompted further EPR investigations on ozonized Fe(III)-doped Whatman paper, as described in the next section.

5.5 EPR investigations on Fe(III)-doped papers

Further studies have been focused on the effect of thermal and oxidative treatments on Whatman standard paper samples, undoped and doped with ferric sulfate solutions at different concentration and interesting results came out from this investigation.

Papers, doped with the highly-concentrated Fe(III) solutions and stored in the oven at 105°C for 24 hours, showed EPR radical signals, attributable to one or more cellulose radicals.

The same signals have been also detected in ancient paper in previous EPR studies.[37, 54-56] This aspect is particularly interesting because these species represent the main intermediates in paper oxidation reactions and therefore their study can provide useful information about paper degradation mechanisms.

In the recent years, much research has been carried out in this area, especially as regards the simulation of hydrolytic damage of paper leading to the depolymerisation of cellulose, taking no notice of the oxidative component and the oxidative-hydrolytic synergic effects, underpinning the autocatalytic mechanism of natural cellulose degradation. However, the oxidation and autoxidation reactions proceeding during the natural ageing of paper can become predominant in certain cases and therefore make these systems more complex and difficult to reproduce in the laboratory.[5-8, 50] In the last few years, much work has been performed in order to shed light on this class of reactions and on the reactive species, which promote and catalyze them. Many evidences have been collected on the role of reactive oxygen species (ROS) in the cellulose natural oxidation reactions, on their ability to induce paper radical reactions and to produce radical species in ancient papers.[9-13] In general, nowadays serious and complete studies of paper radicals and, in particular, of their correlation with the paper oxidation by-products are not present in literature. In this sense, further efforts have been done towards the optimization of an ozonation protocol, able to

reproduce the formation of these open-shell species on paper and to allow for a deeper study of their nature and their effect on the writing support.

5.5.1 Experimental section

18 samples of paper standards have been prepared and undergone various degradation treatments. Pure cellulose Whatman papers were cut in 1*1 cm^2 and immersed into 10^{-1} M EDTA solution, in order to wash out residual metal ions. They were rinsed with bidistilled water and left to dry for one night. They were divided into three groups and treated with ferric sulfate solutions at different concentration (Table 14).

An third of them underwent a 4-hour-long ozonation treatment, another third was placed in the oven at 105°C for one day and the last group did not undergo any ageing treatments. In the first two cases, after the treatments, the samples were stored in the freezer in order to stop any induced degradation process.

Paper samples have been analyzed by means of EPR techniques at different temperatures.

Table 14: Summarizing table of ozonized samples.

Doping solution concentrations (M)/ Treatments	No treatment	Thermal treatment	Ozone treatment
0	1	7	13
$1x10^{-1}$	2	8	14
$5x10^{-2}$	3	9	15
$1x10^{-2}$	4	10	16
$5x10^{-3}$	5	11	17
$1x10^{-3}$	6	12	18

5.5.2 Analysis results

5.5.2.1 Untreated Samples

At room temperature, Sample 2, the one with the highest amount of Fe(II), shows a gaussian-shaped signal (peak-to-peak width 100 mT) at 250-350 mT, typical of Fe(III) in quasi-cubic or pseudooctahedral symmetry and attributable to hydrated Fe(III) or Fe(III) weakly bound to cellulose (Fig. 43a). Overlapped to this signal, a narrower one appears (peak-to-peak width 20 mT) with a quasi Lorentzian shape ascribed to Fe(III) in a octahedral environment. In the other paper samples, the lower Fe(III) did not allow for the detection of Lorentzian signal,

while the Fe(III) guassian component is always present, getting narrow and changing its shape as a result of the concentration decrease.

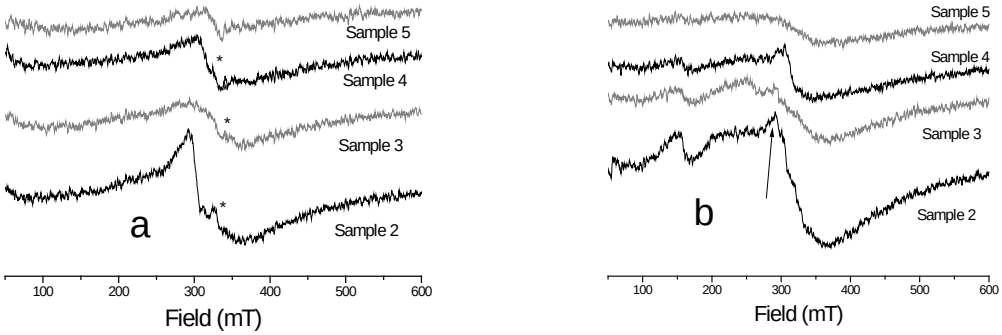

Figure 43: EPR spectra of unaged samples at 290 K (a) and at 200 K (b). The asterisk * indicates a background signal due to the probehead.

The Sample 2 EPR spectrum recorded at 200 K (Fig. 43b) shows an intensity increase of the Fe(III) rhombic component at 150 mT, while the pseudooctahedral signal exhibits a more anisotropic shape (broader at low field and narrower at high field). The narrower signal at 300 mT (indicated by the arrow), previously detected in the Sample 2 spectrum recorded at room temperature, appears in the EPR spectra of the other samples as well.

5.5.2.2 Thermally aged samples

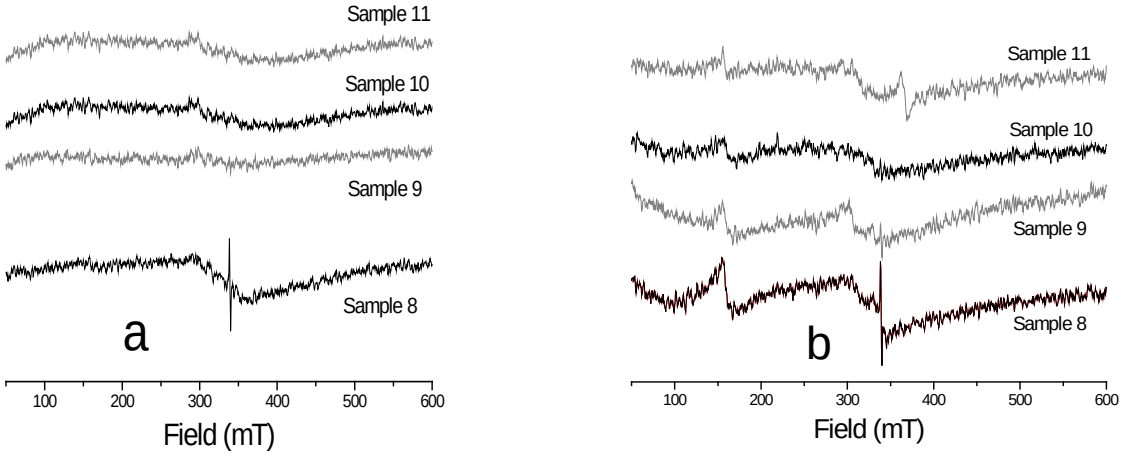

Figure 44: EPR spectra of thermally aged samples at 290 K (a) and at 200 K (b). The asterisk * indicates a background signal due to the probehead.

As a result of the thermal ageing, the octahedral, gaussian-shaped Fe(III) EPR signal strongly decreases (Samples 8-11, Fig. 44a). The narrow Lorentzian signal in the sample more

concentrated, sample 8, is no more present. The narrow signal, that appears only in the Sample 8 spectrum (339 mT, peak-to-peak width about 1 mT), is particularly interesting as it is due to the presence of one or more cellulose radicals.

In the spectra recorded at 200 K (Fig. 44b), a clear signal of Fe(III) in rhombic site appears simultaneously with a strong decrease in intensity of the pseudooctahedral Fe(III) signal. With the decrease of Fe(II) concentration, all the EPR signal intensities decrease, especially the rhombic Fe(III) one.

5.5.2.3 Ozonized Samples

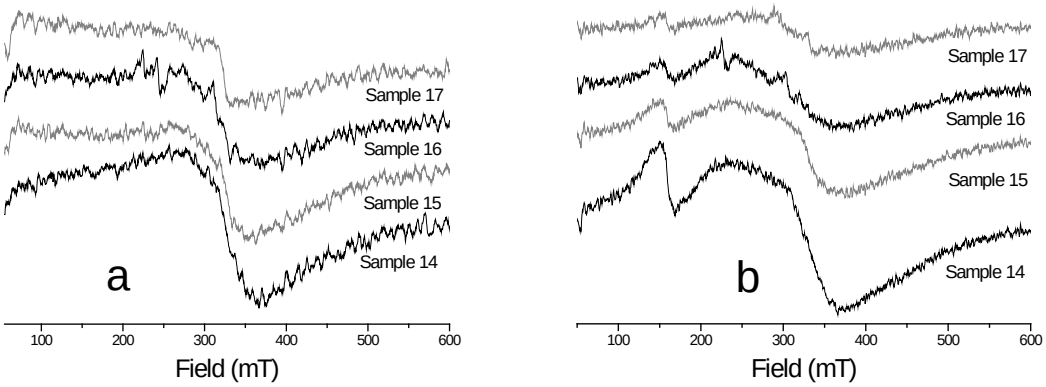

Figure 45: EPR spectra of ozonized samples at 290 K (a) and at 200 K (b). The asterisk * indicates a background signal due to the probehead.

The spectra recorded on ozonized samples at room temperature are dominated by a strong Gaussian component of Fe(III) in a pseudooctahedral site (Fig. 45a). With the decrease of the concentration, the signal intensity seems to reduce and the Gaussian line tends to get narrow and changes its shape. At 200 K, the Fe(III) line has a marked anisotropic shape, similar to the one detected in the EPR spectra of unaged samples, while the narrower component is completely absent (Fig. 45b). The signal attributed to Fe(III) in a rhombic site appears and it is more intense, than the one detected in the unaged samples.

5.5.3 Discussion of the EPR results on Fe(III)-doped papers

In spite of its simple components (basically water and cellulose), paper is a very complex material: its composition in terms of crystalline and amorphous regions, as well as its texture and morphology can also change within the same sheet of paper. Therefore, small changes in the spectra are also observed in samples obtained in apparently identical conditions. Taking

into account these limitations, the EPR study conducted so far, however, shows some interesting aspects related to Fe(III) signals in the paper samples. In the literature, EPR spectra of ancient papers, which has been recorded at a low temperature (140 K), are normally characterized by two main types of signal: the Fe(III) in a pseudooctahedral site and the Fe(III) in a rhombic site signals.

The first ones fall at 250-350 mT with a nearly Gaussian shape and are generally assigned to Fe(III) hydrate complexes or Fe(III)-cellulose complexes, where Fe(III) is weakly coordinated to the cellulose hydroxyl groups or to water molecules in pseudooctahedral complexes. The Gaussian shape is due, in this case, to the envelope of several signals of different width and position, which reflects the existence of several slightly different coordination sites.

The signal of Fe(III) in rhombic site falls at around 150 mT and it is assigned to Fe(III) strongly bound to cellulose.

The examination of EPR spectra recorded on the Fe(III)-doped and undoped paper samples, ozone and thermally treated, provides the following indications:

1) The signal of Fe(III) in rhombic site becomes evident only in the EPR spectra recorded at low temperatures and this phenomenon is likely due to spin-lattice and spin-spin relaxation processes. We can suppose that strongly bound Fe(III) complexes are characterized by a rigid structure, with a slow conformational dynamics on the EPR timescale, the so-called *slow-motion regime*. Increasing temperature increases the conformational dynamics and, in the slow-motion regime, this brings about line broadening, which involves EPR signal reduction. This effect explains why, in all the observed cases, the EPR rhombic signal increases on lowering temperature.

2) The signal of Fe(III) in octahedral site strongly decreases after thermal aging. This datum confirmed its assignment to Fe(III) ions weakly bound to water molecules and/or cellulose complexes: the loss of water caused by heating causes the disappearance of these complexes in favor of iron oxides, hardly visible because they give rise to very large EPR signals;

3) The Fe(III) EPR Gaussian signal in the samples decreases its line width and slightly change its shape on lowering the iron concentration. This is probably due to the distribution of Fe(III) octahedral complexes into a smaller number of more stable sites, which give rise to more structured and less broad signal;

4) At the lowest temperature (200 K), the water in the paper pores is frozen, and the complexes get blocked. In these conditions, the signal of Fe(III) in octahedral site assumes

the typical form of an anisotropic powder EPR spectrum, where the signal is the envelope of the EPR spectra due to complex blocked in all the possible orientations. This aspect could not be appreciated in the EPR spectra of ancient papers because this signal is normally overlapped to Cu(II) and Mn(II) signals.

This is also an indication that the octahedral Fe(III) complexes are quite mobile, probably involving one or more Fe(III)-water bonds.

5) After thermal aging, the EPR spectrum of the paper sample doped with the highest concentration of Fe(III), recorded at room temperature, shows a significant radical signal. This signal is not observed in the samples containing a lower amount of Fe(III) and this evidence indicates that Fe(II)/Fe(III) ions have a key role in the paper radical oxidation processes.

A Lorentzian-shaped signal appears in the spectrum of the most Fe(II)-concentrated unaged sample recorded at room temperature. Although its origin is not clear, it could be attributed to iron(III) oxide nanoparticles, which form likely when the Fe(III) ions exceed the number of the most stable coordination sites present in cellulose.

The narrow octahedral Fe(III) signal appears neither in the ozonized nor in the thermally aged samples. We can speculate that the oxidation induced by the ozonation caused the formation of functional groups capable of coordinating the Fe(III) ions, providing more cellulose sites, while thermal aging caused the growth of the oxide nanoparticles up to oxide microparticles, which results in a broader and undetectable EPR signal.

Chapter 6

6. Conclusions

In this work, the analysis of degradation by-products from ancient papers and the development of an innovative artificial ageing method were presented. The principle inspiring the work is that only a comparison between artificially and naturally aged paper by-products can provide, on one side, useful indications to set-up artificial ageing methods able to mimic the natural ageing, and, on the other side, to assess reliably the actual "health" state of paper document or book.

In the first part of the work, for the first time in literature, we demonstrated that wash waters obtained in routinely deacidifying treatments in book conservation workshops contain a large amount of degradation by-products and that their analysis provides a deep insight in the "health" condition of the book. The main by-products formed on the most damaged leaves of the "*De Divina Providentia*" were strongly oxidized and unsaturated cellulose oligomers, while the analyses performed on the water extracts of the non-degraded sheets have further confirmed and highlighted the protective role of the gelatin towards the paper over the centuries. The study has shed light on the role of metallic ions and gelatin size in the paper degradation processes, through a comparison of degraded and non-degraded leaves: this is a very special case where degraded and non-degraded leaves were present in the same book, therefore sharing the same fate, so that we can safely attribute the different conservation state to differences in the chemical composition of the leaves. Particularly, we observed an overall low amount of metallic ions in the Extract 3 together with a high content of hydrolyzed gelatin: low metal content and high gelatin sizing of these leaves could have cooperated in the preservation of the cellulose chain. In general, the differences in composition between the most degraded samples and the non-degraded ones suggest that the sheets, from which the analyzed solutions were extracted, belonged to different reams. This method and its analytical protocol could represent a fundamental step forwards in the field of the artificial ageing methods. The chemical and physical features detected by the application of the above-reported, wide range of techniques could make available specific indications, which will allow for a closer reproduction of the naturally aged conditions in artificial and accelerated ageing methods.

In the second part of the work, we proposed an innovative artificial ageing method base on ozone as trigger of oxidation: the method takes into account the literature results, which indicate ozone as the species able to reproduce the oxidative degradation by-products found in naturally aged papers. The first tests have shown that ozonation generates carboxyl and carbonyl functions, as observed in the paper natural ageing, and is able to induce decarboxylation processes, a type of reactions observed in ancient papers, as determined also by our study on the "*De Divina Providentia*" book leave extracts. For the first time, EPR measurements have been applied on artificially aged papers, providing interesting results, such as the occurrence of radicals in ozonized Fe(III)-doped papers. The interesting results obtained by the first ozonation tests represent only the beginning of a huge study, which will be complementary to the data already present in literature, aimed at investigating deeply the mechanism of paper degradation reactions.

New studies, which have been carried out on the ozonized Fe(III)-doped papers, will involve in future a multitechnique analytical approach: paper samples will be investigated by means of combined EPR and HPIC techniques. The crossing of the results will allow for a wider and more complete insight into the paper degradation mechanisms, establishing, for the first time in literature, the correlation between a specific class of paper by-products and the open-shell species, which promote their production.

Chapter 7

7. An Insight into the Metal Coordination and Spectroscopic Properties of Artistic Fe and Fe/Cu Logwood Inks

7.1 Introduction

Logwood inks are prepared basically by boiling heartwood chips from the tree *Haematoxylon Campechianum*, a species indigenous to Mexico, Central America, and the West Indies, mixing the decoction with a variety of inorganic salts such as $AlK(SO4)_2 \cdot 12H_2O$ or other alums, $FeSO_4 \cdot 7H_2O$, $Fe(NO_3)_2$, $CuSO_4 \cdot 5H_2O$, or K_2CrO_4, and adding a solution of dextrin or a gum as binding medium.[74-76] Gum Arabic was commonly added to give mixture fluid writing properties and keep particles in suspension. Even though it is known that the dyestuff from the logwood tree was already used by the Maya in pre-Columbian times for dying textiles and body painting, and its value as a dye for textiles was later discovered by the Europeans in the 16th century,[77] it is still uncertain when the first logwood ink formulations were developed. The presence of a logwood ink has been reported on a 18th century manuscript [78] and, in manuals from the second half of the 18th century, some recipes call for the addition of logwood extract to improve the coloring properties of iron-gall inks [75] that had been, for more than a thousand years, the material of choice for writing, along with carbon-based black inks. Iron-gall inks do not assume their full color intensity when freshly applied, and depending on the relative concentrations of the basic ingredients (gallotannic or gallic acids and an iron salt, usually $FeSO_4 \cdot 7H_2O$),[79, 80] it may take several hours, or even days until they became a deep brown or bluish black. This was an important shortcoming of iron gall inks; therefore colorants, such as logwood and indigo, were recommended in order to increase their chromatic intensity.[75] But rather than just improving the properties of iron gall inks, logwood inks found a place of their own among the artists' materials and writing inks. In a study of a group of drawings by Van Gogh, it was discovered that he did not use a 'traditional' iron-gall ink (as initially suspected on the basis of the visual appearance of these works of art), but rather relatively new formulations of logwood.[81, 82] The coloring matter of logwood in its native state is mainly in the form of the colorless compound *hematoxylin* (Htx, Fig. 46), which rapidly oxidizes to the red *hematein* (Hm, Fig. 46) when exposed to oxygen.[83, 84] The crude logwood extract has

been reported to contain, in addition to the main colorant, small amounts of a derivative of brazilein, quite larger quantities of five other, still unidentified, colorants, and large amounts of tannins.[77] Different inorganic salts are added to the logwood extract solutions to impart them certain hues. When combined with alum salts, the deep red Hm solution changes to a violet or deep violet-black; when $FeSO_4 \cdot 7H_2O$ is used it acquires a greenish shade that gradually changes to brownish-black or black upon drying; the hue is blacker when $CuSO_4 \cdot 5H_2O$ is used instead of an iron salt; K_2CrO_4 is reported to impart a black color.[75] These hues may be modified by changing the proportions of the ingredients mentioned above, or by adding others, such as acids and/or other metal salts. For example, a red ink can be obtained by mixing a solution of the logwood extract with alum, copper acetate, dextrin, and small amounts of H_2SO_4.[74, 75]

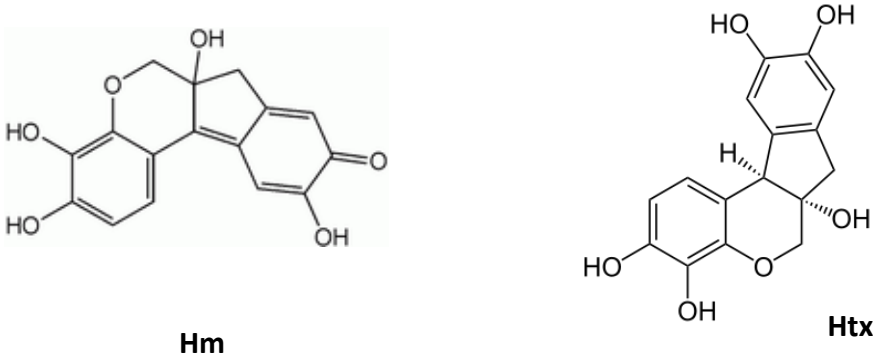

Hm **Htx**

Figure 46. Hematein (Hm) and hematoxylin (Htx) molecules structures.

A group of inks have been prepared following historic recipes found in early manuals and have been characterized by several techniques in order to determine the coordination environments of the different metallic ions in the colorants and in order to ascertain whether the complexes, as powders and as applied on the papers substrates mixed with a binder, have different structures.

Their solutions were analyzed by means of UV-Vis and EPR spectroscopy, while the powders obtained by their evaporation and the ink applied on paper substrates were characterized by a combination of FTIR, Raman, FTRaman, EPR and ESI-MS techniques.

7.2 Experimental

7.2.1. Sample preparation

Three logwood inks were prepared for the present study: Fe logwood (FL), Fe logwood with oxalic acid (FLO), and Fe/Cu logwood (FCL). For the ink FL, 3 g of logwood chips (Aurora Silk) in 50 ml of water were boiled for one hour. The solution was left to cool down and it was then filtered. 3 g of $FeSO_4 \cdot 7\ H_2O$ (Fisher Scientific) and 1,5 g of Arabic gum (Sigma-Aldrich) were added to 60 ml of an 8% acetic acid solution (vinegar was recommended in the historic recipe), and this solution was mixed with the logwood chips filtrate and then filtered.

The FLO ink was prepared by dissolving 2 g of logwood extract (Aurora Silk) and 3 g of ferrous sulfate (Fisher Scientific) in 40 ml of water. The solution was heated up to 70°C for 30 minutes. After cooling down, 10 g of sodium carbonate (Aldrich Chemical Company, Inc.) and 2 g of oxalic acid (Aldrich Chemical Company, Inc.) were added. The solution was filtered and 1.5 g of Arabic gum (Sigma-Aldrich) were added to the filtrate. After a second filtration step, the ink was ready for use. For the FCL ink, 6 g of logwood chips (Aurora Silk) in 40 ml of water were boiled for one hour. The resulting solution was left to cool down and it was filtered. 3 g of ferrous sulfate (Fisher Scientific), 0.75 g of copper sulfate (Fisher Scientific), 1.5 g of Arabic gum (Sigma-Aldrich) and 0.75 g of sugar were added to the filtrate, and the resulting solution was filtered.

The freshly prepared FL and FCL inks had a black grey color that became brighter when applied on Whatman® filter paper and dried, while the FLO ink had a dark blue hue that became lighter when it was applied on the Whatman® filter paper and dried.

7.2.2. Spectroscopic analyses: FTIR, UV-Vis, Raman, EPR, and ESI-ToF

The powders obtained by evaporating the inks in a Petrii dish and the inks applied on Whatman® filter paper were characterized by FTIR using a Bruker Vertex70® spectrometer coupled to a Hyperion® microscope.

The samples were mounted between the windows of a diamond anvil cell and observed in the transmission mode with a spectral resolution of 4 cm^{-1}.

The UV-Vis spectra of the ink solutions in solvent were acquired in a Varian Cary 50 Bio UV/visible spectrophotometer. This analysis was used to confirm the occurred ink formation.

Raman spectroscopy measurements were carried out using a Renishaw System 1000 coupled to a Leica DM LM microscope. A 785 nm laser excitation was used for the inks applied on

paper, and a 514 nm laser was employed for analyzing the ink powders. The two lines were focused on the samples using a 50x objective lens. A 1200 lines/mm grating was used in conjunction with the 785 nm laser excitation, and a 1800 lines/mm grating was employed with the 514 nm excitation; a thermoelectrically cooled CCD detector was used, with integration times between 10 and 40 s.

Continuous-wave electron paramagnetic resonance (EPR) spectra of the ink solutions and of the inks applied on paper were acquired on a Bruker ER200 instrument, equipped with a TE102 probehead. The microwave frequency was set at about 9.5 GHz, the modulation amplitude at 0.2 mT and the microwave power at 2 mW. The spectra of the inks applied on paper were recorded at room temperature. The spectra of the pure ink solutions were acquired at 200 K, where the ink solutions are frozen in a glassy phase, since at room temperature no EPR spectrum of the liquid inks could be detected, due to the fast tumbling of the iron(III) complexes, leading to a strong line broadening. The EPR spectra at 200 K of the inks applied on paper were similar to the corresponding EPR spectra at room temperature, and therefore we report in this work only the latter ones.

Mass spectra were recorded using an electrospray ionization source (ESI-ToF) operating in the positive-ion mode with a PerSeptive Biosystem Mariner instrument (Framingham, MA).

1 ml of 10^{-2} M ink solution (this concentration is approximate and it was estimated based on the amount of $FeSO_4.7H_2O$ used in each ink recipe) was diluted with 500 µl of MeOH. The mobile phase used was a 1:1 acetonitrile-water solution with 0.1% formic acid. For the assignments of the m/z values to possible chemical structures, the factors considered were the m/z values, the hematein structure, and the presence or absence of the isotopic Fe and Cu peaks since the concentrations used were high enough to allow for the detection of these peaks and differentiate them from the background noise.

7.3 Results and Discussion

7.3.1. Fe logwood ink (FL)

ESI-MS revealed that the main components are complexes of Fe(II) with catechols and bicyclic compounds,[85] formed by the breakdown of the hematein (Hm) macromolecules whose peak at 301 m/z was not detected. These species are similar to the ones contained in iron gall inks, Fe(II)-pyrogallates. These are unexpected results, so additional experiments were performed in order to better understand at which point of the ink preparation the Hm

break down to the catechol and bicyclic species occurred. The assignments of the FL ink mass spectrum, acquired using electrospray ionization (ESI-MS), are listed in Table 15, and the structures of the different species are shown in Fig. 47.

By comparison, solutions containing only logwood chips were prepared and, respectively, heated (70°C) and boiled; ESI-MS spectra of these solutions were recorded. These solutions showed a red coloration, typical of Hm aqueous solutions before heating. The main peak in the mass spectra of both samples was observed at 301.08 m/z (Fig. A1 and A2 in Appendix A), confirming the presence of Hm as the main component. Immediately after the addition of $FeSO_4 \cdot 7H_2O$, the mass spectra of both samples revealed the Hm breakdown (Fig. A3 and A4 in Appendix A), as observed for the FL ink (Fig. A5 in Appendix A)

Table 15. Assignments of the ESI-MS m/z values observed for the ink FL. See Fig.47 for the assigned fragments.

Fragments	m/z value	Possible attribution	Calculated m/z value
I	182,985	$[M+H]^+$	182,892975
II	196,9972	$[M]^+$	196,908625
III	234,9446	$[M+H]^+$	234,892375

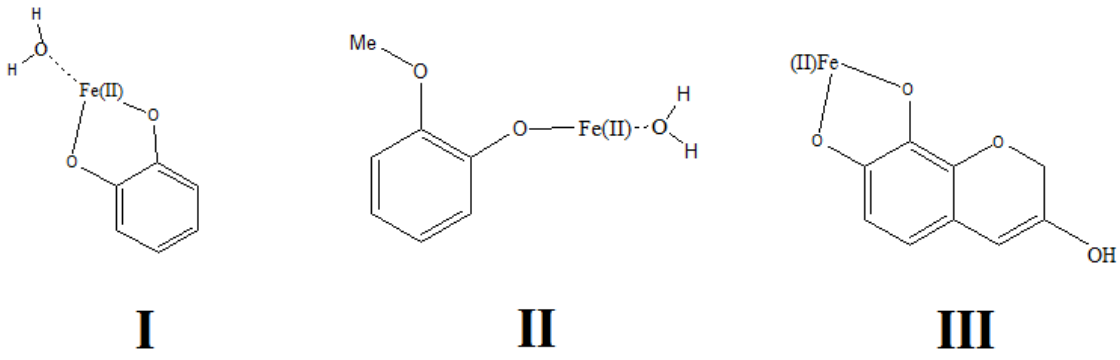

Figure 47. Proposed structures assigned to the ESI-MS peaks listed in Table 15.

Upon the addition of $FeSO_4 \cdot 7H_2O$, the color of the solution resulting from boiling the logwood chips turned brown and the color of the one resulting from heating the chips was similar to that of the brown-black FL ink. Therefore, it is possible to conclude that the addition of $FeSO_4 \cdot 7H_2O$ during the ink preparation, rather than the increase of temperature,

is responsible for the breakdown of the Hm leading to the formation of catechol and of bicyclic Fe(III) complexes.

The EPR spectra performed on the ink applied on paper and of the liquid ink (respectively Fig. 48a and 48b) confirmed the presence of Fe complexes. The EPR spectrum of the ink on paper (Fig. 48a) shows a broad asymmetric signal at *ca.* 3250 G that has been attributed to Fe(III) complexes in a pseudosymmetric environment, i.e. Fe(III) complexes that have a pseudooctahedral symmetry. This feature has been observed in hydrated Fe(III) or weakly bound Fe(III) complexes.[54-56] The sharp signal, expected at ca. 1580 G (g=4,3) for Fe(III) in a distorted (rhombic) environment and that usually occurs in paper for Fe(III) strongly bound to a matrix, is very weak in this spectrum.

In the EPR spectrum of the pure ink, which is in glassy phase at the measurement temperature of 200 K (Fig. 48b): the signal due to Fe(III) in an octahedral environment is still visible, but the line assigned to distorted Fe(III) at *ca.* 1580 G is strongly increased with respect to the sample on paper. This effect is mainly related to the distortion induced on the iron(III) complexes by the frozen solvent, and the general profile of the EPR spectrum it is typical for iron(III) complexes in glassy phase.

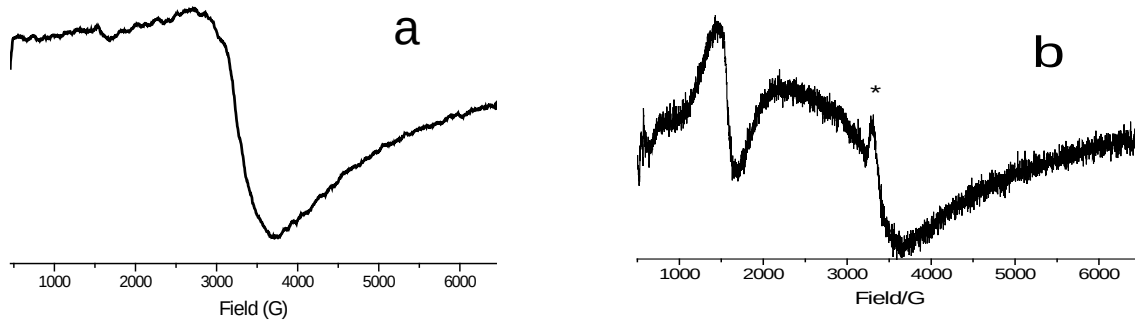

Figure 48. EPR spectra at room temperature of the FL ink applied on Whatman filter paper (a) and the EPR spectrum at 200 K of the pure ink (b). The asterisk * indicates a background signal due to the probehead.

Raman and FTIR spectra were acquired not only to complete the chemical characterization of the compounds but also to create reference spectra that can be used for the identification of the inks in works of art, particularly in a non-invasive manner by Raman spectroscopy.

In the FTIR spectrum of the FL ink powder (Fig. 49a) two broad bands are present at *ca.* 1643 and 1092 cm^{-1} respectively. The first band has contributions from the antisymmetric stretching of carboxylic acids, alkene ν(C=C) stretching, aromatic ν(C=C) stretching, ν(C=O) stretching, C–H bending, ring bending, water O-H bending, while the second feature is due to

ν(C-O) stretching of secondary alcohols, ν(C–C) stretching, C–H bending, and SO_4^{2-} vibrational modes.[86-88] The residual ferrous/ferric sulfate contributes to the absorptions at *ca.* 1092 cm^{-1} and at 976 cm^{-1}.[89] The weak peaks in the region between 1500-1300 cm^{-1} suggest the presence of residual Hm inside the ink (Fig. 49c). The ν(Fe-O) frequencies are expected in the 606-645 cm^{-1} range but they are not visible in the recorded spectra.[47]

The Raman spectra characteristic of the complexes in Al logwood inks were previously reported and assigned assuming to be due to Hm complexing Al(III) ion.[90] Although the ESI-MS data indicated the breakdown of Hm molecules and the formation of Fe(II)/Fe(III) cathecol complexes, the assignment of the FL ink powder Raman spectrum (Fig. 50a) was based on the comparison with the pure Hm powder (Fig. 50c) and Al Logwood ink Raman spectra (Fig. 50b). Indeed, the functional groups complexing the Fe ions in the ink were the same of the catechol and bicyclic compounds composing the hematein original molecule (species I, II, and III in Fig. 47).

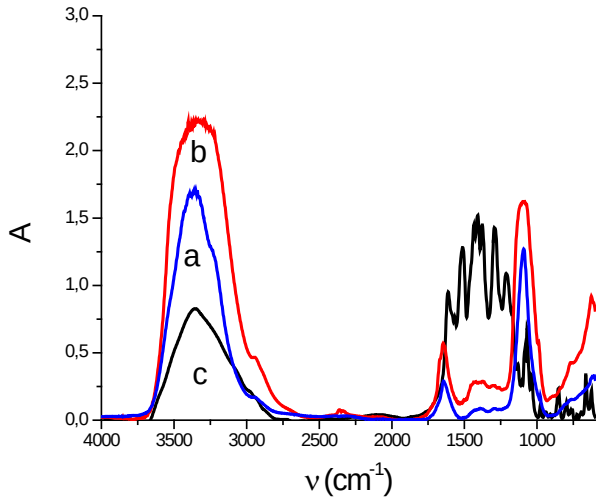

Figure 49. FTIR spectra of FL (a) and FCL (b) ink powder and Hm (c).

With respect to the Hm Raman spectrum, the lower frequency of the bands assignable to the cyclic and/or bicyclic rings, C=C,C-O and COH functional groups and the Fe-O features in the fingerprint region of the ink spectrum confirm the formation of the Fe complexes.[86, 91-94] The Raman spectrum shows medium strong signals at 1434, 1386 and 1339 cm^{-1}. By overlaying the two spectra, the peak at 1339 cm^{-1} could be attributed to the COH bending mode of the unreacted Hm still present in the ink, while the other two bands could be assigned to the several vibrational modes of acetate/acetic acid.

In the low-frequency region, the Raman spectrum of FL ink powder shows bands at 498 cm^{-1}, at 574 cm^{-1}, at 627 cm^{-1} and at 709 cm^{-1}. Lee and others studied the iron gall ink Raman spectra: they indicated the broad band, due to multiple peaks, at 500-620 cm^{-1} as one of the major characteristic peaks of those samples. The Raman spectrum of the yellow ochre pigment, made by FeO(OH) and calcite, shows a band at 556 cm^{-1} as well.[95, 96] Xia et al. applied the Raman technique to the study of Fe(III)-Phenolate Complexes and they assigned the band at 643 and 896 cm^{-1} to the Fe-O stretching.[97] This attribution was also confirmed by DFT calculations.

Therefore, the bands observed in the FL ink powder could be assigned to convolution of bands attributed to Fe-O and Fe-C stretching and aromatic ring deformation modes, which fell in the same region (472 and 538 cm^{-1}).[33, 49, 93, 98, 99]

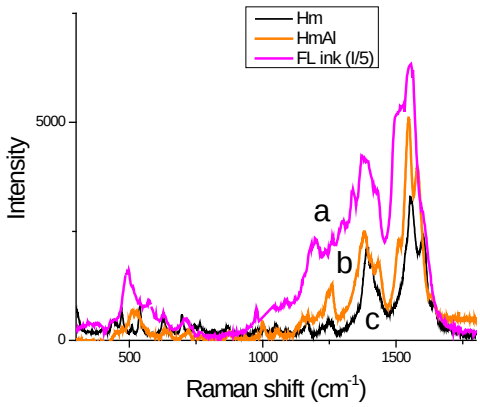

Figure 50. Raman spectra of Fe logwood ink powder (a), Al Logwood ink (b) and Hematein (c).

The ink signals were identified also in the Raman spectra of painted paper covered by 4 ink layers (Fig.A8 in Appendix A), particularly in the regions where Raman bands of paper are not present:

- 450-800 cm^{-1}: the strong bands at 580 and 715-736 cm^{-1} were assigned to the Fe-O stretching;
- 1200-1400 cm^{-1}: the strong signal at 1338 cm^{-1} was assigned in the ink spectrum to the COH bending;
- 1500-1600 cm^{-1}: the bands at 1497, 1541 and 1607 cm^{-1} were assigned to C=O and aromatic C=C stretching.

The four layers painted paper Raman spectrum show clear and strong ink signals. In particular, the interaction between the ink and the paper seems to enhance the intensity of

the bands attributed to Fe-O stretching and it causes a shift of the bands assigned to C=O and aromatic C=C vibrational modes.

The ability to identify the ink signals on the paper support is useful from an historical and conservational point of view. Raman reveals itself as a not destructive, sensitive and selective technique useful for the identification of inks in the works of art.[90, 100]

7.3.2. Fe/Cu logwood (FCL) ink

The EPR spectra acquired in the FCL ink are completely different from the spectra of FL ink. The EPR spectrum of FCL ink applied on paper shows the typical features of dispersed Cu(II) complexes: a four line pattern at low field (so-called "parallel region") characteristic of Cu(II) complexes in well-defined sites (Fig. 51a).[54-56] From these results, it is possible to deduce that Cu(II) is bound to the organic matrix, while the bound Fe(III) signal is not visible in this spectrum. The spectrum of the pure ink in glassy phase at 200 K is dominated by the typical Cu(II) signal, as well (Fig. 51b).

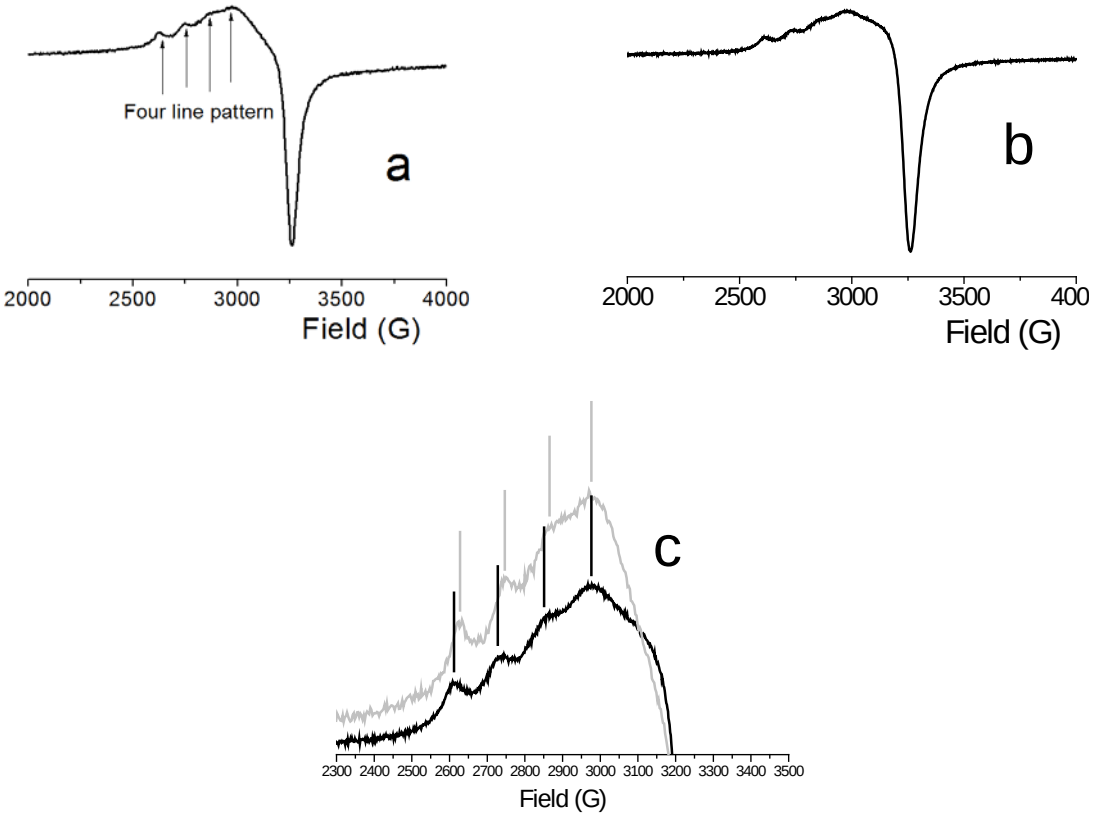

Figure 51. EPR spectra of the Fe/Cu (FCL) logwood ink applied on Whatman® filter paper at room temperature (a) and of the same, pure ink at 200 K (b). Detail of the four line pattern range in the spectra a and b (c).

EPR is a valuable technique to assess coordination around Cu(II), and has been widely applied to characterize Cu(II) sites in proteins, due to its non-invasive and non-perturbative features. Blumberg and Peisach have shown that the so-called parallel region, i.e. the four lines observed at low fields, indicated by arrows in Fig. 51a are very sensitive to coordination of copper.[101] These authors provide diagrams (B-P diagrams) that relate the position and distance of these four lines to the type of atoms coordinated to the copper center. The position of the line quartet is given by the parallel g-factor, g_{par}, whereas the distance between lines is given by the parallel hyperfine constant A_{par}.

When the four line pattern of the ink applied on paper (Fig. 51a) and that of the liquid ink (Fig. 51b) are compared it is possible to see that the position and distance between the lines in the pattern are similar for both samples (a detail of the relevant range is shown in Fig. 51c). This is a very important piece of information because, as stated above, this region is very sensitive to coordination changes, and clearly indicates that the Cu(II) complexes are similar in the liquid ink and in the ink applied on paper.

Through a simulation it is possible to estimate the parameters A_{par} = 150 x 10^{-4} cm^{-1} and g_{par}=2.41. According to the B-P diagrams, these values characterize doubly charged Cu(II) complexes (i.e., the ligands around Cu(II) are neutral) with a 4 O configuration, i.e. the equatorial ligands are OH groups. The overall spectrum is not like the expected one for pure copper aquo complexes, therefore we assign tentatively the spectrum to Cu(II) complexes with OH ligands from components of the mixture and water.

The formation of Cu(II) complexes is also confirmed by the ESI-MS results (Table 16 and the structures proposed for the fragments observed Fig. 52): the ESI-MS results show the presence of Cu(II) complexes with catechol rings in the ink (Fig.52, structure II), together with the Fe(II) complexes (Fragments I and III), also observed in the mass spectrum of the Fe logwood ink (Fig. A6).

The FTIR spectrum recorded for the FCL ink (Fig. 49b) is similar to that of the FL ink (Fig. 49a), as it shows weak peaks in the range between 1500 and 1300 cm^{-1}, suggesting the presence of residual Hm in the ink (Fig. 49c), a broad band at 1643 cm^{-1} with a shoulder at 1670 cm^{-1}, probably due to the presence of a second metal ion species, and another broad band at 1088 cm^{-1}. The ferrous and copper sulfates contribute with their vibrational modes to the bands at 1261 cm^{-1} and at 1088 cm^{-1},[89] while the glucose bands may enhance the intensities of the band at 1435, 1088 and 989 cm^{-1}.[88]

Table 16. Assignments of the ESI-MS m/z values observed for the ink FCL. See Fig.52 for the assigned fragments.

Fragments	m/z value	Possible attribution	Calculated m/z value
I	182,9852	$[M+H]^+$	182,892975
II	189,977	$[M+H]^+$	190,598975
III	234,9474	$[M+H]^+$	234,892375

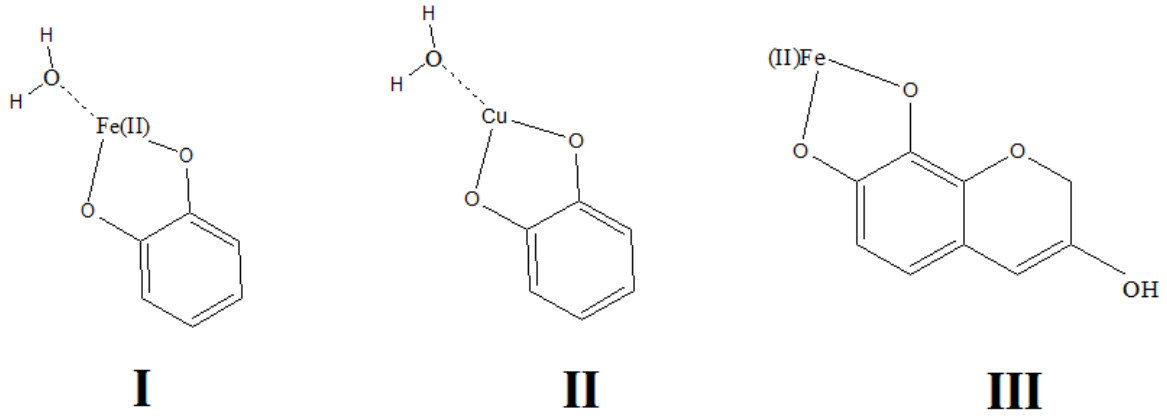

I II III

Figure 52. Proposed structures assigned to the ESI-MS peaks listed in Table 16.

The Raman spectrum of the FCL ink powder (Fig. 53a) resembles that of the FL ink discussed above, with just some minor differences. The main difference could be found in the finger print zone: a narrow and sharped peak appear at 395 cm^{-1} and the band at 495 cm^{-1} is more intense and sharper than the same one in the Raman spectrum of FL ink. Nakamoto and others attributed the bands at 420 and 541 cm^{-1} in the mooloite Raman spectrum, the bands at 291 and 451 cm^{-1} in the $Cu(acac)_2$ Raman spectrum and the band at 360 cm^{-1} in the Cu-glycine complex to Cu-O stretching.[98] Frost and others assigned the band at 558 cm^{-1} to the Cu-O stretching in the mooloite Raman spectrum.[102] All blue and green Cu based pigments (Azurite, Malachite and Brochantite) show bands around 400 cm^{-1} in their Raman spectra.[103-106] Therefore, it could be possible to attribute the band at 395 cm^{-1} to the Cu-O stretching or at least it could be a marker of the presence of copper inside the ink. Unfortunately, the other Cu-O vibration modes bands are covered by the iron signals. Iron amount used in the ink preparation is higher than the copper one: the iron signals are expected to be more intense than the copper one. However, the band at 495 cm^{-1} is more shaped and intense in FCL ink Raman spectrum: this evidence could indicate that the Cu-O

stretching signal contributes to the shape and the intensity of this band. Glucose presents medium strong Raman signal at 400 cm^{-1}, a strong one at 543 cm^{-1} and a medium weak one at 651 cm^{-1}, as well, so it is possible that the bands at 395 cm^{-1} and the particular shape of the band at 495 cm^{-1} could be due to the presence of sugar as well.[107] The bands in the region between 1500 and 1700 cm^{-1} (Aromatic C=C and C=O stretching) show the same lower wavenumbers shift, already found in the Raman spectra of the FL ink. Glucose Raman bands also contributes to the large peak at 1374 cm^{-1} and to the peaks around 1200 cm^{-1}.

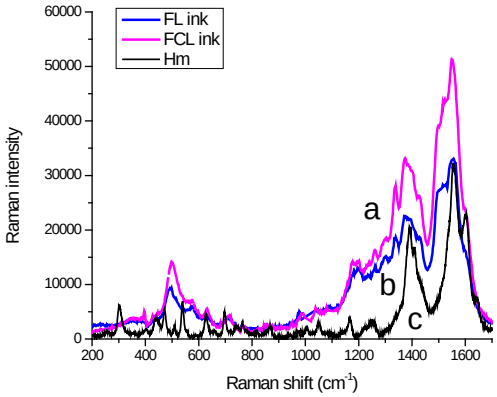

Figure 53. Raman spectra of FCL ink powder (a), FL ink (b) and Hematein (c).

Also in this case, the Raman spectrum of four-layer painted paper shows clearer and stronger ink signals (Fig. A9 in Appendix A) in the low-frequency region. As seen in the Fe logwood ink, the interaction between the ink and the paper seems to enhance the intensity of the bands attributed to Fe-O stretching.

7.3.3. Fe oxalate logwood (FLO) ink

The EPR spectrum acquired in the FLO ink applied on Whatman® paper shows similar signals to those discussed in section 3.2 for the ink FL (Fig. 54a): the sharp signal at 1580 G (g=4,3), attributed to Fe(III) in a distorted environment, and the broad asymmetric signal at 3250 G attributed to Fe(III) complexes in a more symmetric environment, i.e. Fe(III) complexes close to octahedral symmetry, and related to hydrated Fe(III) or weakly bound Fe(III) complexes. However, the signal at 1580 G appears to be much stronger in the FLO ink than in the ink FL, whereas the octahedral signal is weaker in the FLO ink than in the ink FL.

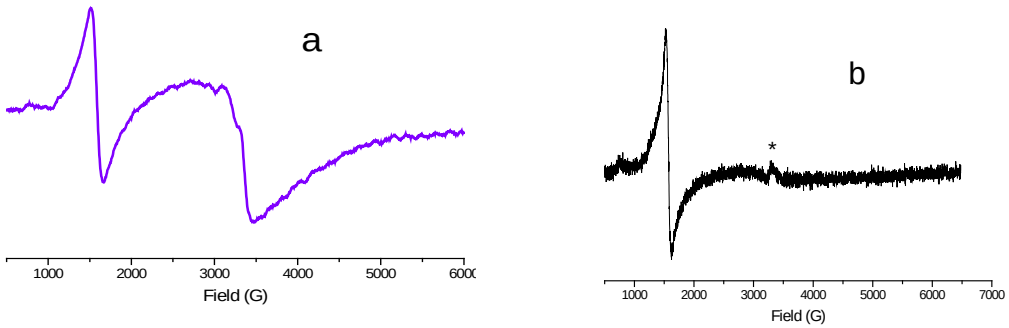

Figure 54. EPR spectra at room temperature of the FLO ink applied on Whatman filter paper (a) and the EPR spectrum at 200 K of the pure ink (b). The asterisk * indicates a background signal due to the probehead.

In the spectrum of the pure FLO ink (Fig. 54b) in glassy phase at 200 K, the signal due to the rhombic Fe(III) is sharper and stronger than for FL ink, whereas the one corresponding to octahedral Fe(III) has almost disappeared, compared to the FL one.

On the base of the general consideration that Fe(III) strongly bound to the ligands gives rise to a sharp and strong signal at 1580 G, these results indicate that in the FLO ink the Fe(III) is more strongly bound to the ligands than in the ink FL. Likely, the difference between the two inks could be due to the presence of oxalates and probably oxalates-Fe complexes, because both inks are similar except for the addition of oxalic acid.

Table 17. Assignments of the ESI-MS m/z values observed for the Fe oxalate logwood ink. See Fig. 55 for the assigned fragments.

Fragments	m/z value	Possible attribution	Calculated m/z value
I	126,0042	M^+	126,04515
II	167,0223	$[M+H]^+$	167,084275
III	171,9976	$[M+Na]^+$	172,058995
IV	235,009	$[M+H]^+$	234,892375

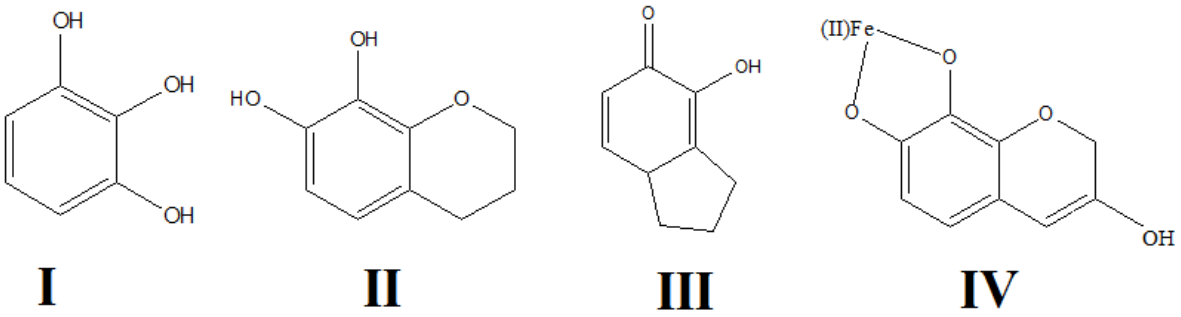

Figure 55. Proposed structures assigned to the ESI-MS peaks listed in Table 17.

The presence of a high salt content, in particular oxalates, affected the ESI-MS measurements. Indeed, the interference of the salts did not allow us to acquire the mass

spectrum of the ink in both the ion polarities. For this reason, the ink was titrated with a $CaCl_2$ solution to remove the oxalate species and, after this, the mass spectrum of the ink was recorded (Fig. A7 in Appendix A). The proposed assignments of the mass spectrum peaks are reported in Table 17 and in Fig. 55. The main peaks can be attributed to bicyclic compounds, the Hm component rings that could complex Fe(II) ions. In particular, the pyrogallol (a) was identified among the components of the ink. This compound was already found by Bettinger as a fragment in the Hm mass spectra.[84]

By the comparison between the FT-IR spectra of the pure Hm and of the FLO ink powder (Fig. 56), it is possible to deduce that the most part of the Logwood extracts, used in ink preparation, reacted with the ferrous sulfate, forming the respective complex. The spectrum shows also the formation of ferrous and ferric oxalate, due to the addition of oxalic acid to the ferrous sulfate and Logwood extract mixture.[49]

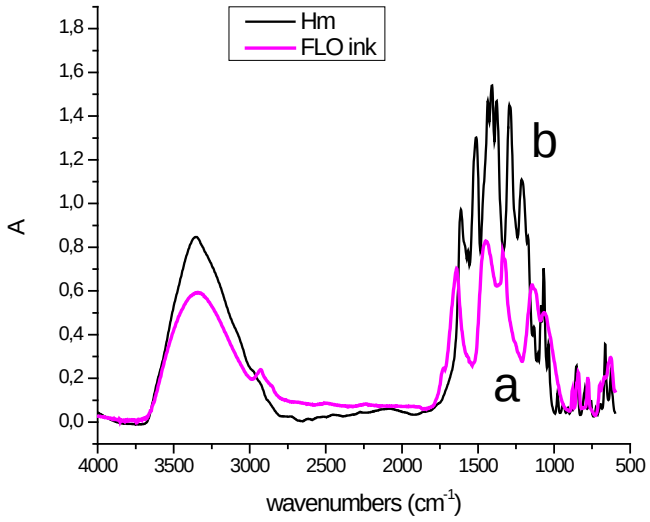

Figure 56. FTIR spectra of FLO (a) and Hm (b).

The bands assigned to Fe-O (539, 574, 628 cm^{-1}) and Fe-C stretching in the Raman spectrum of FL ink powder (Fig. 57b) are clearly present in the Raman spectrum of FLO ink powder, as well (Fig. 57a), confirming the attribution. Also for this ink, the four layers painted paper Raman spectrum shows clearer and stronger ink signals (Fig. A10 in Appendix A).

The bands in the region between 1500 and 1700 cm^{-1} (aromatic C=C and C-O stretching) fall at the same frequency as those detected in FL ink Raman spectrum. A band at 1079 cm^{-1} is visible in the Raman spectrum of the FLO ink on paper, completely lacking in the Raman spectra of the other two samples. This band could be attributed to Arabic gum C-C and C-O-C

stretching modes.[108] In the low-frequency region of the spectrum of FLO ink on paper (Fig. A10 in Appendix A) a medium strong band at 746 cm^{-1} is visible, attributable to Fe-O oxalate stretching

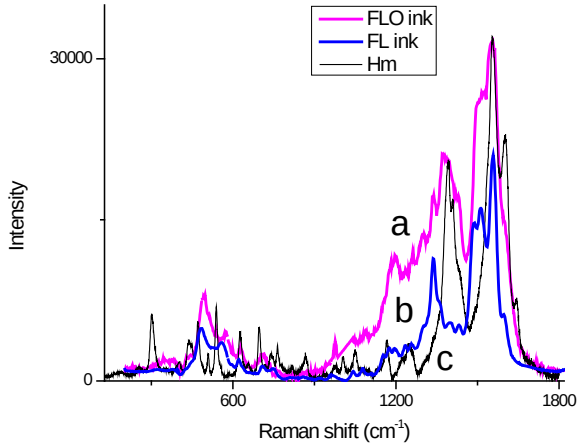

Figure 57. Raman spectra of Fe oxalate logwood (FLO) ink (a), Fe logwood (FL) ink (b) and Hm (c).

The presence of Fe(II)/Fe(III) oxalates could be deduced also by the peak at 1437 cm^{-1}, particularly strong in the FLO ink painted paper.[49] Other oxalate bands could convolve to the bands at 484-562, at 710-752 cm^{-1} and at 1597 cm^{-1}, making them broaden and increasing their intensity. Oxalate bands at 900 cm^{-1} and the Raman peaks of ferrous sulfate and ferrous/ferric sulfate (respectively at 1025 and 980 cm^{-1}) are completed hidden by the aromatic ring deformation bands.[108] The peak at 484 cm^{-1} could be a convolution of bands attributed to aromatic ring deformation modes, oxalate modes and to the Fe-O stretching.[33, 49, 93, 98, 99]

7.4 Conclusions

The multi-technique approach carried out on the Fe and Fe/Cu inks sheds light on the coordination environment of the metallic ions in the colorant matrix, allowing us to better understand the structure of the complexes responsible for the ink colors. Unexpected results were obtained by the ESI-MS analyses: for the first time in literature, MS analysis of Logwood inks has demonstrated the breakdown of Hm molecules during the ink preparation, as just complexed cathecols and/or byciclic compounds were identified as the main component of the three inks. These chemical species are very similar to the ones, which compose the iron gall inks: the Fe(II)/Fe(III)-pyrogallates.

On the other hand, the UV-VIS and FT-IR spectra provide a first indication of the occurred complexation of the metallic ions by the coloring Logwood organic matter, while the Raman spectra show that the coordination of the metallic ions takes place through the carbonyl and hydroxyl groups in the molecule, and that the aromatic rings are also involved in the interaction. EPR confirms the ESI-MS analysis results, giving information about the coordination environment of the metal ions. In this work, it turns out, together with ESI-MS, as the only technique, among the applied ones, that can provide a unique outline for each ink.

Another ink, which was deeply studied but whose data are not reported here, is a Chromium based ink. It is very interesting, as well, because Van Gogh used likely a Cr- based ink for his drawings. The confirmation of this hypothesis is the presence of Cr detected by the XRF measurements carried out on some of them.

The painted paper samples, already characterized by the multiple spectroscopic analyses reported above, will undergo to three different artificial ageing treatments: we will apply the ozonation degradation method, we have been already applying and developing on paper, and the Scientific Department of the MET will use means such us fade-ometer and controlled R. H. Chamber.

In this way it will be possible to compare the results obtained from the different artificial ageing method with the spectroscopic data already collected on the works of art in order to figure out which method is the one that better simulates the degradation of the ink once applied on paper, which reactions Van Gogh's drawings have been undergoing and which conservation treatment could be the best for their restoration and their preservation.

Appendix A

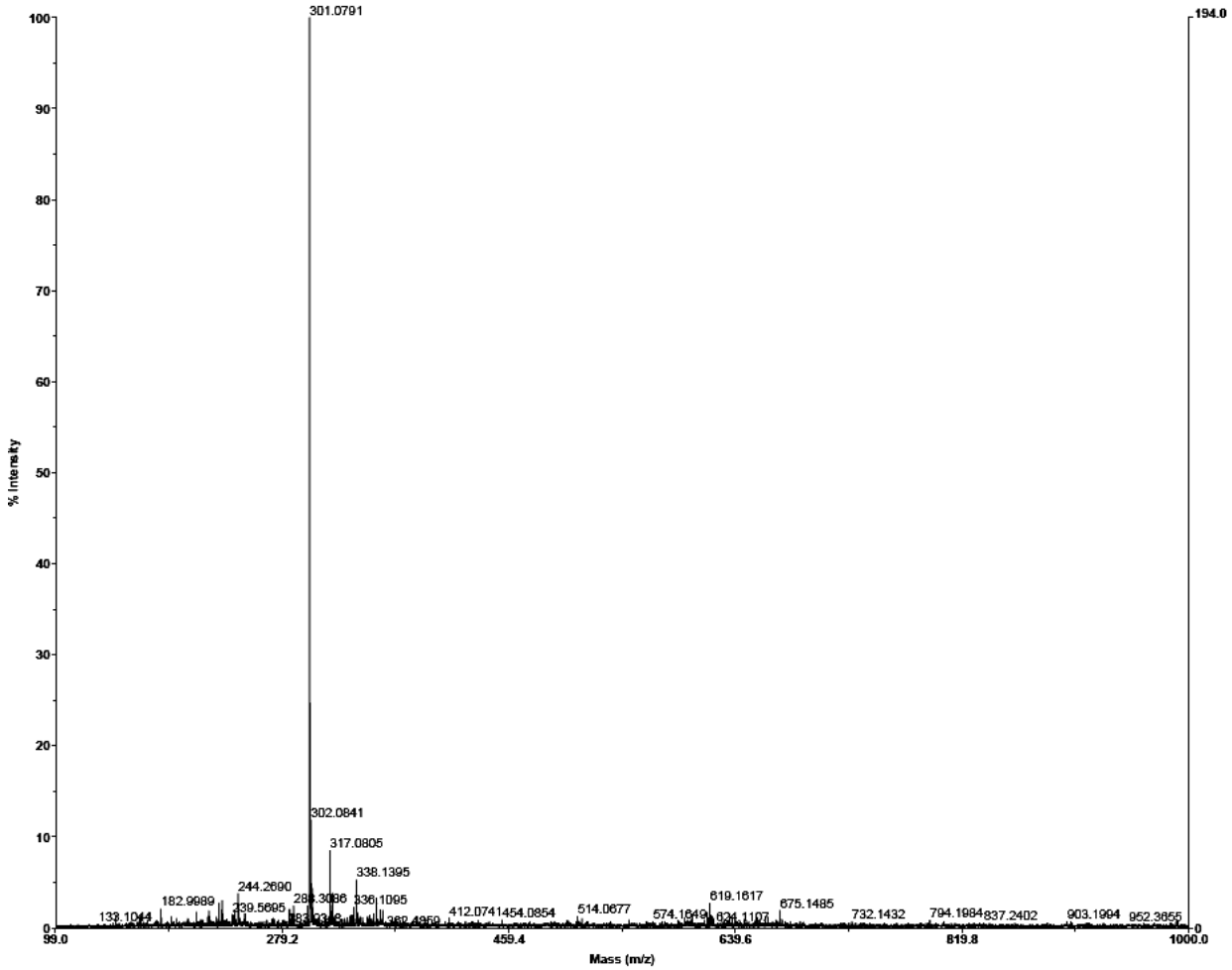

Figure A1. ESI-MS spectrum of boiled logwood chips solutions.

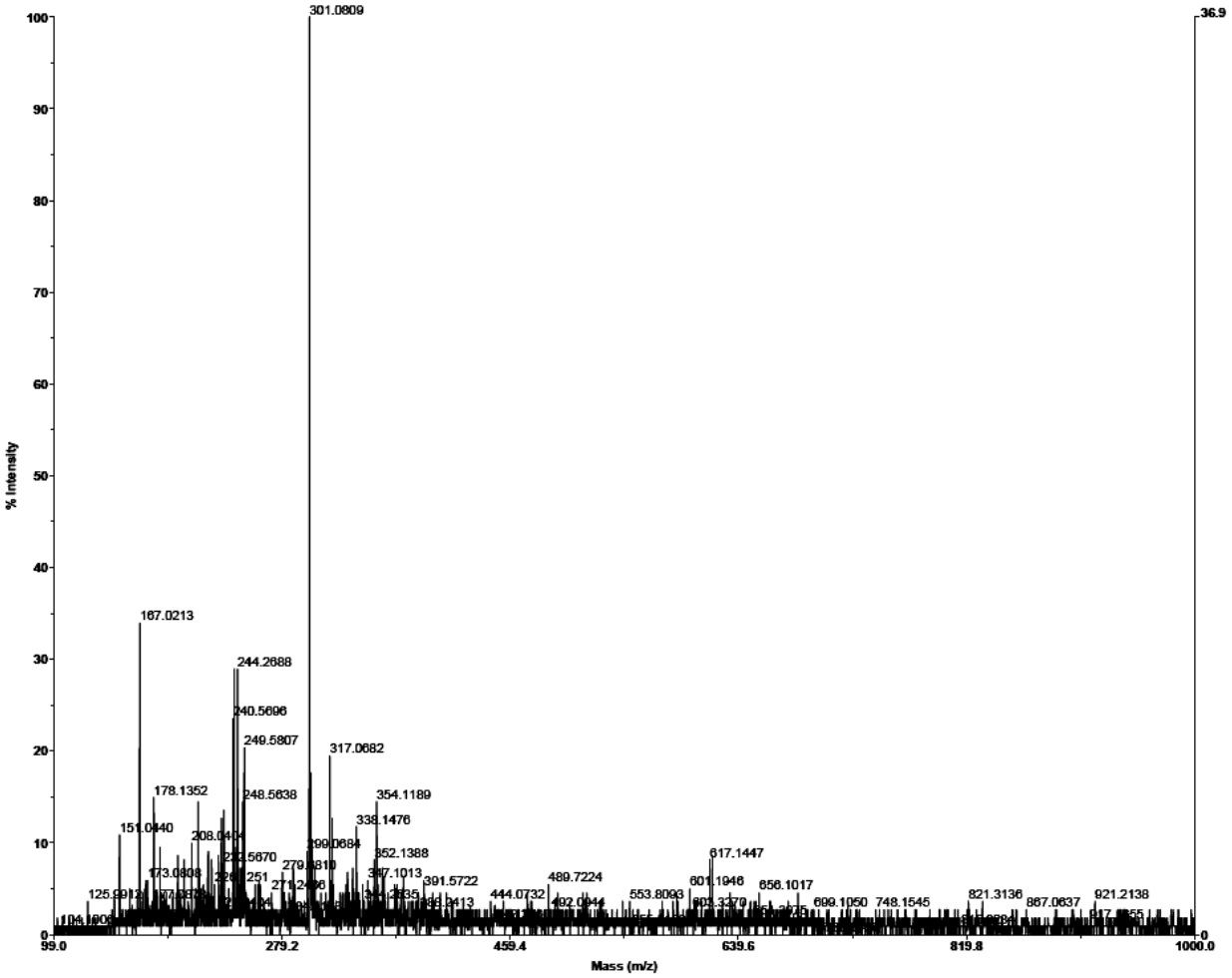

Figure A2.ESI-MS spectrum of heated up to 70°C logwood chips solutions.

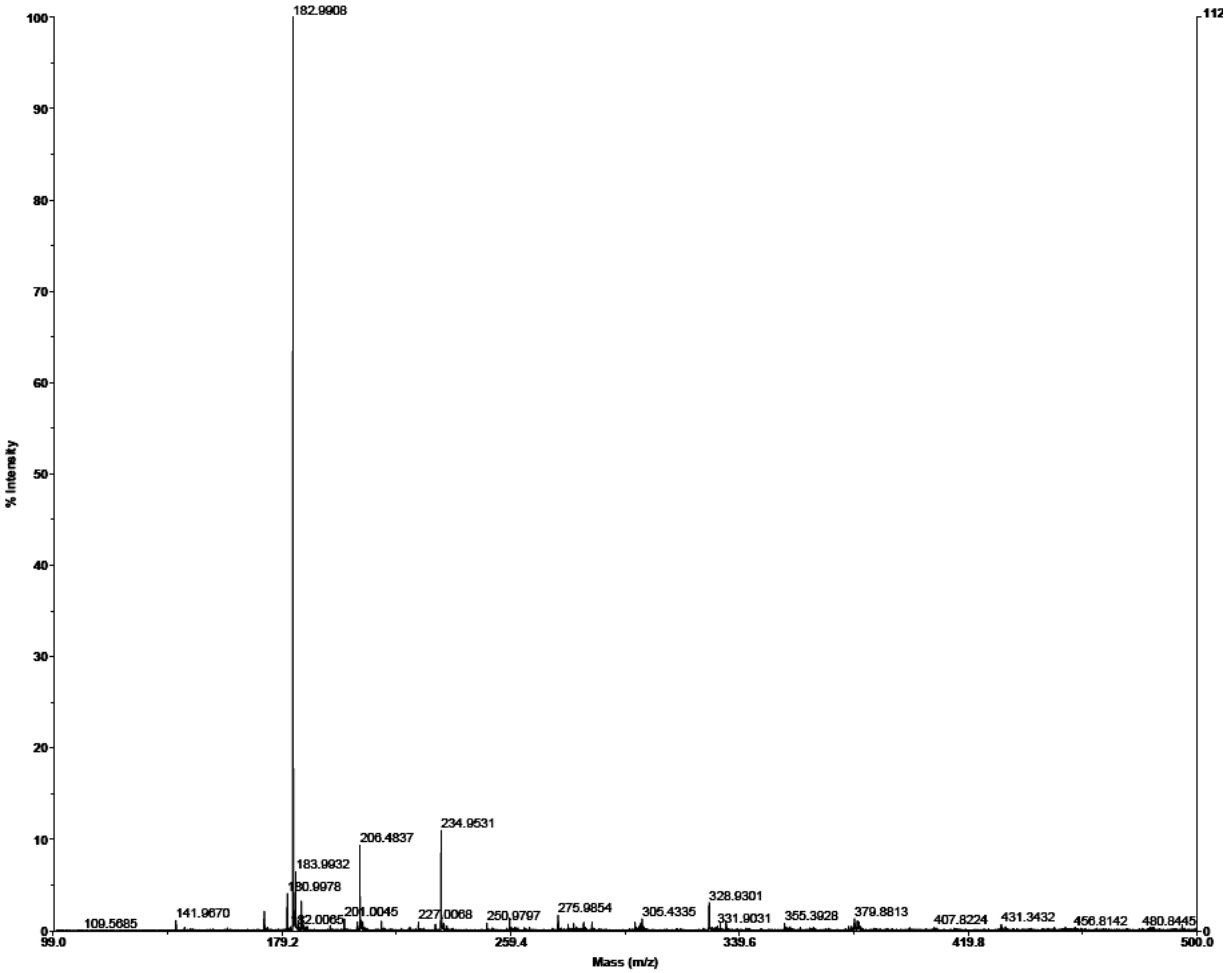

Figure A3.ESI-MS spectrum of boiled logwood chips solutions after the addition of $FeSO_4 \cdot 7H_2O$.

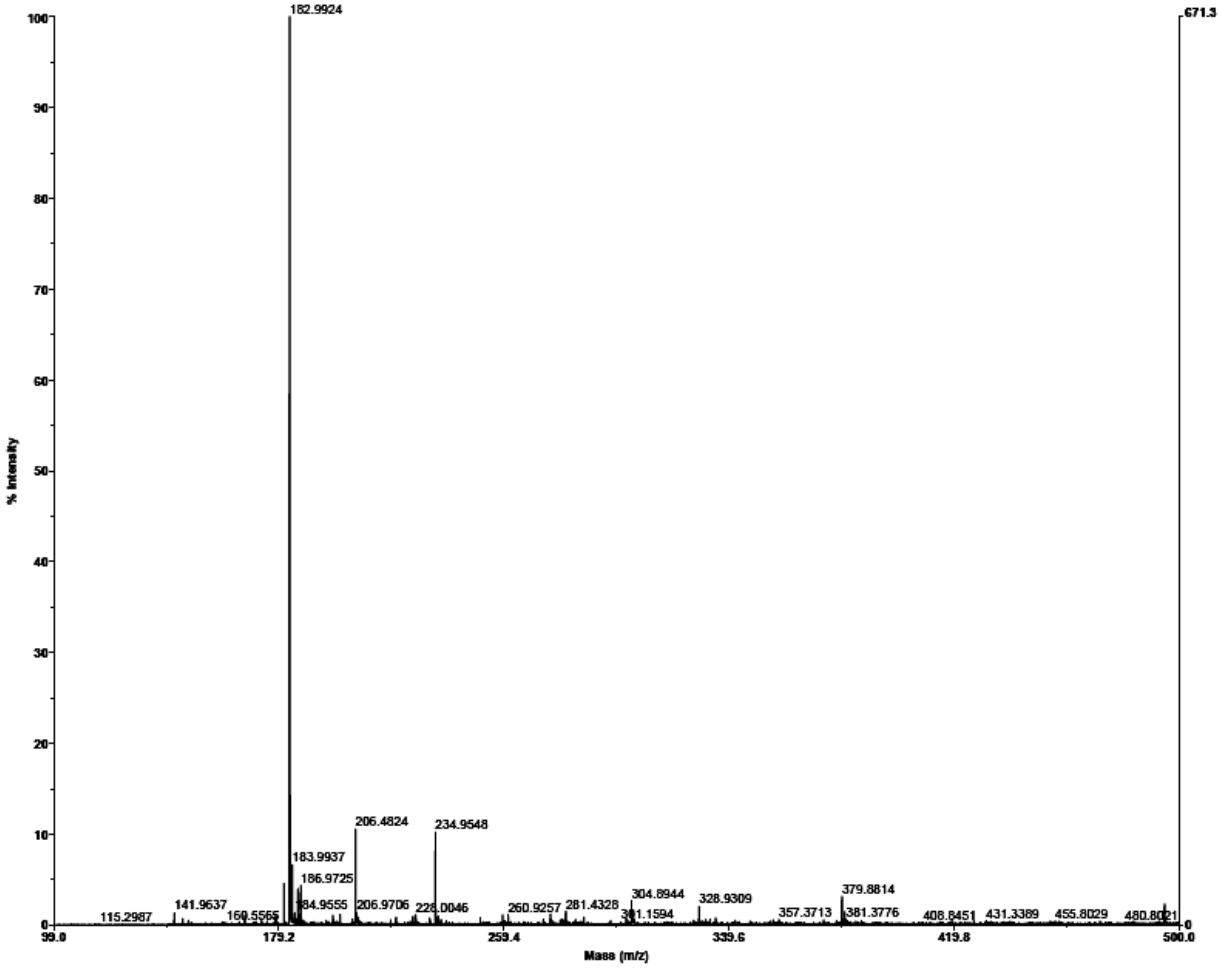

Figure A4. ESI-MS spectrum of logwood chips solutions heated up to 70°C after the addition of $FeSO_4 \cdot 7H_2O$.

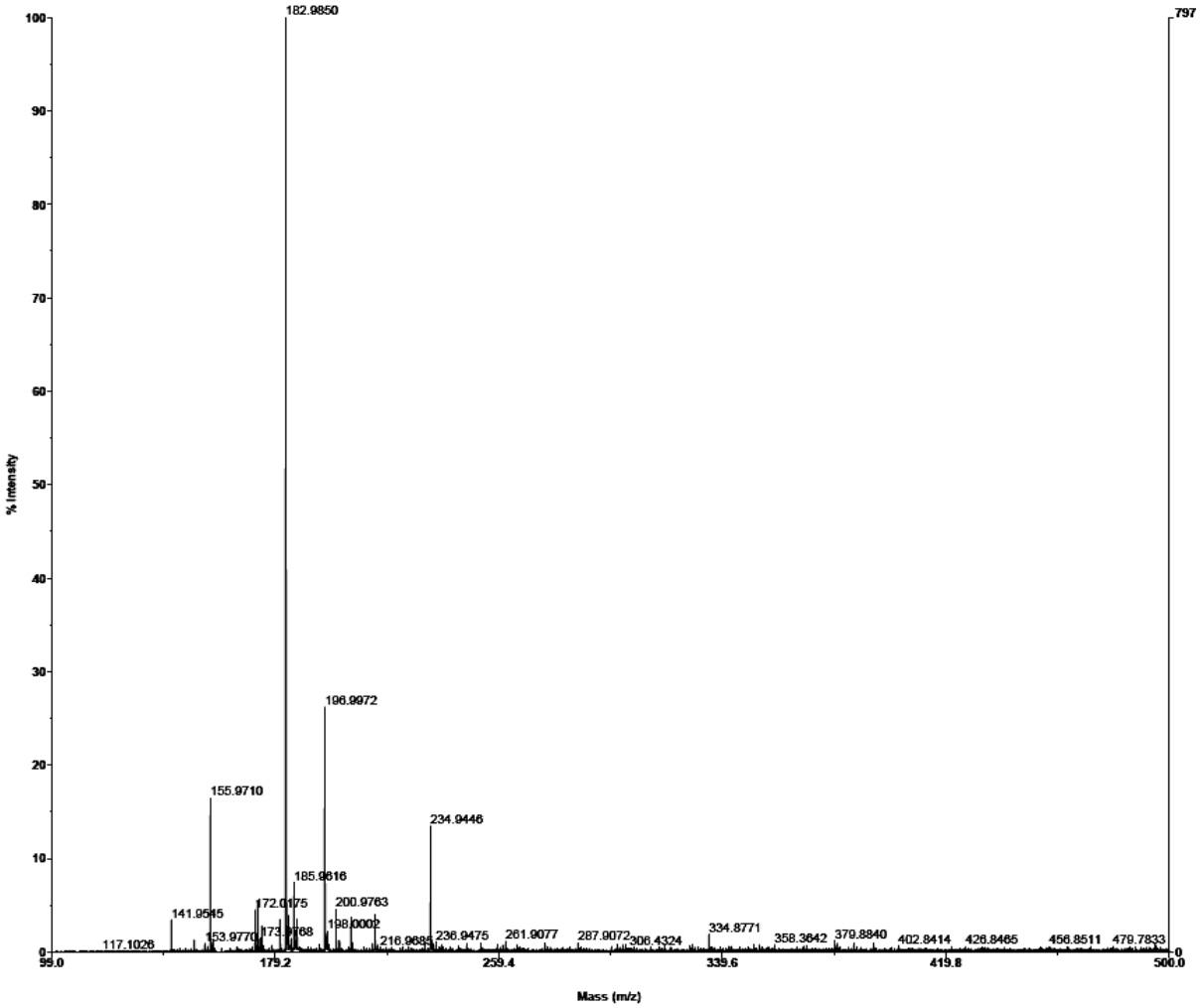

Figure A5. ESI-MS spectrum of iron logwood ink (FL).

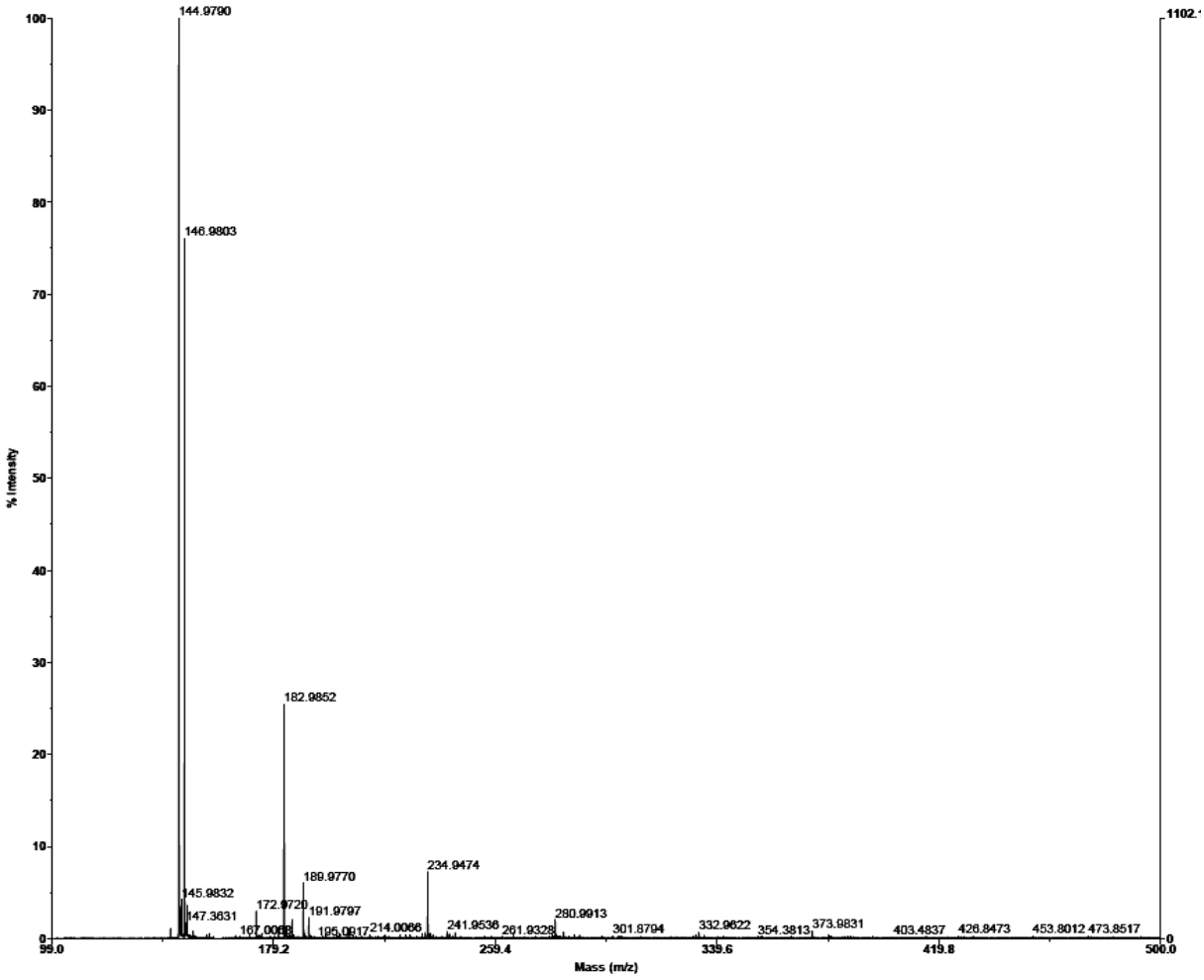

Figure A6. ESI-MS spectrum of Fe/Cu logwood ink (FCL).

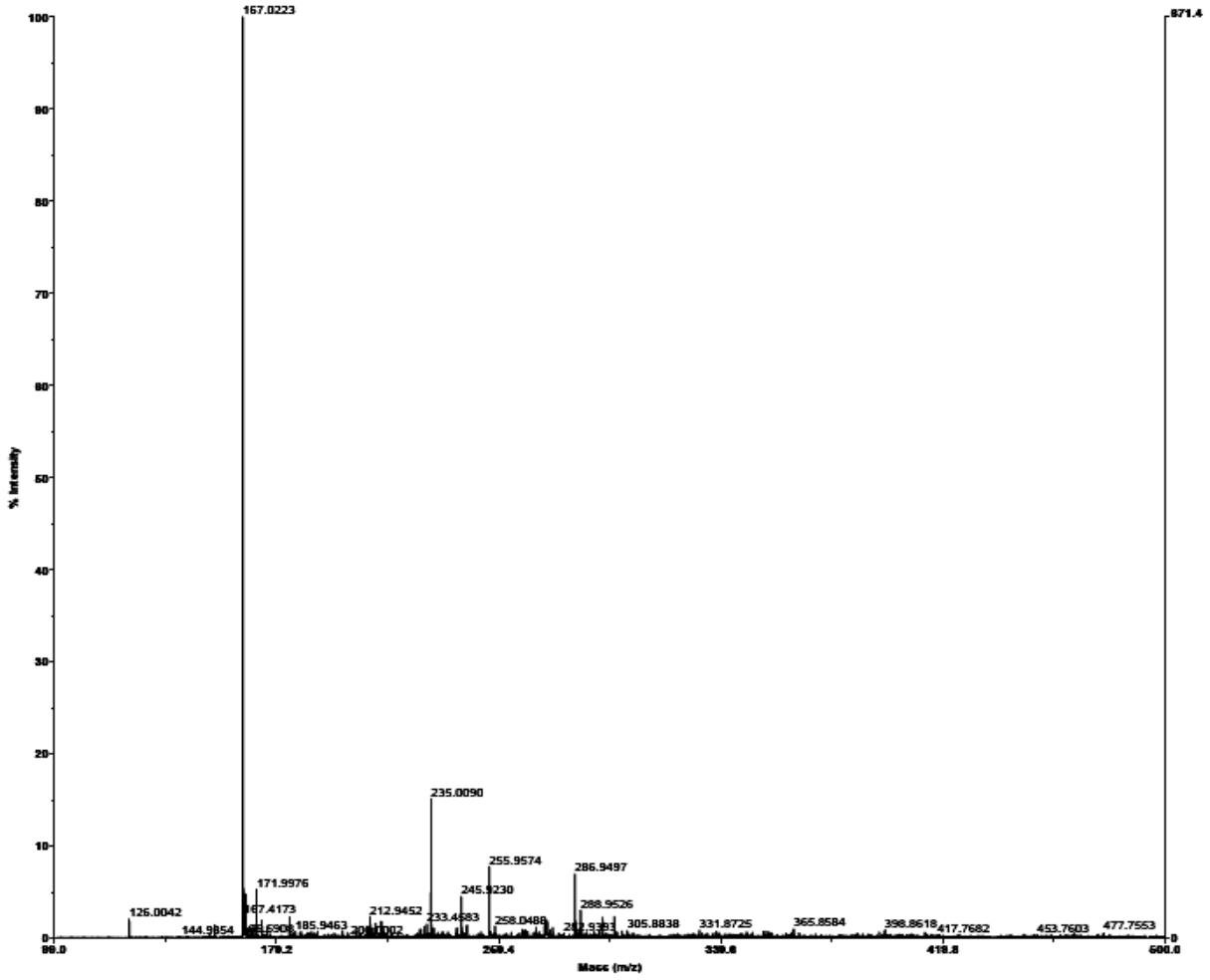

Figure A7. ESI-MS spectrum of Fe oxalate logwood ink (FLO).

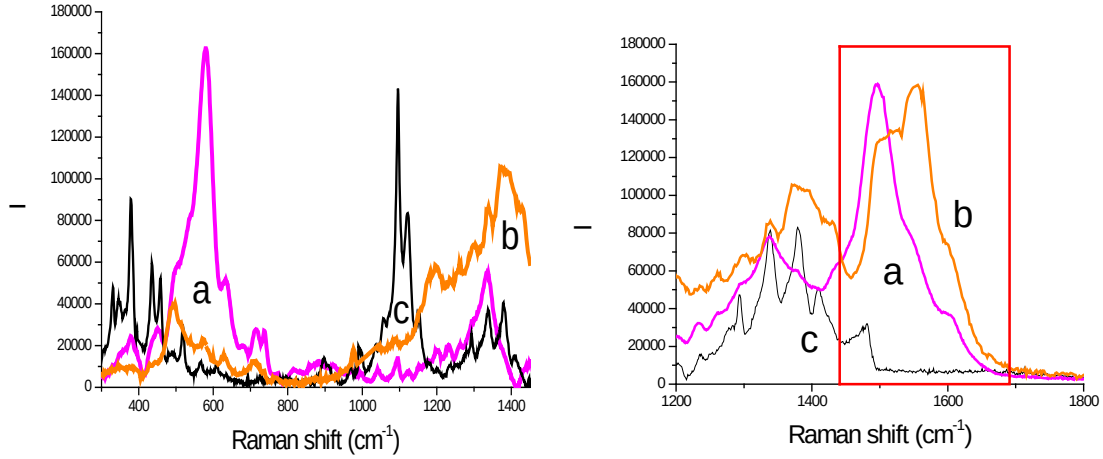

Figure A8: Raman spectra of FL four layers painted paper (pink, a), FL ink powder (orange, b) and paper (black, c).

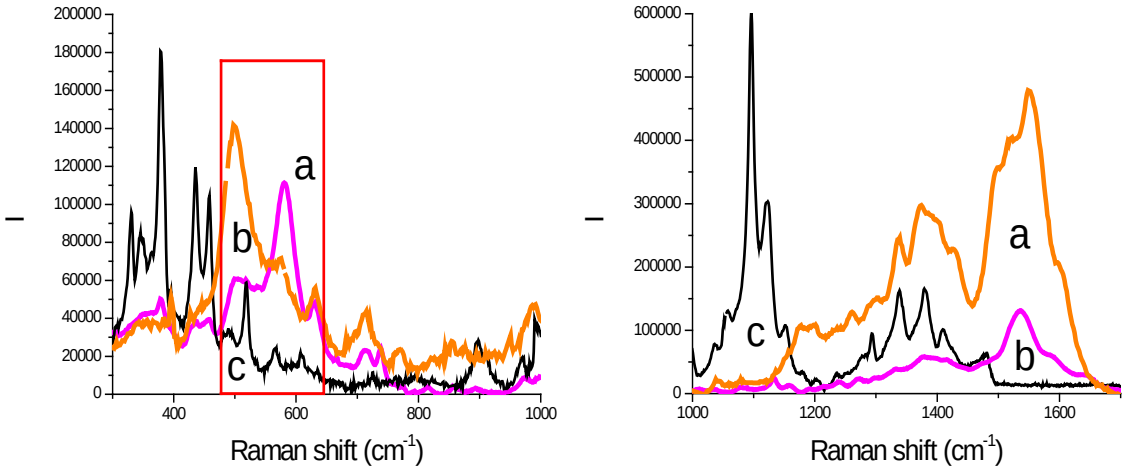

Figure A9: Raman spectra of FCL four layers painted paper (pink, a), FCL ink powder (orange, b) and paper (black, c).

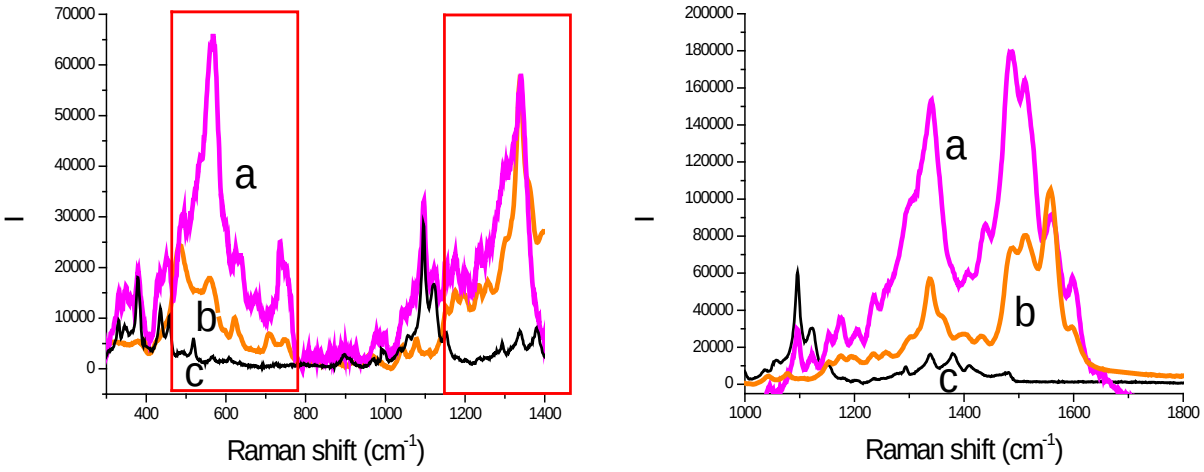

Figure A10: Raman spectra of FLO four layers painted paper (pink, a), FLO ink powder (orange, b) and paper (black, c).

Appendix B

1. Origin of paper

The paper invention is historically attributed to the Chinese dignitary Ts'ai Lun in 105 B.C., although he likely only perfected papermaking process, making paper more suited to be used as writing support. For many centuries the papermaking process was limited to the Chinese area, and only in the 7th century it was introduced in Korea and Japan. In 751, after the Talas Battle, Arabs learned the secrets of the papermaking from some Chinese prisoners, and afterwards they began to build paper mills in their territory: from Samarkand (751) to Baghdad (793), Damascus and up to Fez and, in the early 12th century, even in the European occupied territories, Spain (Jativa) and Sicily (Palermo). Perhaps, the foundation of the first paper mills in Fabriano in the first decades of the 13th century could be attributed to the Arabic domination. Other Italian centers, which based their economic system on the paper industry, were Amalfi, Venice, Genoa, Palermo and University cities such as Padua and Bologna.

2. Paper in the pre-industrial society

The first material used for papermaking was the paper mulberry bark (Brussonetia Papyrifera) and bamboo china-grass in the East, while in the West rags were used as raw materials. White or light colored rags of vegetable origin (cotton, hemp, and flax) were the most suitable ones for the papermaking. The linen fabric was the most common in Europe and it provided the best paper quality. However, it did not exclude, in particular for lower-quality papers, additions of colored rags, ropes, fishing nets and also silk and wool. Rag materials, after a first sorting needed to separate the different qualities and colors, were deprived of buttons and metal seam lines and cut. The rags were then beaten to get rid of dust and mud, washed and leached, so as to degrease and soften the tissue with a consequent color bleaching, accentuated by subsequent drying in the sun. After a further washing to remove the lye, the rags were cut into strips, which were washed again and left to macerate for four to seven weeks. Rags, once reduced to almost pure cellulose, were sent to the shredder in order to separate the fibers and thus be transformed into a paste or pulp. In ancient times, the Chinese people carried out this process only manually; subsequently, Arabs renewed this technique introducing the *follo*, a machine consisting of hand-operated

stone tubs (*pile*) with pestles (*magli*). In Fabriano, at the end of the 13th century, they were able to automatically operate the pestles by means of a water wheel.

In 1680 a new shredding rags machine was invented in the Netherlands, the so called "*pila olandese*". It was composed by a stone tub, where a steel blade-covered cylinder revolved. The rag shredding occurred more rapidly than with the pestles, the defibration was thinner and lasted thirty to forty times less, the raw material loss was much more reduced. Its use allowed for a more uniform paper sizing and it avoided the maceration step. However, the thus produced paper was composed by shorter fibers resulting less resistant. With the discovery of chlorine and its use for the textile bleaching (by Berthollet in 1789), also colored rags could be used for the paper production of white papers. The degradation effect induced by application of chlorine on paper imposed, a few decades later, a resort to special anti-chlorine treatments on the bleached pulp, firstly based on the use of sodium hyposulfite and, afterwards, of sodium bisulfite solutions.

Once obtained, the pulp was introduced into a vat and appropriately diluted, according to the type of paper. The fiber distribution was kept homogeneous by a constant stirring of the pulp at the constant temperature of 25°C. The sheet was formed introducing into the vat a rectangular wooden frame (*forma*): it is composed by a thin brass wires grating (*vergelle*), in which the wires were arranged very close one to each other, parallel on the longer side and superimposed and linked to other brass wires (*filoni)*, thicker and more distant than the *vergelle* and perpendicularly organized to them. The *filoni* were fixed into thin wood strips (*colonelli*), which surmounted and fastened them. The frame, holding the pulp fibers and filtering the water, formed the sheet. In the 16th century, a new wooden frame of suited thickness (*cascio* or *coperta*) was introduced, in order to allow one to make sheets of different thickness.

In correspondence of the loom wires, because of their thickness, paper was more subtle and transparent: in order to eliminate this flaw, in 1757 the Englishman John Wattman introduced a flat filtering frame consisting of a dense mesh, which allowed for a more uniform sheet. The thus produced paper was called tissue paper (*velina*), from the word *velino*, which was the most valuable ancient parchment made by the skin of dead born lambs or calves. (Their skin was indeed very thin and white, flawless, more uniform and very durable.)

This type of frame was used for the first time in 1781, and then its use spread throughout Europe. The adoption of the new loom was especially necessary to compensate for the greater subtlety of the fibers produced by the *pila olandese*, which were easily filtered through the vergelle.

The manual papermaking process allowed for the production of seven to eight sheets per minute, with a daily production, for small to medium size papers, of about 4250 sheets. Of course the production amount varied according to the size and quality of the paper. Once formed, the sheets were superimposed giving rise to a stack, normally composed by 160 to 420 sheets, where the leaves were interspersed with several felts.

In the filtering frame, a thin copper wire depicting an image, a sign or a letter was inserted and linked to the *vergelle* and *filoni* nets. This seam was called *watermark* and it represented the trademark of the paper mill. The brand was needed to ascertain the origin of the paper and for the identification of the paper type and size. Watermarks were probably introduced by the Fabriano paper mills in first decades of the 13th century.

The sheets, intercalated by several felts, were piled and pressed by hand-presses (later hydraulic presses), in order to obtain well flattened and unwrinkled papers and to reduce the drying times. After other two pressing steps, called the *soppressatura* and *scotolatura*, necessary to remove the residual water, to reduce the paper grain and to favor a more uniform sizing, the sheets were then separated and arranged to dry initially exposing them to the sun, then in the drying rooms.

3. Paper and the industrialization of the paper mills

The great social revolutions of the late 18th century brought, especially in France, the science liberalization, the freedom of speech and expression. The press became more and more a means of political and philosophical propaganda, in particular in the new middle class. Therefore, the demand for periodicals increased, with the consequent need of increasing production of paper, in shorter times and at lower prices.

The first device, which introduced the basis of the industrial papermaking, revolutionizing the pace, the technique and the costs of the paper industry was the “continuous papermaking machine”, invented in 1798 by Frenchman Nicholas Louis Robert. The invention was firstly implemented in England and made a working machine by the engineer Bryan Donkin in 1803. The engine was composed by a vat, consisting of a metal wire net, in which a

continuous strip entered. The paste was deposited by a palette cylinder on the strip, then the continuous sheet was deposited on a felt.

Further improvements provided an even bigger and faster equipment, even if the quality of the paper was not comparable to the manual produced one.

Almost simultaneously with Robert's paper machine, in 1797 Michael Leistenschneider introduced the roll continuous papermaking machine. In this equipment, the plane strip was replaced by a cylindrical frame covered by a copper wire grating, similar to the manual papermaking frame. The cylinder, called *creator drum*, was immersed for three quarters of its volume into the tank containing the paste. Its rotation created a pressure gradient between the inside and the outside, which induced the water to penetrate through the net, while the fibers were retained on the surface. Then, fibers were deposited as a sheet on a felt flowing over the bath. The paper produced by this machine had an intermediate quality between the continuous papermaking machine and the manual produced ones.

4. The new paper raw material

The rag shortage and the increasing demand for paper boosted the search for alternative raw materials. The new results from the natural sciences and the birth of chemistry as a science favored the first experiments on plants, aimed at obtaining a paste suitable for the papermaking. In 1765 G. C. Schoeffer proved the possibility to produce paper from several plants: wood of different tree species (softwood, broad-leaf), pruning of vines, nettles, moss and straw, several leaves, cabbage, brooms.

Initially the use of these materials was excluded for the manufacture of white paper, as the bleaching methods, necessary for whiten vegetable fibers, were unknown. After the introduction of chlorine and the development of the bleaching treatments, white printing and writing paper began to be produced from vegetable raw materials. Wood was firstly used in the second half of the 19^{th} century. The obtained sheets were white, smoothed and they were used for the printing of some of the most famous English periodicals. The wood-pulp was obtained by leaving these materials macerate with lime, soda and caustic potash. Afterwards, they were washed and beaten with pestles or with the roll continuous papermaking machine. In order to obtain whiter paper, plant fibers were whitened with chlorine and successively washed with dilute sulfuric acid.

However, the thus produced pulp still contained all the no-cellulosic substances (encrusting substances) present in the plant (especially in wood), that were not useful in the paper manufacture, but that, instead, could strongly damage the paper quality. For this reason, chemical methods, aimed at the removal of these substances and at the production of paper with higher cellulose content, were studied. The use of the chemical pulp became widespread only after the 1880 with the introduction of C. D. Ekman's sulfite process and C. F. Dahl's sulfate process.

The wood-pulp papers can be classified into three main categories, in relation to the degree of fibrous material purity and to the extraction processes:

a) mechanical pulp paper (or wood-pulp): it is obtained by the wood mechanical defibration. It contains all the wood impurities: hemicelluloses (polysaccharides with a low degree of polymerization), lignin, tannins, resins, natural gums. This paper is not expensive, but it is composed by fibers of low mechanical strength and it is characterized by a strong opacity.

b) chemical pulp paper: it is obtained by treating the wood or other plant materials with acidic, such as calcium or sodium bisulfite (sulfite process), or alkaline chemicals, such as sodium sulfate, lime (sulfate process), in order to eliminate the encrusting substances present. These substances quickly and uniformly penetrate into the plant matrix and dissolve the non-cellulosic substances. For this purpose, the use of autoclaves under pressure at 120-170°C is necessary. This process does not guarantee the total elimination of the harmful substances, as it would imply a great loss of cellulose and its excessive degradation.

c), semi-chemical or chemi-mechanical pulp paper: it is obtained by impregnating the wood with chemical reagents, so as to weaken the cohesion between the cellulosic fibers, followed by the wood mechanical defibration.

References

1. Buringh E., Van Zanden J., L. *J. Econ. Hist.* **2009**, 69, 409-445;
2. Hey M., *The Paper Conservator* **1979**, 4, 66-80;
3. Zou X., Uesaka T., Gurnagul N., *Cellulose* **1996**, 3, 243-267;
4. Whitmore P. M., Bogaard J., *Restaurator* **1994**, 15, 26-45;
5. Margutti S., Conio G., Calvini P., Pedemonte E., *Restaurator* **2001**, 22, 67-83;
6. Potthast A., Rosenau T., Kosma P., Saariaho A. M., Vuorinen T., Sixta H., *Cellulose* **2005**, 12(1), 43-50;
7. Jeong M. J., Dupont A.-L., de la Rie E.R., *Cellulose* **2012**, 19, 1135-1147;
8. Strlič M., Kolar J., Evaluating and enhancing paper stability - the needs and recent trends, in 5th EC Conf. “Cultural Herit. Res.: Pan-Eur. Challenge” **2002**: Krakow;
9. Bronzato M., Calvini P., Federici C., Bogialli S., Favaro G., Meneghetti M., Mba M., Brustolon M., Zoleo A. *Chem. Eur. J.* **2013**, 19, 9569-9577;
10. Mosca Conte A., Pulci O., Knapik A., Bagniuk J., Del Sole R., Łojewska J., Missori M. *Phys. Rev. Lett.* **2012**, 108(15), 169902;
11. Łojewski, T., Miśkowiec, P., Missori, M., Lubańska, A., Proniewicz, L. M., Łojewska, J., *Carbohydr. Polym.* **2010**, 82, 370-375;
12. Porck H. J., Rate of Paper Degradation: The Predictive Value of Artificial Aging Tests, European Commission on Preservation and Access, Amsterdam, **2000**;
13. Shahani C. J.; Hengemihle F. H. In *Historic Textile and Paper Materials. Conservation and Charaterization*; Needle, H., Zeronian, S. H., Eds.; Series 212; Am. Chem. Soc.: Philadelphia, USA, **1986**; pp. 387–410;
14. Calvini P., Gorassini A., Luciano G., Franceschi E., *Vib. Spectrosc.* **2006**, 40, 177-183;
15. Calvini P., Silveira M., *e-Preserv. Sci.* **2008**, 5, 1-8;
16. Ali M., Emsley A. M., Herman H., Heywood R. J., *Polymer* **2001**, 42, 2893-2900;
17. Buslov D. K., Nikonenko N. A., Sushko N. I., Zhbankov R. G., *J. Appl. Spectrosc.* **2001**, 68, 917-923;
18. Proniewicz L. M., Paluszkiewicz C., Weselucha-Birczyńska A., Majcherczyk H., Barański A., Konieczna A., *J. Mol. Struct.* **2001**, 596, 163-169;
19. Bicchieri M., Sodo A., Piantanida G., Coluzza C., *J. Raman Spectrosc.* **2006**, 37, 1186-1192;

20. Bellot-Gurlet L., Pagès-Camagna S., Coupry C., *J. Raman Spectrosc.* **2006**, 37, 962-965;
21. Smith E., Dent G., *Modern Raman Spectroscopy: A Practical Approach*, Wiley;
22. Creighton J. A., Eadon D. G., *J. Chem. Soc.* **1991**, 87, 3881-3891;
23. Lombardi J. R., Birke R. L., Lu T., Xu J., *J. Chem. Phys.* **1986**, 84, 4174-4180;
24. Lombardi J.R., Birke R. L., *J. Phys. Chem*. **2008**, 112, 5605-5617;
25. Amendola V., Meneghetti M., *J. Mater. Chem.* **2007**, 17, 4705-4710;
26. Mantler M., Schreiner M. *X-Ray Spectrom*. **2000**, 29, 3-17;
27. Ardrey R. E., *Liquid Chromatography- Mass Spectrometry: an Introduction.* **2003**, New York: J. Wiley and Sons;
28. Grossman P. D., Colburn, J. C. in *Capillary Electrophoresis. Theory and Practise.* **1992**;
29. Dupont A. - L., Egasse C., Morin A., Vasseur F., *Carbohydr. Polym.* **2007**, 68, 1-16;
30. Souguir Z., Dupont A. - L., *Biomacromolecules* **2008**, 9, 2546-2552;
31. Łojewska J., Missori M., Lubańska A., Grimaldi P., Zięba K., Proniewicz L. M., Congiu Castellano A., *Appl. Phys. A* **2007**, 89, 883-887;
32. Łojewski T., Zięba K, Knapik A., Bagniuk J., Lubańska A., Łojewska, J., *Appl. Phys. A* **2010**, 100, 809-821;
33. Socrates, G., *Infrared and Raman Characteristic GroupWavenumbers, Tables and Charts*. **1994**, NewYork: JohnWiley & Sons;
34. Łojewska J., Miśkowiec P., Łojewski T., Proniewicz L. M., *Polym. Degrad. Stab*. **2005**, 88, 512-520;
35. A. - L. Dupont, *Restaurator* **1996**, 17, 1-21;
36. Casieri C., Bubici S., Viola I., De Luca F. *Solid State Nucl. Magn. Reson.* **2004**, 26, 65-73;
37. Attanasio D., Capitani D., Federici C., Segre A. L. in *Multidimensional Spectroscopy of Polymers* (Eds.: M. W. Urban, T. Provder), Am. Chem. Soc., Washington, **1995**, pp. 335-353;
38. Varma, A. J., Chavan, V. B., Rajmohanan, P. R., Ganapathy, S. *Polym. Degrad. Stab*. **1997**, 58 257-260;
39. Tahiri C., Vignon M. R., *Cellulose* **2000**, 7, 177-188;
40. Moulthrop J.S.; Swatloski R. P., Moyna G., Rogers R. D. *Chem. Commun.* **2005**, 12, 1557-1559;
41. Martínez M., León de Pinto G., Sanabria L., Beltran O., Igartuburu J. M., Bahsas A., *Carbohydr. Res.* **2003**, 338, 619-624;

42. Flugge L. A., Blank J. T., Petillo P. A., *J. Am. Chem. Soc.* **1999**, 121, 7228-7238;
43. Benabdillah K., Mahfoud Bousetta J. C., Engel R., Vert M. *Macromolecules* **1999**, 32, 8774-8780;
44. Higham C. W., Gordon - Smith D., Dempsey C. E., Wood P. M. *FEBS Lett.* **1994**, 351, 128-132;
45. Marcq O., Barbe J. M., Trichet A., Guilard R., *Carbohydr. Res.* **2001**, 333, 233-240;
46. Marcq O., Barbe J. M., Trichet A., Guilard R., *Carbohydr. Res.* **2009**, 344, 1303-1310;
47. Cariati F., Rampazzi L., Toniolo L., Pozzi A. *Stud. Conserv.* **2000**, 45, 180-188;
48. Frost R. L., Yang J., Ding Z., *Chin. Sci. Bull.* **2003**, 48, 1844 –1852;
49. D' Antonio M. C., Wladimirsky A., Palacios D., Coggiola L., González-Baró A. C., Baran E. J., Mercader R. C., *J. Braz. Chem. Soc*. **2009,** 20(3), 445-450;
50. Sistach M.C., Ferrer N., Romeo M. T., *Restaurator* **1998**, 19, 173-186;
51. Ferrer, N., Sistach M. C., *Book Pap. Group Ann.* **2007**, 26, 21-25;
52. Calvini P., Gorassini A*., Restaurator* **2002**, 23, 48-66;
53. Calvini P., Gorassini A., Chiggiato R., *Restaurator* **2006**, 27, 81-89
54. Attanasio D., Capitani D., Federici C., Segre A. L., *Archaeometry* **1995**, 37, 377-384;
55. Zoleo A., Confortin D., Dal Mina N., Brustolon M., *Appl. Magn. Reson.* **2010**, 39, 215-223;
56. Zoleo A., Vecchia F., Brustolon M., *Appl. Magn. Reson*. **2009**, 35, 213-220;
57. Lund Myhre C. E., Nielsen, C. J., *Atmos. Chem. Phys.* **2004**, 4, 1759-1769;
58. Back R. A., *Can. J. Chem.* **1984**, 62(8), 1414-1428;
59. Max J. J., Chapados C., *J. Phys. Chem. A* **2004**, 108, 3324-3337;
60. Dupont A. - L, *Restaurator* **1996**, 17, 145-164;
61. Wiltscheck R., Kammerer, R. A., Dames, S. A., Schulthess T., Blommers M. J. J., Engel J., Alexandrescu A. T., *Protein Sci.* **1997**, 6, 1734-1745;
62. Saitò H., Yokoi M., *J. Biochem.* **1992**, 111, 376-382;
63. Dupont A. - L. *J. Chromatogr.* A **2002**, 950, 113-124;
64. Dupont A. - L. *Gelatine sizing of paper and its impact on the degradation of cellulose during aging.* Ph.D. Thesis, University of Amsterdam, Amsterdam, **2003**;
65. Stephens C. H., Whitmore P. M., Morris H. R., Bier M. E., *Biomacromolecules* **2008**, 9, 1093-1099;
66. Holen A. K., Christensen P. K., Moe S. T. In *Investigation of Reaction Products from the Ozonation of Cellulose Model Compounds by NMR Spectroscopy*, Int. Pulp Bleaching

Conf., Washington, **1996**, pp. 499-502;

67. Holen A. In *Reaction products from ozonation of dissolved carbohydrates*, *Int. Pulp Bleaching Conf.*, KCL, **1998**, pp. 481-486;
68. Lemeune S., *J. Appl. Polym. Sci.* **2004**, 93, 1219-1223;
69. De Laat J., *Environ. Techn. Lett.* **1995**, 16, 1035-1038;
70. Angibaud P., Defaye J., Gadelle A. In *Cellulose and its Derivatives;* Kennedy J. F. et al., Eds.; Ellis Horwood Ltd: New York, **1985**; pp. 161-171;
71. Lemeune S., *Ozone-Sci. Eng.* **2000**, 22, 447-460;
72. Sakai K., *J. Fac. Agr.* **1991**, 36(1-2), 45-53;
73. Butorac V., *Croat. Chem. Acta* **2007**, 80(3-4), 533-539;
74. Lehner S. In *Ink Manufacture including Writing, Copying, Lithographic, Marking, Stamping and Laundry Inks*; 5th ed.; Scott, Greenwood and Company: London, **1914**;
75. Ainsworth Mitchell C. In *Inks: Their Composition and Manufacture;* Charles Griffin and Company Ltd: London, **1904**;
76. Gettens R. J., Stout G. L. In *Painting Materials. A Short Encyclopaedia;* Dover Art Instruction: New York, **1966**;
77. Cardon D. In *Natural Dyes. Sources, Tradition, Technology and Science;* Archetype, Eds: London, **2007**;
78. Bicchieri M., Monti M. Piantanida G., Sodo A., Tanasi M. T. In *9th International Conference on NDT of Art*, Section "Inside the parchment", May 25-30, **2008**, Jerusalem, Israel;
79. Krekel C., *Int. J. Foren. Doc. Examiners* **1999**, 5, 54-58;
80. Neevel J. G., Mensch C. T. J. I the ICOMCC 12th Triennial Meeting, Section "The behaviour of iron and sulphuric acid during iron gall ink corrosion", August 29–September 3, **1999**, Lyon, France;
81. Centeno S. A., in *Vincent Van Gogh. The Drawings*; S. A. Stein, C. Ives, S. Van Heugten, M. Vellekoop, Eds.; The Metropolitan Museum of Art, Van Gogh Museum, Yale University Press: New York, Amsterdam, New Haven, **2005**; pp. 356;
82. Shelley M., in *Vincent Van Gogh. The Drawings*; S. A. Stein, C. Ives, S. Van Heugten, M. Vellekoop, Eds.; The Metropolitan Museum of Art, Van Gogh Museum: New York, Amsterdam, New Haven, **2005**; pp. 348;
83. Kahr, B., Lovell S., Subramony J. A., *Chirality* **1998**, 10, 66-77;

84. Bettinger C., *Histochemistry* **1991**, 96, 215-228;
85. Joshi K. C., *Coord. Chem. Rev.* **1977**, 22, 37-122;
86. Mostafa S.I., *Transit. Met. Chem.* **1999**, 24, 306-310;
87. Sorrell T. N., *Inorg. Chem.* **1990**, 29(9), 1687-1692;
88. Ibrahim M., Alaam M., El-Haes H., Jalbout A. F., de Leon A., *Ecl. Quím.* **2006**, 31(3), 15-21;
89. Senvaitiene J., Beganskiene A., Kareiva A., *J. Vib. Spectrosc.* **2005**, 37, 61-67;
90. Centeno S. A., Ropret P., Del Federico E., Shamir J., Itinf B., Jerschowg A., *J. Raman Spectrosc.* **2010**, 41, 445-451;
91. Becker E.D., *J. Phys. Chem.* **1991**, 95, 2818-2823;
92. Nonella M., *Chem. Phys. Lett.* **1997**, 280, 91-94;
93. Bellamy L. J., In *The Infrared Spectra of Complex Molecules*; John Wiley & Sons Ltd: New York, **1962**;
94. Szabó A., Kovàcs A., *J. Mol. Struct.* **1999**, 510, 215-225;
95. Lee A. S., Mahon P. J., Creagh D. C., *J. Vib. Spectrosc.* **2006**, 41, 170-175;
96. Lee A. S., Otieno-Alego V., Creagh D. C., *J. Raman Spectrosc.* **2008**, 39(8), 1079-1084;
97. Xia H., Sun K., Sun K., Feng Z., Li W. X., Li C., *J. Phys. Chem. C* **2008**, 112, 9001-9005;
98. Nakamoto K., In *Infrared and Raman Spectra of Inorganic and Coordination Compounds*; 4th ed: **1986**;
99. Lin-Vien D., Colthup N. B., Fateley W. G., Grasselli J. G., In Handbook of Infrared and Raman Characteristic Frequencies of Organic Molecules; Academic Press: San Diego, **1991**;
100. De Souza R. F. V., *Spectrochim. Acta Part A* **2005**, 61, 1985-1990;
101. Peisach, J., Blumberg, W.E., *Arch. Biochem. Biophys.* **1974**, 165 (2), 691-708;
102. Frost R. L., *J. Raman Spectrosc.* **2002**, 33(4), 252-259;
103. Burgio L., *PNAS* **2010**, 107(13), 5726-5731;
104. Frost R. L., *Anal. Chim. Acta* **2004**, 517, 207-214;
105. Gilbert B., *Analyst*. **2003**, 128, 1213-1217;
106. Nastova I., Grupče O., Minčeva-Šukarova B., Turan S., Yaygingol M., Ozcatal M., Martinovskac V., Jakovlevska-Spirovskac Z., *J. Raman Spectrosc.* **2012**, 43, 1729-1736;
107. Söderholm S., Roos Y. H., Meinander N., Hotokka M., *J. Raman Spectrosc.* **1999**, 30, 1009-1018;
108. Bicchieri M., Monti M., Piantanida G., Sodo A., *Anal. Bioanal. Chem.* **2013**, 405, 2713-

2721.

Acknowledgments

So many people supported me in these three years and I would like to thank everybody, because everyone around me was important for the realization of this project.

My first and sincere thank you goes to my family, who always supports me unconditionally, encouraging me to follow my dreams.

A special gratitude is for my boyfriend Mario: thank you for your love, for your support, for believing in me and inciting me to do so. Thank you for always being beside me!

I wish to express my deep gratitude to my supervisor Dr. Alfonso Zoleo for giving me the opportunity to work in the amazing and inspiring world of the Cultural Heritage and to fully experience the librarian and archival reality.

I would like to thank Prof. Carlo Federici and Prof. Melania Zanetti for allowing us to work on very rare samples and therefore acquiring unique data, which made our research one of the most cutting-edge one in this field.

I would like to thank Prof. Calvini for his useful advice, which helped us scientifically address our work.

I wish to express my appreciation to all the researchers and professors of the Chemical Science department, who took part to this project, for their availability and the fruitful discussions and advices:

- Professor Moreno Meneghetti for giving us the opportunity to use the UV-Vis and Raman spectrophotometer and for his help in the article redraft;
- Professor Danilo Pedron and Dr. Lorenzo Franco for allowing us to record FTIR ATR spectra of our samples;
- The whole analytical chemistry department: Professor Tapparo for his useful indications and his group, in particular Dr. Lidia Soldà, for the HPIC analysis, Dr. Valerio di Marco for the ICP-MS analysis, Dr. Sara Bogialli and Dr. Gabriella Favaro for the HPLC analysis;
- Dr. Miriam Mba Blazquez for carrying out the catalytic hydrogenation of our samples;
- Prof. Stefano Mammi and his research group for recording the NMR spectra of our samples: in particular thank you to Dr. Ileana Menegazzo for her availability and competence;

- Dr. Luca Nodari and Dr. Marta Maria Natile, for recording of spectra XRF and XRD of our samples;
- The lab technicians Sabrina Mattiolo and Emanuela Zangirolami, for their help, their kindness and their sympathy.

Furthermore, I would like to deeply thank Dr. A. - L. Dupont and Dr. Silvia Centeno, who gave me the opportunity to work in their team, in most famous research centers all over the world, and in general all the people I met during these two amazing experiences. A special thank you goes to Chiara, Sabrina, Olivier, Sophie, Lorena, Lisa and Natalya, who were more than simple colleagues, they were real friends and they helped me to feel like home. I hope to see you soon!

I would like to thank the whole EPR group and in particular the Ph.D. students Tommaso, Francesco, Annalisa and Dr. Marco Bortolus: it was a pleasure to share the office with you during this period, thank you for the supporting chats and the cooking advices.

I would like to thank all my old friends and new friends: thank you so much for the relaxing and funny moments we had and we will have together.